FACULTY
OF MATHEMATICS
AND PHYSICS
Charles University

MASTER THESIS

Bc. Tomáš Malina

Artificial light-harvesting antenna based on an aggregation of bacteriochlorophyll c with selected pigments

Department of Chemical Physics and Optics

Supervisor of the master thesis: doc. RNDr. Jakub Pšenčík, Ph.D.

Study programme: Physics

Specialization: Biophysics and chemical physics

Prague 2020

I declare that I carried out this master thesis independently, and only with the cited sources, literature and other professional sources.

I understand that my work relates to the rights and obligations under the Act No. 121/2000 Coll., the Copyright Act, as amended, in particular the fact that the Charles University has the right to conclude a license agreement on the use of this work as a school work pursuant to Section 60 paragraph 1 of the Copyright Act.

In Prague, May 25th 2020 Tomáš Malina

First of all I would like to thank my supervisor doc. RNDr. Jakub Pšenčík, Ph.D. for his patient mentoring, for the numerous discussions, and all his help when I was writing this thesis.

Also, I would like to thank RNDr. David Bína, Ph.D. for making it possible for me to perform some of the measurements at the University of South Bohemia.

Last but not least I would like to thank all my friends and family who motivated as well as distracted me and for their good humour.

Název práce: Umělá světlosběrná anténa založená na agregaci bakteriochlorofylu c s vybranými pigmenty

Autor: Tomáš Malina

Katedra: Katedra chemické fyziky a optiky

Vedoucí diplomové práce: doc. RNDr. Jakub Pšenčík, Ph.D., KCHFO MFF UK

Abstrakt: Sluneční energie je jedním z nejdůležitějších zdrojů energie pro všechny živé organismy v přírodě. Její záchyt probíhá ve specializovaných světlosběrných komplexech zvaných antény, které typicky obsahují proteinovou kostru s navázanými pigmenty. Výjimečnými jsou v tomto případě chlorosomy, světlosběrné antény zelených bakterií, ve kterých se pigmenty organizují spontánně, bez pomoci proteinů. Tuto vlastnost spontánní agregace mají pigmenty bakteriochlorofylu (BChl) *c*, *d* nebo *e*, které jsou v chlorosomech zastoupeny nejpočetněji. Díky této vlastnosti lze vytvořit umělé světlosběrné antény na stejném principu a rozšiřovat jejich absorpční spektrum pomocí dalších pigmentů.

V této práci byly studovány antény vzniklé agregací BChl c s β-karotenem a BChl a dvěma metodami, rychlou a pomalou. Nejprve byla zkoumána účinnost přenosu energie mezi těmito pigmenty. Přenos energie mezi BChl *c* a BChl *a* dosahoval až 95 %, zatímco přenos z β-karotenu na BChl *c* má účinnost nižší. Důležitou vlastností β-karotenu v umělých agregátech podobně jako v přirozených chlorosomech však bylo jeho účinné zhášení tripletních stavů BChl *c*, které jinak mohou generovat singletní kyslík. Ten by anténu poškozoval. Pro studium struktury jednotlivých agregátů bylo použito mikroskopie atomárních sil. U některých agregátů byla též zjištěna vyšší oscilátorová síla emisních dipólů než u monomerů, což zvyšuje účinnost přenosu excitační energie.

Klíčová slova: Umělá fotosyntéza, světlosběrné antény, přenos excitační energie, superradiance, zelené fotosyntetické bakterie

Title: Artificial light-harvesting antenna based on an aggregation of bacteriochlorophyll c with selected pigments

Author: Tomáš Malina

Department: Department of Chemical Physics and Optics

Supervisor of the master thesis: doc. RNDr. Jakub Pšenčík, Ph.D., KCHFO MFF UK

Abstract: Solar energy is one of the most important energy sources for all living organisms. The light harvesting takes place in specialised photosynthetic complexes called antennas; they typically contain pigments held by a protein scaffold. Antennas of green bacteria, chlorosomes, are unique in this respect, for they do not need proteins to organise the pigments. The pigments contained in chlorosomes, bacteriochlorophyll (BChl) *c*, *d* or *e*, aggregate spontaneously. This self-aggregation can be used to form an artificial light-harvesting antenna the absorption spectrum of which can be extended by addition of other pigments.

Antennas based on aggregation of BChl c with β-carotene and BChl a were prepared by a fast and slow method. The excitation energy transfer efficiency between these pigments was studied. The efficiency of energy transfer from BChl c to BChl a reached up to 95 %, the efficiency of energy transfer from β-carotene to BChl c was lower. An important role of β-carotene in artificial aggregates as well as in chlorosomes is its efficient quenching of BChl c triplet states, which could otherwise generate singlet oxygen harmful to the antenna. Atomic force microscopy was utilised to study the structure of individual aggregates. In some aggregates, a larger emission dipole strength compared to monomeric BChl c was observed, allowing for more efficient energy transfer.

Keywords: Artificial photosynthesis, light-harvesting, excitation energy transfer, superradiance, green photosynthetic bacteria

Table of contents

1 Introduction

A lot of the energy stored on our planet is of solar origin. Photosynthetic bacteria, algae, and plants have been converting solar energy into chemical form for several billions of years by the process of photosynthesis. If humans were ever able to master photosynthesis for their own use, there would be no need for fossil fuels. However, we still do not understand all the mechanisms of photosynthesis to be able to utilise it for energy production efficiently.

Currently, there are two main branches of artificial photosynthesis research. The first one is trying to develop an artificial photosynthetic unit that would produce desired molecules suitable for other processing – e.g. hydrogen ((1), (2), (3), (4)) or hydrocarbons ((2), (3), (4)) as a fuel. This fuel could then be utilised to generate electricity or power a vehicle. The other branch is trying to synthesise a photosynthesis-based solar cell that would directly output electric power ((5), (6), (7)). Both of these devices would have some advantages and drawbacks in different applications. However, neither of these products are ready for manufacture yet, although both have been demonstrated in laboratory conditions as a proof of concept ((1), (2), (4), (5), (6), (7)).

Currently, there are several problems with the organic photovoltaics. First and foremost, it is the low overall efficiency (5). Should it be based on chlorophyll pigments, those absorb only in two narrow bands in the visible spectrum, leaving much of the energy hitting Earth to go to waste. Long term stability is also not very good at the moment – the organic pigments used in photosynthesis are sensitive to oxidative damage (4) and are protected by sophisticated mechanisms in living cells (8). There is therefore a lot of room for improvements.

The electromagnetic spectrum hitting Earth is different from blackbody radiation that the Sun more or less emits. As determined by the Wien's displacement law, the emission spectrum of Sun corresponds to a blackbody of temperature around 5800 K. Due to temperature variations on the surface and the absorption and emission of specific wavelengths by the atoms and molecules of which it is constituted, the spectrum is not a perfect blackbody radiation spectrum (9). Nevertheless, this spectral

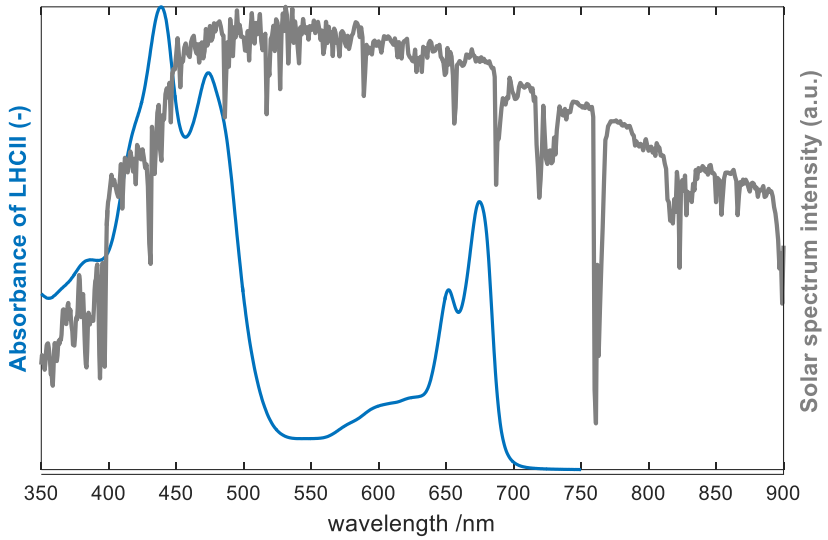

Figure 1: Absorption spectrum of LHCII, the most abundant photosynthetic antenna on Earth, overlaid on top of solar spectrum at sea level.

profile hits the top of our atmosphere. There, due to absorption by atmospheric gases (mostly water vapour, carbon dioxide, oxygen and ozone), this spectrum is modified.

To compare the amount of energy hitting Earth (at sea level) and the spectral range that is not utilised, see Figure 1. For artificial applications, this is a significant drawback as the maximum efficiency is noticeably lowered.

1.1 Photosynthesis

Photosynthesis is a process converting light into chemical energy. This process takes place in unicellular and multicellular organism, in prokaryote and eukaryote, in plants, algae, cyanobacteria, and photosynthetic bacteria. The purpose is straightforward: to produce energy-rich compounds that can be transported where energy is needed or stored for later. It can be divided into two phases: the light phase which involves the absorption of light and conversion of this energy into fast-metabolised macroergic molecules, and the dark phase, which processes these products of light phase into more stable energy reservoirs or cellular structural elements. These final products of the dark phase are called saccharides and in the end serve as energy source for not only photosynthetic organisms, but in turn to almost all organisms in general (10). Photosynthesis is therefore a vital part of life on Earth and without it, only less effective mechanisms of metabolisms would have evolved (11).

Without photosynthesis, there are other mechanisms that could in theory supply energy into the food chain. Organisms that utilise temperature gradient could run a nature's version of Carnot's cycle. This would be limited only to places that offer large temperature differences over small distances, e.g. in the proximity of volcanic vents or thermal geysers. Osmotic or pH gradient could also supply energy for some – but the location of this mechanism would also be limited to an interface of two sufficiently different environments. Redox reactions utilising elements and minerals in the Earth's crust could supply some energy, but only to a point where all of the free elements are fully oxidised. Electric field can also supply energy in the nature, e.g. piezoelectricity, but the application of such a mechanism would be also strictly limited. Last, the oxidation of energy-rich compounds such as saccharides is a very efficient way to get energy. However, the production of these energy-rich compounds is complicated and requires a constant influx of sufficient amount of energy, which is why photosynthesis is the most suitable mechanism of harvesting energy on Earth (11).

The formation of Earth is dated approximately 4.6 billion years ago, and the exact time when photosynthesis first appeared is still disputed. There is evidence that it might have been as early as 3.8 billion years ago ((12), (13), (14)). A date that the scientific community agrees on is for the existence of oxygenic photosynthesis. The concentration of oxygen in atmosphere started to rise 2.4 billion years ago during the Great Oxidation Event (15). This is the latest possible instant that oxygenic photosynthesis could have occurred. However, anoxygenic photosynthesis is surely older ((12), (13), (14)). Thus photosynthetic bacteria are deemed to be one of the first inhabitants of Earth.

1.1.1 Light-harvesting molecules

The photons are captured by various pigment molecules, the most prominent ones are from a group called chlorophylls. The exact chemical structure differs by organism, but they are all derived from a tetrapyrrole macrocycle. The common features are the central ion, typically Mg^{2+}, a fifth cyclopentanone ring fused to pyrrole C, reduced ring D in most chlorophylls (Chls) and additional reduction on ring B in most bacteriochlorophylls (BChls), and a long esterified alcohol chain attached to the D ring. They are the main light-harvesting pigments in most of the photosynthetic antennas, complexes specialised for absorption of solar energy (10).

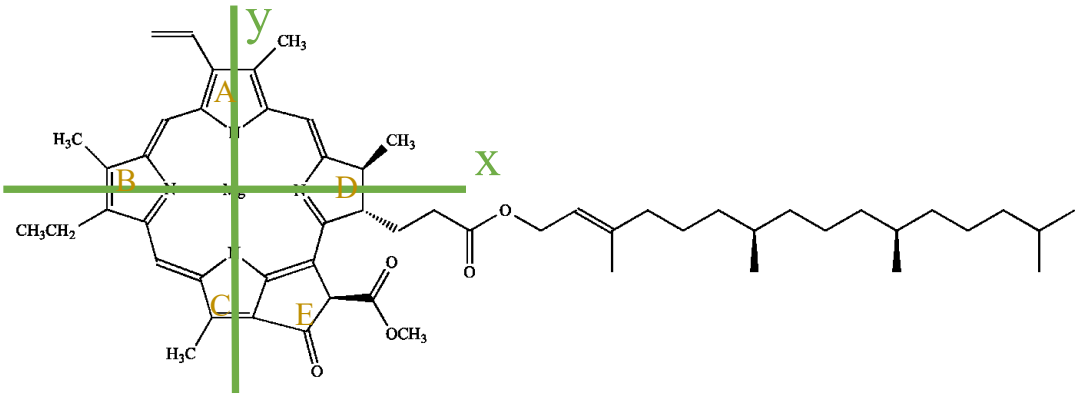

Figure 2: Structure of Chl *a*, the most abundant of chlorophylls on Earth. Edited from (16).

The chlorophyll molecules have two distinct absorption bands, the Q bands, corresponding to the S_0 to S_1 (so-called Q_y band) and S_0 to S_2 transition (Q_x band), and the Soret band (sometimes called the B band), corresponding to the S_0 to S_3 (B_y band) and S_0 to S_4 (B_x band) transition. They are denoted x and y depending on the orientation of transition dipole moment with respect to the axis convention. Due to electron density shifts resulting from the transitions, which are more significant along the y axis and less significant along the x axis, the transitions along the x axis are less pronounced. ((17), (8)).

The prosthetic groups bound to the tetrapyrrole ring change the position of the absorption bands (see Figure 3). Therefore, even though all the chlorophylls have the two distinct bands in common, the actual energy of the electronic transitions is different from pigment to pigment. Furthermore, due to molecular interactions, even two pigments of the same structure will absorb at different wavelengths in two

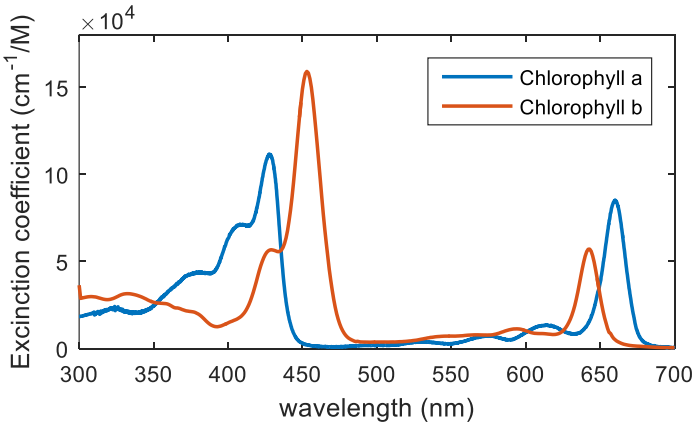

Figure 3: Spectra of Chl *a* and *b* in diethyl ether. Data taken from (18).

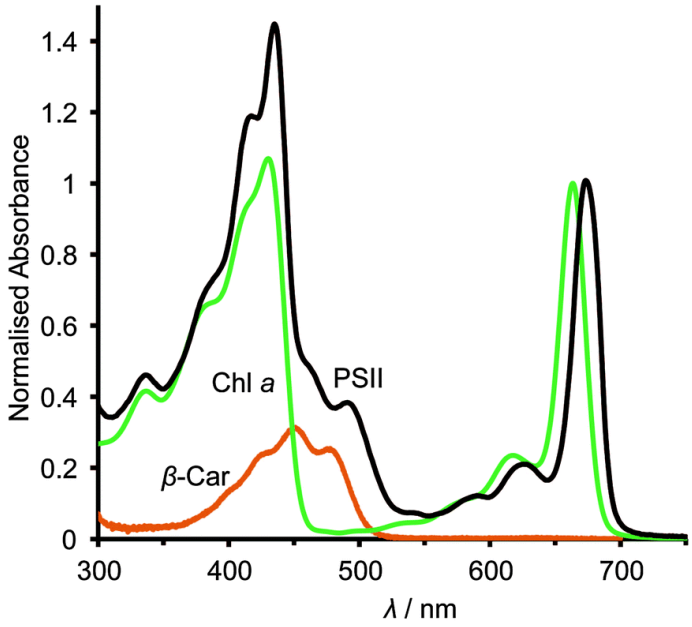

Figure 4: UV-Vis absorption spectra of Chl *a* (in methanol, green), β-carotene (in hexane, red) and PSII (in MES buffer, black). Image taken from (19).

different surroundings. This can be demonstrated by measuring the absorption spectrum of Chl *a* free in solution and in a protein complex (see Figure 4).

Apart from molecules of chlorophyll, there are also other pigments present in the light-harvesting complexes. Those are not the main pigments that mediate energy harvesting, but they supplement absorption of chlorophylls for the organism to gain an advantage in its habitat, to protect the light-harvesting complexes from degradation, or serving as a structural component of membranes. The second most common group of pigments are carotenoids. Those terpenoid lipophilic molecules are usually rigid components of a light-harvesting complex. They absorb in the blue-green region of visible spectrum and extend the absorption range at the red-end of the Soret band. The efficiency of singlet-singlet energy transfer from certain carotenoids to chlorophyll is in some cases very high, reaching up to nearly 100 % (10). A noteworthy function of theirs is the protection from oxidative stress they provide to the photosynthetic complexes. They are also involved in regulation of photosynthesis ((20), (21)).

Other pigments in cyanobacteria and algae are phycobilins which extend the absorption spectrum. They are, just like chlorophylls, constituted of four pyrrole molecules, but the pyrroles here are not connected into a ring form; rather, they remain linear. They are contained in special antennas called phycobilisomes, positioned

farthest from the so-called reaction centres (RCs), a photosynthetic unit accepting energy from the light-harvesting antennas in order to conduct charge separation and begin the electron transport chain. These phycobilins absorb in the green to orange region and help the cyanobacteria to survive under the water surface where organisms can afford little light to be wasted (10).

Also, pheophytins, pigments differing form chlorophylls only in missing the central magnesium ion, are present in many reaction centres to help to mediate the electron transfer (10).

1.1.2 Light phase and dark phase

First part in the chain of reactions is the light phase, and at the very beginning an absorbed photon excites an electron. The excited electronic state may evolve in many different ways. Depending on the state, the fastest processes are vibrational relaxations, bringing the electron to the lowest vibrational state of the electronic state. Next, if the excited electronic state is a higher excited state, it relaxes into the lowest allowed excited electronic state (in case of (B)Chls it is the S_1 state). (10)

From this point, the de-excitation pathways vary. The excited state may undergo a fluorescence decay, a relaxation into its ground state while emitting a photon. Another option is the intersystem crossing (ISC) where the spin of the electron flips and now the relaxation into the ground state is spin-forbidden. Internal conversion is another way an excited state may decay, transforming the energy of the excited electron into thermal energy and vibrations. Leaving all these unwanted processes behind, the energy of the excited electron (called exciton) is needed to be transferred to other pigment molecules in order for photosynthesis to work. An energy gradient of the excited states directs the exciton to reaction centres where the excited electron separates completely from its host molecule, ionising a so-called special pair – two chlorophyll molecules. This ionised electron is no longer in risk of losing the energy on a nanosecond timescale like the exciton while it continues the electron transport chain. However, the lost electron in the reaction centre needs to be replaced. Therefore, an electron donor is necessary to fill the electron holes in reaction centres. In oxygenic photosynthesis, this is the role of water, providing electrons and being oxidised into pure oxygen. Anoxygenic photosynthesis utilises different electron donors (see section 1.1.3). (10)

In the end, the separated electron is carried from the reaction centre via pigments in the centres structure to electron transporters and then to enzymes producing NADPH, a hydrogenated form of NADP (nicotinamide adenine dinucleotide). Along the transport chain, proton gradient over photosynthetic membrane (in plants it is the thylakoid membrane, in bacteria it is the plasma membrane) is created. The proton gradient is processed by ATP-synthase creating ATP (adenosine triphosphate). These two molecules enter the second step, the dark phase. (10)

In the dark phase, NADPH and ATP help to reduce carbon dioxide into saccharides in a series of steps called the Calvin cycle or its alternatives. A part of the process runs similar to glycolysis, only backwards and with the use of different enzymes, while the rest of the cycle is needed to regenerate the original reactants. These reactions are the most efficient part of photosynthesis, reaching the efficiency of approximately 90 %. However, the overall efficiency of photosynthesis is below 30 % because of other processes like non-photochemical quenching and photorespiration. (10)

1.1.3 Bacterial photosynthesis

Photosynthesis in bacteria is almost as old as life itself. However, that does not mean the processes are simple or even fully understood. There are several types of photosynthetic bacteria, divided into groups of purple or green bacteria, sulphur or non-sulphur bacteria. Each of these groups of bacteria utilises a different apparatus to achieve the single goal of creating macroergic molecules. The main difference from oxygenic photosynthesis in plants, cyanobacteria, and algae is in the ultimate electron donor used – instead of taking electrons (and protons) from water, they utilise various other electron donors like hydrogen sulphide or elemental sulphur in case of sulphur bacteria, or e.g. hydrogen molecules or lactate in case of non-sulphur bacteria (22). Also, while plants and algae use specialised organelles for the harvesting of light, bacteria do not have any special compartments and therefore photosynthesis has to take place on the plasma membrane (except for cyanobacteria). Some bacteria possess specialised parts of the membrane for photosynthesis, so-called chromatophores (23) or membrane invaginations of various shapes (10). This creates an interface between two separated parts of the cell and therefore allows for transmembrane processes generating electrical and concentration gradients to be generated, which can be converted into macroergic molecules.

Instead of Chl molecules, bacteria use BChl molecules which are adapted for longer wavelengths reflecting their usual habitats. These may include for example seabed or pond bottoms (i.e. short wavelength light is either scattered before reaching the bottom or absorbed by other organisms like algae floating on the surface) and other aquatic habitats. (21)

In this thesis, parts of green bacteria are used and studied.

1.1.3.1 Green bacteria

Green bacteria contain mostly BChl *c*, *d*, *e*, or potentially *f* (24) with some minor amounts of carotenoids and BChl *a*. The BChl *a* present in green bacteria serves two functions – it is a pigment aiding the transfer from BChl *c*, *d*, *e* to reaction centres and a small amount serves as the reaction-centre pigment itself. The light-harvesting is performed mainly by the BChl *c*, *d*, *e* in specialised structures called chlorosomes. There are three bacterial phyla with members containing chlorosomes: the green sulphur bacteria, the green filamentous bacteria (formerly known as green non-sulphur bacteria), and acidobacteria. (10)

1.1.3.1.1 Chlorosomes

Chlorosomes are the largest photosynthetic antenna discovered so far. They are unique in several ways. The first remarkable feature is the amount of pigments partaking in light harvesting. Every chlorosome contains thousands of bacteriochlorophyll molecules. In contrast, eukaryotic antennas contain no more than 100 chlorophylls. Being a thousand times richer in pigments, the chlorosome is well equipped for low-light conditions. (10) Apart from bacteriochlorophylls, chlorosomes contain a significant amount of carotenoids – between 4 and 30 % of the pigment content, depending on the species and the light conditions. ((25), (26))

An unusual feature of chlorosomes interior is the lack of protein scaffold. Antennas of other photosynthetic organisms require a specific protein structure in order to grant efficient performance to their host – the orientation and distances between pigments are fine-tuned to its optimum. However, there are no proteins inside chlorosomes holding the bacteriochlorophyll pigments. The light-harvesting is conducted by aggregates of bacteriochlorophylls resembling a lipid multilayer, a stack of lamellae that are organised spontaneously into shapes reminiscent of concentric cylinders ((27), (28)). The large structure of bacteriochlorophylls displays a significant red shift in the

Q_y absorption band due to strong excitonic interactions between the molecules. The red shifts are similarly large as those observed in J-aggregates, although there is no band-narrowing observed. ((10), (29))

Strong excitonic coupling is observed in structures called J-aggregates. In those, transition dipole moments of individual molecules align in a way that the aggregated super-structure has a combined dipole moment larger than the individual molecule. The interactions result in excitonic splitting of energy levels; if two molecules are interacting, then there are two available transitions, one red-shifted and the other blue-shifted. However, these two states possess different symmetries and therefore, only one of them is allowed. In J-aggregates, only the transition to the red-most shifted level is allowed. In so-called H-aggregates, the transition to the blue-shifted level is allowed. The peaks of J-aggregates are often distinctly narrowed in comparison to the bands of monomers.

However, in chlorosomes, there are many molecules interacting and the resulting Q_y absorption band of BChl aggregates is a sum of a large number of variously shifted peaks that result from various numbers of molecules interacting together. Moreover, chlorosomes usually contain multiple homologs of bacteriochlorophyll, leading to more structural disorder and broadening the absorption band even more. This is desirable as the absorption can take place over a wider spectral range. (29) As a result of excitonic interactions, the excitation tends to be delocalised over multiple BChl molecules and allows for the excitation energy to travel extremely fast throughout the chlorosome interior, the energy transfer times being on the order of tens of fs. (30)

The only proteins in chlorosomes are in the lipid-like monolayer encasing the aggregate. The role of some of them is structural (31), but in the region of the envelope called baseplate, there are pigment-protein complexes containing BChl *a*. The baseplate has two major functions. First, it attaches the chlorosome to the photosynthetic membrane. Second, the BChl *a* transfers the energy captured by the chlorosome towards reaction centres (via other complexes). Without the baseplate, the exciton would travel randomly throughout the chlorosome, albeit at an immense speed. The BChl *a* in baseplate forms an energy trap for the exciton and siphons the energy from the aggregate on the order of 10-100 ps depending on the bacterium species ((32), (33), (34)). Without the baseplate, the energy transfer from chlorosomes to the next link in the exciton transfer chain would take nanoseconds. (29)

1.1.3.1.2 Green sulphur bacteria

After the absorption in chlorosomes, the exciton travels to the baseplate which absorbs at approximately 795 nm. From there, the exciton is passed to the FMO protein complex, a BChl *a* containing trimeric protein. The FMO protein absorbs around 810 nm, which makes it an ideal acceptor of excitation energy from the baseplate. From the FMO, the exciton is then transferred to the core antenna and the reaction centre P840 (indicating the protein complex has an absorption maximum at 840 nm). All the parts except for the chlorosome interior are utilising BChl *a*. (29)

In the reaction centre, a special pair of two BChl *a* molecules accepts the exciton and an electron separates from this pair. This positive charge hole is filled by an electron from an adjacent cytochrome *c* reactivating the reaction centre. Meanwhile, the separated electron travels through a series of transient acceptors (chlorophyll *a*, quinone, Fe-S protein) to ferredoxin, an electron transporter. This electron transport then follows one of the two following paths. One, it can recombine with the ionised cytochrome *c* and close the lap. This is called a cyclic electron flow and is typical for photosynthesis in stress situations where not enough reducing agents are available (35). Two, it can travel to an enzyme called Ferredoxin-NAD^+ reductase (FNR, EC 1.18.1.3) at the outer side of the plasma membrane and help to reduce an oxidised NAD^+ to NADH, a macroergic molecule. The reaction centre working with the iron-sulphur protein transporters is called Type I reaction centre, named after its similarity to the green-plant reaction centre of photosystem I. ((29), (36))

The green sulphur bacteria are strictly anaerobic, employing mechanisms quenching the excited states in presence of oxygen to prevent oxidative damage. Chlorosomes and BChl *c* from the green sulphur bacterium *Chlorobaculum* (*Cb*.) *tepidum* were used in this work.

1.1.3.1.3 Green filamentous bacteria

The exciton energy transfer in green filamentous bacteria is fairly similar to the transfer in green sulphur bacteria. From the baseplate of the chlorosomes, the exciton is transferred directly to the core antenna of the reaction centre (called B806-866) without the help of FMO proteins. This energy transfer step is efficient due to the large spectral overlap between the 795 nm absorption of the baseplate and the B806 bacteriochlorophylls of the core antenna. The reaction centre is further red-shifted,

with the primary donor absorbing around 870 nm, and is called P870. From this point on, the processes are rather different. ((29), (8))

First, there are no iron-sulphur proteins like in the type I reaction centres. Green filamentous bacteria possess type II reaction centres (similar to green-plant photosystem II) and the energy transport is conducted by bacteriochlorophyll, bacteriopheophytin and quinones. The reduction of the special pair in the reaction centre is performed by a different kind of cytochrome *c*. The reduced quinones (quinols) travel through the membrane to a so-called Alternative Complex III (37), where the electrons are thought to be transferred to a water-soluble auracyanin (38) directing the electron towards a reaction centre, where it reduces the local cytochrome *c*. This cytochrome can then reduce the special pair. ((29), (8))

During the electron transport (in all photosynthesis), protons are pumped through the membrane. This leads to a proton gradient that can be processed by the ATP-synthase into ATP, another macroergic molecule. (21)

Chloroflexus (*Cf.*) *aurantiacus* belongs to this group and their chlorosomes are used in this work.

1.1.4 Carotenoids in photosynthesis

A surplus of 1100 carotenoids has been identified as of December 2019 (39). Out of this number, approximately 150 have been identified in photosynthetic organisms (29). They function as light-harvesting pigments, absorbing at wavelengths where chlorophylls do not. For some organisms, this extension of absorption spectrum is vital: they live below other photosynthetic organisms absorbing the standard chlorophyll spectrum. However, carotenoids in photosynthetic organisms are essential also for another reason. They provide photo-protection to the light-harvesting complexes in case of too strong light. (21)

Some light-harvesting antennas and reaction centres can be assembled in living organisms without any carotenoids (provided a mutation to make them carotenoid-less is introduced), but they will not survive long in their natural environments. This is due to almost omnipresent oxygen that is toxic to most photosynthetic organisms. Carotenoids provide a mechanism to cope with the toxicity of oxygen. That is why they are present in all photosynthetic organisms. Experiments on purple bacteria ((40),

(41)) (and other photosynthetic organisms (42)) were performed to prove the essential role of carotenoid protection in photosynthesis, the strains without carotenoids or with carotenoids containing low number of conjugated bonds were quickly killed under semi-aerobic conditions. (21)

When (B)Chls get excited, one of the decay pathways is intersystem crossing (ISC). Under high intensity light, the reaction centres are not capable of processing all the absorbed energy, which results in excited electrons staying longer in the antenna chlorophylls. The longer the (B)Chl molecule stays excited, the higher is the probability of ISC. This pathway generates an excited triplet state that can decay by phosphorescence or by interacting with another molecule. Since phosphorescence is a forbidden transition (electron spin needs to flip during the relaxation), those excited states are long lived (microseconds to seconds), and therefore the probability of an interaction with another molecule is increased. If that molecule happens to be oxygen (which is triplet in its ground state and its excited singlet energy level lies lower than (B)Chl triplet, allowing for a triplet-triplet energy transfer), a highly reactive species called singlet oxygen is generated. ((20), (21))

Singlet oxygen is a strong oxidising agent that can damage and destroy biomolecules. To prevent its generation, carotenoids accept triplet excitations from (B)Chls. In carotenoids that are typically present in photosynthetic complexes, the triplet state has a lower energy than the singlet state of oxygen, therefore carotenoids cannot populate it. In order for the (B)Chl triplet quenching by carotenoids to be efficient, carotenoids need to be in the vicinity of (B)Chls. For this reason, carotenoids are present in antennas and reaction centres alike. Once the triplet energy is transferred to a carotenoid, it can safely dissipate to heat. Carotenoids can also accept excitation energy directly from singlet oxygen itself. ((20), (21))

Quenching of BChl triplet states occurs also in the interior of chlorosomes, where no protein scaffold holds carotenoids and BChls together. (43)

Another known role of carotenoids is the regulation of light harvesting efficiency. In most plants, the photosynthesis apparatus can get saturated quickly under relatively low light intensity; then additional excitation is harmful. Plants have evolved a series of mechanisms collectively known as non-photochemical quenching where carotenoids are also important. Probably the best known so far is the xanthophyll cycle,

where carotenoids are switching between two states, violaxanthin with higher energy excited states and low quenching activity (for low-light conditions) and zeaxanthin with lower energy excited states and high quenching activity (for high-light conditions). Under high-light conditions, Chl *a* is quenched intensively in its singlet state to avoid over-excitation. One of the hypotheses proposes that this is due to the lowest excited state of zeaxanthin having a lower energy than the excited state of Chl *a*, while the first excited level of violaxanthin is higher, and therefore it is possible to enable and disable the energy transfer. ((44), (20)) Other mechanisms of xanthophyll cycle photoprotection have also been described (45).

1.2 Organic solar technology

While photosynthesis is the nature's way of getting energy, so far, humans have been using mostly fossil fuels. With the growth in world's population and a rising demand for energy in everyday lives, the energy consumption will continue to grow in the coming years. Therefore, other energy sources need to be found in order to meet the growing demand while fossil fuels reserve is thinning and in order to find alternatives that are less harmful to our environment and climate. An apparent solution is at hand, since nature has been using photosynthesis to generate huge amounts of energy. Thus, devices converting solar energy into electricity are in development. ((46), (47))

So far, there are three generations of solar cells. Crystalline silicon is used in the first generation, while the second generation includes e.g. thin film solar cells composed of amorphous silicon, CdTe, and copper indium gallium (di)selenide (CIGS). The third generation focuses on design of organic solar cells (OSC), dye-sensitised solar cells (DSSC), and quantum dot solar cells. While the first and second generation are most common nowadays in practical applications, they suffer from various drawbacks, namely: high energy requirements for manufacturing, scarcity of rare elements used for manufacturing, and difficult recycling of the solar cells itself and the compounds used in manufacturing. ((46), (47)) To tackle these issues, OSCs and DSSCs use parts that are inspired by photosynthesis in terms of environmental non-toxicity, flexibility, high power conversion efficiency, natural availability, and are promising see-through power-generating windows. ((46), (48))

The idea of using highly absorbing sensitisers to capture light is already well implemented in DSSCs. There are reports of such solar cells reaching an overall

efficiency of more than 10 % using ruthenium based dyes ((49), (50), (51)). Although these types of solar cells are much less demanding on manufacturing costs, these ruthenium dyes still possess the same disadvantages such as high cost, complex synthesis and global resource limitations of ruthenium ((46)). Therefore, there have been attempts to prepare DSSCs using natural dyes. Those attempts used various pigments extracted from fruits, flowers, or leaves which makes them much more available than dyes based on much scarcer ruthenium. However, the efficiency of such solar cells was lower, mostly below 1 % ((46)). In order to achieve efficiency above 10 %, synthetic dyes are currently needed, although some synthetic dyes have helped to achieve this feat without any rare metals ((52), (53)).

In DSSC technology, the electrolyte solution allowing for charge recombination lowers the efficiency. The selection of proper electrolyte in DSSCs is currently an issue because there appears to be a trade-off between evaporation and corrosion versus ionic conductivity. Also, the DSSCs are very limited in the semiconductor thickness, so far to the micrometre scale. (46)

Since the natural pigments started being tested for more sustainable alternatives to ruthenium dyes, the field has been extended to include photosynthetic complexes as sensitisers. This presents two main problems before such a sensitiser can be used. First, the photosynthetic complexes that collect and convert photons into electrons need to be isolated and the freed electrons need to be directed into an electrical circuit. Second, the oxidised photosynthetic complexes need to be reduced back into neutral states by the electrons returning from the circuit. An illustration of this happening is seen in Figure 5. (46)

In order to solve those problems, one needs to immobilise the photosynthetic complex on the surface of the electrode in a desirable orientation, find a cost-effective and rapid electron donor to reduce the oxidised complex and design a mechanism of transfer the electrons back from the counter-electrode to the electron donor. (46)

There are several reports of multiple photosynthetic complexes being immobilised on the electrode surface, including reaction centres (RC) of purple bacteria, complexes of photosystem I and II (PSI and PSII) from plants and cyanobacteria, or whole thylakoid membranes with the combination of both PSI and PSII, as reviewed in (46). Each of

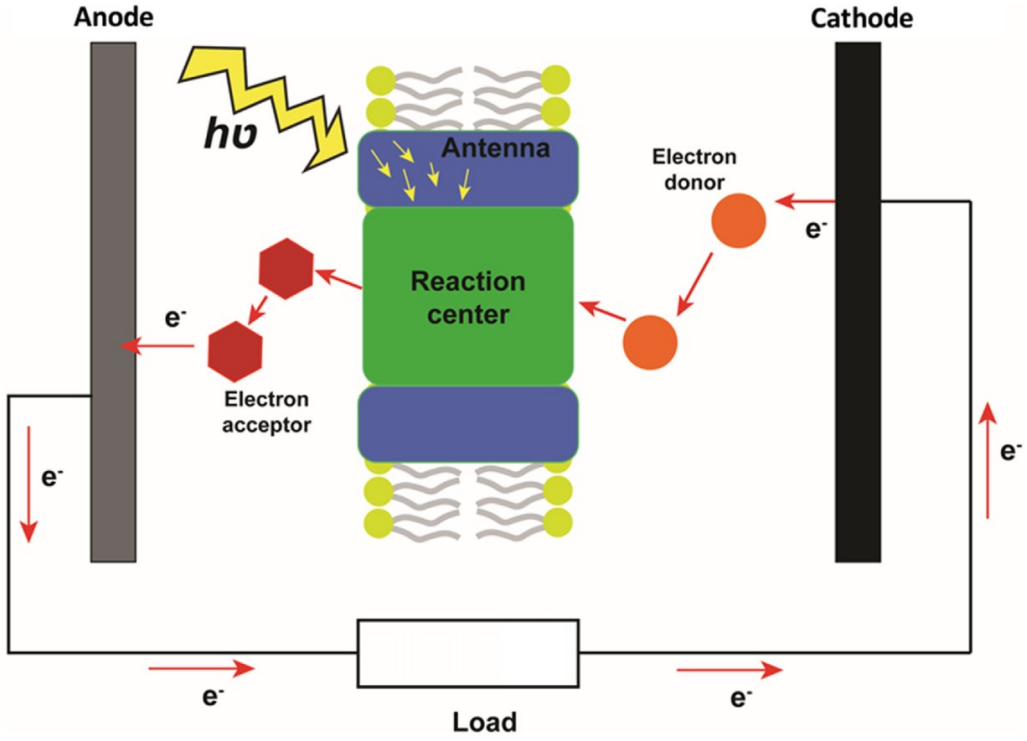

Figure 5: The principle of operation of a general biohybrid solar cell. A photosynthetic complex inside a lipid bilayer is used as sensitiser. The electron acceptor and donor can be either free in solvent (as depicted), or the photosynthetic complex can be firmly attached to the electrode(s). Image taken from (46).

those complexes has certain advantages and disadvantages. RC of purple bacteria are the smallest known complexes to perform light-induced charge separation, allowing for immobilisation of more RCs on the electrode surface. Also, those RCs are relatively easy to extract from the bacteria, making them readily available to studies ((54), (46)). The advantage of PSII as a sensitiser lies with its high redox potential in an oxidised state (higher than both the RC of purple bacteria and PSI) and with the oxygen evolving complex that is retained after isolation. Therefore, PSII can use water as the electron donor even in solar cells. However, it is less stable in vitro (46). Finally, whole thylakoid membranes combine the advantages of both PSI and PSII. Moreover, the complexes are more stable in their native environment of a thylakoid lipid membrane. The drawbacks are, however, the excess of parts that are inactive in the absorption processes, such as lipids, which lower the absorbance of the sensitiser. (46)

For a solar cell based on photosynthetic elements to be efficient, the photosynthetic complexes need to absorb strongly in as broad a spectrum as possible (in the visible

region), be firmly anchored to the substrate of the electrode, the resistance between the photosynthetic complex and electrode needs to be minimal, avoid bleaching and photo-degradation, allow for densely packed deposition on the electrodes, and reduce the charge recombination as much as possible. (46)

Right after efficiency of reactions, one of the biggest problems currently is the low stability and degradation. The natural photosynthetic complexes are very susceptible to damage outside their natural environment which provides a multitude of repair mechanisms. Although there has been progress made in minimising the degradation of sensitisers for DSSCs and OSCs, they still decay gradually and irreversibly, mainly due to oxidation. ((46), (48)) Both of these factors impact the overall energy production equally. While OSCs lasting more than 1000 hours have been reported, those cells have a lower power conversion efficiency. Fortunately, a larger active area seems to lead to a higher stability ((48), (55)).

The biggest advantage of organic photovoltaics (OPV), apart from its environmental friendliness and its necessity to replace the diminishing sources of fossil fuels, is the low cost. Although inorganic solar cells are the leading technology in the current market due to the high power conversion efficiency, the OPV can compete in terms of efficiency per unit cost, manufacturing simplicity, and mechanical flexibility. New materials are being tested now to tackle the current problems of those devices. (56)

The first process in a solar cell is the capture of a photon. One of the ways to improve the efficiency of absorption by these cells is to provide them with a light-harvesting antenna that is efficient and easy to prepare. Aforementioned BChls in chlorosomes tend to organise themselves into aggregated structures spontaneously, creating a working antenna without a protein. ((57), (58)) Owing to this spontaneous aggregation, BChl aggregates have been an inspiration for creating a modified light-harvesting antenna with a broadened absorption spectrum.

1.3 Goals of this thesis

This thesis focuses on the preparation of an artificial light-harvesting antenna with an extended absorption spectrum. This is an important feature, since BChls absorb exclusively in the blue and red region of the visible spectrum, leaving the green and yellow part of the spectrum out. This antenna will be based on the self-aggregation of BChl *c* isolated from chlorosomes of *Cb. tepidum* with additional pigments.

The first goal of this thesis it to prepare an artificial antenna with added β-carotene. Then, the efficiency of excitation energy transfer (EET) from the carotenoid to BChl *c* will be measured (see section 1.3.1).

Another important characteristic is the ability to transfer the absorbed energy to the final acceptor on the outside of the antenna. For this purpose, EET efficiency from BChl *c* to the added BChl *a* will be measured (see section 1.3.2).

Additionally, one of the key characteristics of light-harvesting antennas is their stability. In nature, antennas decay and are re-synthesised by complicated mechanisms, but a working proteosynthetic apparatus is necessary for this. In isolated antennas or antennas artificially created, this proteosynthetic apparatus is missing. Therefore, to ensure longer lifespan of the antenna in vitro, the primary goal is to slow its decay.

One of the main factors responsible for the decay of antennas in nature is oxidative damage (as mentioned in section 1.1.4). Oxidative damage can originate from the triplet states of (B)Chls that are usually quenched by carotenoids. In chlorosomes, yet another mechanism is employed to prevent formation of the triplet states – due to strong excitonic interactions, the aggregated molecules of bacteriochlorophyll have a much shorter fluorescence life-time than monomeric BChl *c* (see sections 2.6.1 and 3.5.1) which reduces the probability of a triplet state formation. Combining these two mechanisms makes the chlorosome resistant to photo-damage.

Therefore, the ability of the artificial aggregates to quench BChl *c* triplet states will be studied (see section 1.3.3).

Additionally, the structure of the individual aggregates will be studied (see section 1.3.4).

Finally, the dipole strength is important for excitation energy transfer efficiency and can indicate the internal organisation inside the aggregates. It is studied in this thesis as well (see section 1.3.5).

1.3.1 EET from β-carotene to BChl *c*

When creating an artificial antenna, additional pigments need to be incorporated to cover the gap in the absorption spectrum of BChl *c* and to increase its efficiency, (see Figure 1). Since β-carotene is known to induce aggregation (59), it will be used to prepare artificial aggregates. Then, using absorption spectroscopy and steady-state

fluorescence spectroscopy, the efficiency of energy transfer from β-carotene to BChl *c* will be determined (see section 2.3). In chlorosomes, the EET efficiency from carotenoids to BChls has been reported to be between 50 and 80 % ((60), (61), (62)). A certain type of artificial aggregates was already measured for the EET efficiency from β-carotene to BChl *c*, reporting a value of approximately 30 % (59).

1.3.2 EET from BChl *c* to BChl *a*

For the application of artificial aggregates in photovoltaics, energy transfer from the aggregate to an acceptor needs to happen. The energy needs to be not only captured, but it also needs to be transferred out of the aggregate. An obvious acceptor for the excitation is BChl *a*, which is normally the acceptor of energy in chlorosomes. However, BChl *a* in chlorosomes is contained in the baseplate bound to a protein. It will be therefore studied whether energy transfer between BChl *c* and BChl *a* can occur also when BChl *a* is added freely into the aggregates, not held by a protein structure.

1.3.3 Quenching of BChl *c* triplet state

Since the absorption from the ground state to the T_1 state is forbidden, a peak corresponding to this transition cannot be seen in the absorption spectrum. However, absorption from T_1 to higher triplet states can occur, albeit only on a timescale of microseconds after the population of the T_1 state, before the state decays. In order to find if there are triplet states of bacteriochlorophyll being formed in the artificial aggregates, transient absorption will be measured using the pump-probe method (also called triplet-minus-singlet spectroscopy or flash photolysis).

1.3.4 Shape and size analysis

To obtain information about the physical properties of the artificial aggregates, their shape and size will be studied using the atomic force microscopy (AFM). The results of this measurement will help to draw conclusions about the suitability of the artificial aggregates for depositions onto substrates in solar cells and the difficulty of such a deposition.

1.3.5 Superradiance

The exciton interactions in BChl aggregates cause not only a red shift, but also a significant shortening of the fluorescence lifetimes and lowering of the fluorescence

quantum yields. Reports of superradiance in photosynthetic antennae have been published for several years now ((63), (64)). Superradiance in light-harvesting antennae is interesting because it can reflect the collective dipole-dipole interactions of pigments inside the aggregate as well as indicate high-efficiency energy transfer ((63), (64)). It is a consequence of a dipole strength larger than that of a monomer. The experiments described in this thesis are performed to shed light on processes inside chlorosomes.

Superradiance is a phenomenon that is observed if the emission intensity of an ensemble of molecules is proportional not to the number of molecules, but to their square (65). This is caused by a coherence in the emission, because the molecules no longer emit photons randomly due to their interactions (Figure 6).

The increased dipole strength in the aggregates makes it easier for the molecule not only to emit radiation (as described in section 2.6), but also to transfer energy from one molecule to another.

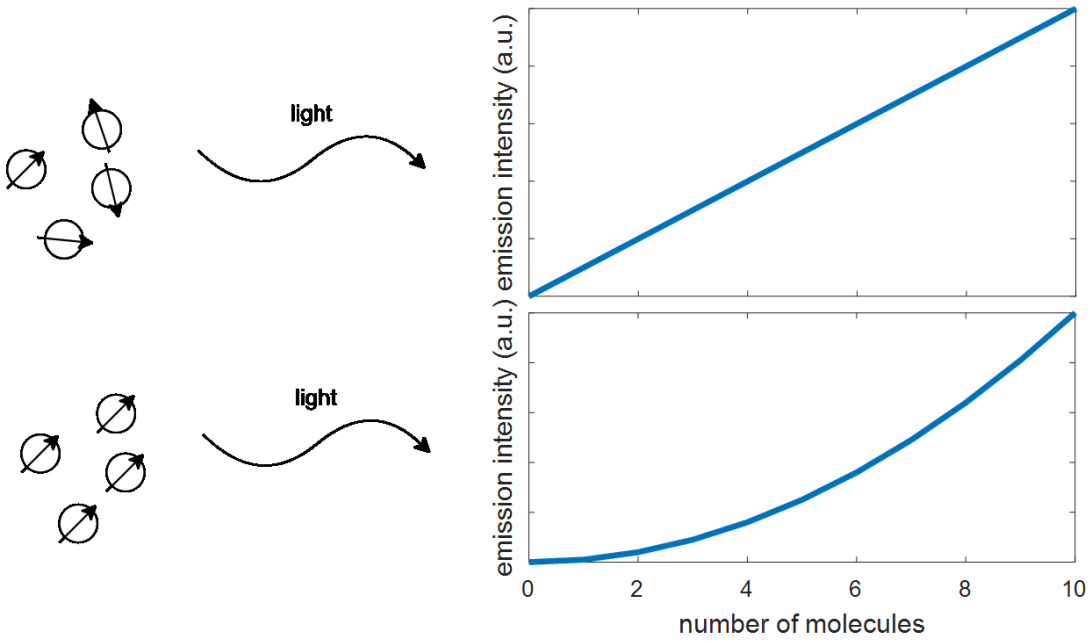

Figure 6: A diagram explaining the nature of superradiance. If the emission dipoles of fluorescing molecules are aligned, the amplitudes of electric field combine in phase, i.e. coherently, resulting in an enhanced emission intensity.

2 Methods

All measurements and preparations were performed at room temperature. The work with dissolved pigments was conducted in dark.

2.1 Isolation of bacteriochlorophyll *c*

High-performance liquid chromatography (HPLC) is a method used in chemistry to analyse or separate components of a mixture. In chromatography in general, the analysed sample is mixed with a solvent (called a mobile phase) which flows through a stationary phase. If the fractions of the mixture interact differently with the mobile and stationary phase, they travel at different speeds and are separated. It is therefore necessary to select a suitable mobile and stationary phases so that the components can be distinguished. The process of separating one component from the other can be based on the different physical (e.g. molecular weight in gel chromatography) or chemical properties (e.g. affinity to the stationary phase in a thin-layer chromatography).

It is common to use a column with alkylated chains inside (acting as the stationary phase) and use a polar mobile phase; this setup is called a reverse phase HPLC. This causes the polar molecules to elute faster than the non-polar molecules; those are slowed down by the interactions with the non-polar stationary phase. After the fractions exit the column, they are analysed, e.g. spectroscopically, and can be identified and collected. A simplified scheme of a HPLC setup is shown in Figure 7.

BChl *c* was isolated from chlorosomes of *Cb. tepidum*, a green sulphur bacterium, as described in (66). The crude pigment extract was provided by Mgr. Martina Matěnová,

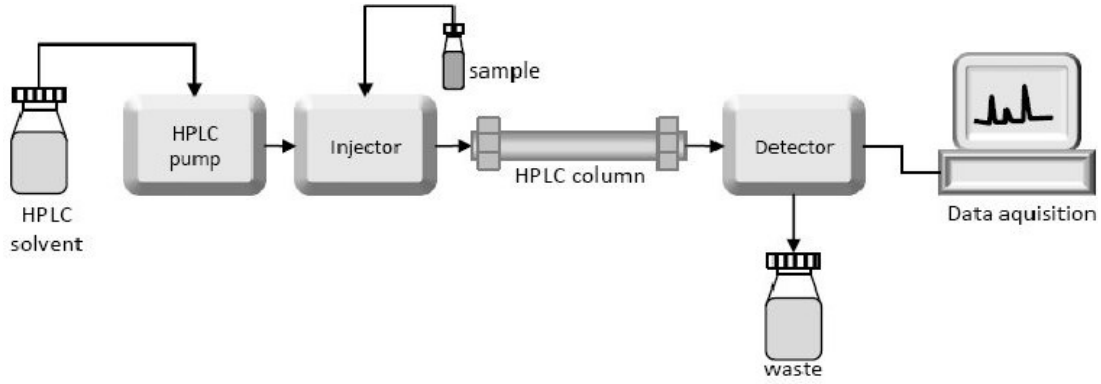

Figure 7: A simplified scheme of HPLC. Image taken from (67).

which was then purified using HPLC (Agilent Eclipse XDB-C18 colon). The four BChl *c* homologs (68) were pooled together, dried in a nitrogen atmosphere and stored at -18°C before use. The pigment decays quickly when dissolved in organic solvents, under light, or exposed to oxygen. Before the preparation of aggregates, the BChl *c* was dissolved in methanol (MeOH) or tetrahydrofuran (THF) for sample preparation.

2.2 Aggregate preparation

Artificial aggregates of BChl *c* can be prepared by multiple methods. Aggregates of BChl *c* were prepared in 20mM tris(hydroxymethyl)aminomethane (further just Tris) buffer stabilised to pH 8.0 by HCl. BChl *c* isolated using HPLC was dissolved either in MeOH (HPLC grade) or THF (spectroscopy grade), depending on the method. Different amounts of β-carotene (Fluka) dissolved in THF (spectroscopy grade) were added to obtain different concentration ratios of the pigments in final aggregates.

After preparation (see below), aggregates were left in the dark at room temperature for a minimum of 24 hours before measurement. This allowed the molecules to stabilise in the aggregated state. After this, samples were stored in the dark at 4°C between measurements to minimise degradation.

To find the concentration of dissolved pigments, absorption measurements were performed and the concentration was calculated using extinction coefficients: BChl *c* 70 $mM^{-1}cm^{-1}$ in MeOH at the Q_y band maximum (69), BChl *a* 68 $mM^{-1}cm^{-1}$ in MeOH at the Q_y band maximum (70), and β-carotene 139 $mM^{-1}cm^{-1}$ in THF at the absorption maximum (71).

2.2.1 Fast-method aggregates

The easier of the two methods is to quickly inject the dissolved pigments into an aqueous buffer and shake vigorously (illustrated in Figure 8). (66) This method is referred to as the fast method. Individual BChls are not hydrophobic enough to form aggregates in an aqueous buffer, therefore it is necessary to add a non-polar agent that induces aggregation. This can be a lipid (e.g. monogalactosyl diglyceride – MGDG, contained in the chlorosome envelope) ((66), (72)), a quinone (vitamin K1 or K2) (73), or a lipophilic pigment – e.g. azulene with a long enough substituted chain ((74), (75))

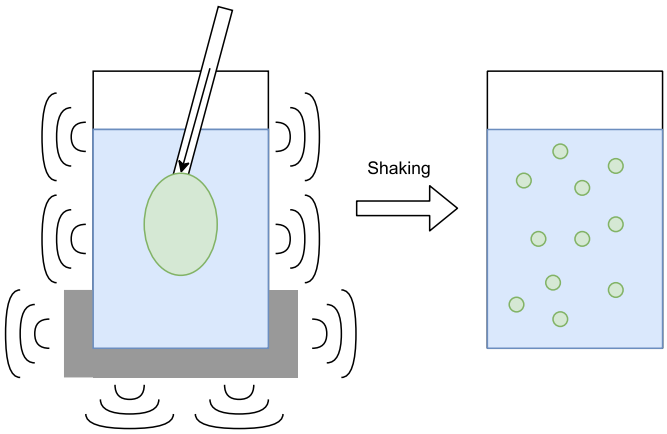

Figure 8: A diagram of preparation of the aggregates by the fast method.

or β-carotene (59). Interestingly, some hydrophobic molecules interact with BChl *c* in some other way than by inducing aggregation, e.g. the carotenoid astaxanthin (76). Aggregates of modified BChls containing a zinc ion instead of magnesium can be prepared by this method as well (72).

First, BChl *c* (and BChl *a* for some aggregates) was dissolved in MeOH and β-carotene in THF and their concentration was determined using absorption measurements. Then the appropriate amounts of pigments were mixed together and this mixture of BChl *c* and β-carotene (and BChl *a* in some cases) was then injected into the buffer as described above. This resulted in formation of aggregates. Aggregates produced by this method exhibit a shift of the Q_y band beyond 715 nm. The tighter are the pigments aggregated, the stronger are the interactions and the more is the Q_y band red-shifted (59). If no aggregation inducing agent is added, BChl *c* tends to form dimers with the Q_y band peaking at approximately 710 nm. The formation of the aggregates was checked spectroscopically according to (59).

2.2.2 Slow-method aggregates

Recently, another method to prepare BChl aggregates was described (77). Instead of injecting the pigments into the buffer, this method used a so-called solvent exchange, a steady change of the solvent from organic to aqueous. BChl *c* is dissolved in a volatile organic solvent (THF) and mixed with a diblock copolymer (PEO-b-PBD - Poly(butadiene(1,2 addition))-block-ethylene oxide) at the molar ratio pigment to co-polymer 13.3:1. This was an optimal ratio; decreasing the amount of the polymer increased the scattering while increasing the amount of the polymer resulted in

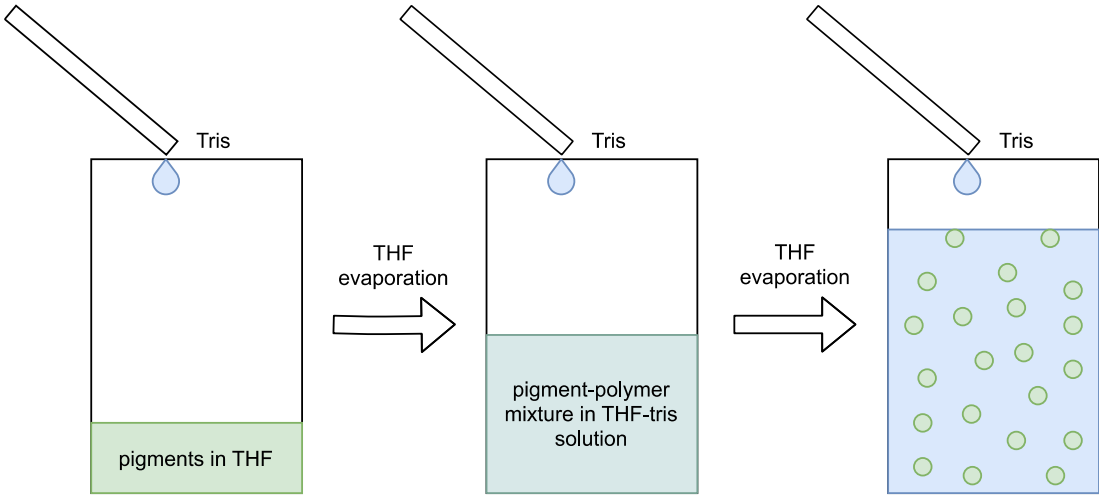

Figure 9: A diagram of preparation of the aggregates by the slow method.

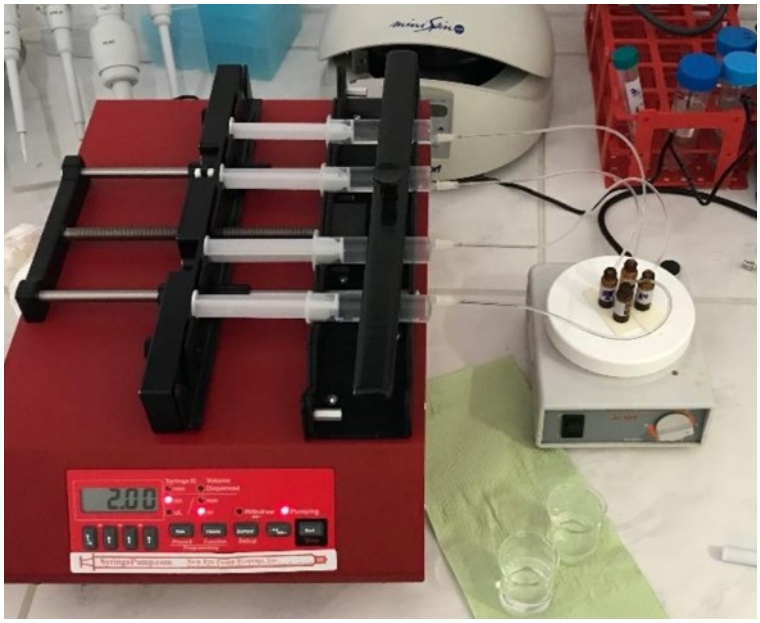

Figure 10: Setup for the preparation of slow-method aggregates using a syringe injector and magnetic stirrer. Samples were protected from light during the preparation.

stronger signal from monomeric BChl *c*. The co-polymer forms a sheath around the aggregate and therefore no other lipophilic aggregation inducing agent is needed (77). The Tris-HCl buffer drips steadily into this mixture from a syringe injector at the rate of 2 ml per hour while the mixture is continuously stirred. In the end, aggregates of BChl *c* enclosed in a co-polymer envelope are formed (illustration in Figure 9). The concentration of BChl *c* in the final solution after infusion was 15 µM. This method is referred to as the slow method.

Due to a fast degradation of the pigments in polar solvents, especially THF, the BChls (*c* and *a*) were usually dissolved in methanol first to determine the concentration of the base solution using absorption measurements. Appropriate amounts were then transferred into preparation vials together with other needed pigments and dried and sealed, and they were re-dissolved in THF right before preparation.

Using this method, BChl *c* molecules aggregate spontaneously even when no co-polymer is added. However, such aggregates exhibit very low absorbance and are not stable.

The first measurements of absorbance showed significantly different red-shifts of the aggregates of BChl *c* with β-carotene depending on the method of preparation. The Q_y band of the slow-method aggregates peaks at approximately 745 nm, while fast-method aggregates are much less red-shifted and peak at approximately 725 nm.

2.3 Measurements for determining EET efficiency

Excitation energy transfer efficiency was measured at the laboratories of Department of chemical physics and optics at the Faculty of Mathematics and physics, Charles University and at the Faculty of Science, University of South Bohemia. Quartz cuvettes by Hellma (1 mm and 10 mm path length) were used to hold the samples.

2.3.1 Steady state absorption measurements

The setup at the Charles University consisted of a dual-beam absorption spectrometer Specord 250 by Analytik Jena operated by WinASPECT software, while the setup at the University of South Bohemia consisted of a single beam spectrometer Shimadzu UV-1800. For a comparison with the fluorescence excitation spectra (see section 3.1), absorbance curve was recalculated into $1-T$ spectrum, where T is transmittance. $1-T$ is proportional to the number of absorbed photons and is related to the absorbance spectrum by $1-10^{-A}$ where A is the measured absorbance.

Data were exported to ASCII, analysed in Matlab, and compared with the fluorescence excitation spectra.

Most of the time, an integrating sphere had to be used due to the scattering nature of all aggregates. Many additional methods to compensate for the scattering have been undertaken, since the integrating sphere available at our lab was a small one where the sample is only attached from the outside instead of being placed inside. This

contributed to the fact that the scattering contribution was not completely removed by the integrating sphere. Other methods have been therefore devised.

First method that was tested was a simple measurement of the sample at different distances from the detector, resulting in different amounts of scattering in the detected spectrum. By subtracting these two measurements, a scattering spectrum was obtained. By multiplying this measured scattering spectrum by an appropriate constant and then subtracting it from the scattering-burdened absorption spectrum, absorption spectrum with a significantly reduced scattering error was obtained. The drawback of this method is the factor of arbitrariness introduced by the "appropriate" constant. Since the aggregates scatter light even at the longest wavelength measured by the absorption spectrometer (1100 nm), one cannot determine the correct amount of scattering to be subtracted with certainty.

Another method was based on Kramers-Kronig relations (also known as the Hilbert transform) linking an absorption spectrum to the specific scattering spectrum, as presented in (78). When the scattering spectrum was obtained (as mentioned in the paragraph above), it consisted of a specific and non-specific contribution. The non-specific scattering is the Rayleigh scattering, while the Hilbert transform of the specific scattering leads to the correct absorption spectrum. It was therefore attempted to separate the two components of the scattering spectrum by fitting – the measured absorption spectrum (which included scattering) was iteratively fitted by two components. The first component was the measured scattering spectrum where only the amplitude was varied. The second component was the Hilbert transform of the specific scattering. The specific scattering was unknown, but it was guessed by an algorithm based on the fact that the specific scattering and the non-specific Rayleigh scattering have to add up to form the full scattering spectrum. Therefore, the scattering itself was fitted by two functions, Rayleigh scattering and the remainder (the presumed specific scattering) in a way that best fits the measured absorption spectrum, i.e. the measured scattering and the Hilbert transform of the presumed specific scatter. By iterating over multiple steps the fit gets better and the estimate of the true absorption spectrum (and true specific scattering spectrum) is reached. However, since the Hilbert transform is in effect composed of Fourier transforms, the edges of the spectra get seriously distorted. In the end, this method provided a reasonably good estimate of the absorption spectrum only in the middle region (green part of the spectrum) where there

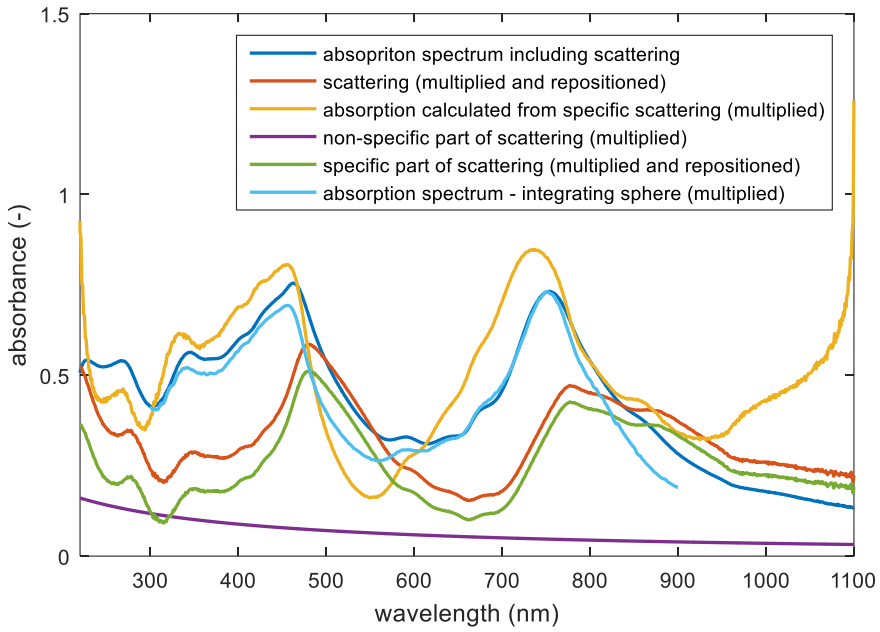

Figure 11: The resulting absorption spectrum (orange) calculated from the estimated specific scattering (green). Combining the non-specific scattering (purple), the specific scattering (green) and the calculated absorbance (orange) results in an approximate fit of the measured absorption (blue). An absorption spectrum as measured with an integrating sphere is shown for comparison (cyan). Some curves are multiplied and repositioned along the y-axis for better visuals (e.g. the specific scattering has a negative contribution at some points).

is almost no signal, while the edges (blue end – Soret band and red end – Q_y band) were affected. For this method to work, a long sequence of buffer points would be needed at the ends of the measured spectra, which was not possible (especially at the blue end of the spectrum) due to measurement limitations of the setup (see Figure 11). The calculations were done on the $1-T$ spectra and then converted to absorbance after finishing.

The calculated absorption in Figure 11 is obviously overestimated at the red end of the spectrum, but this happens surprisingly early, some 300 nm before the longest measured wavelength. Although it is probable that the measured spectrum is shifted towards red (as demonstrated by the attempted removal of the scattering), this result is worse than if a simple subtraction of the measured scattering is done.

However, because both of those methods included steps involving subtraction of spectra multiplied by an arbitrary constant in order to get at least reasonably good results (which were not always guaranteed either), it was decided to measure the absorption spectra using the integrating sphere for consistency. The results were not optimal either way. However, the use of the integrating sphere guaranteed reproducibility.

2.3.2 Fluorescence excitation spectra measurements

In fluorescence excitation measurements, fluorescence is detected at a fixed wavelength. Typically, this is the far-red end of the fluorescence spectrum. The excitation wavelength is scanned through. Therefore, the intensity of fluorescence is directly proportional to the rate of absorption at the excitation wavelength and the conversion efficiency of the absorbed light into fluorescence (known as a quantum yield), since not all absorbed photons are emitted as fluorescence. Other factors such as wavelength dependence of the intensity of the excitation source or wavelength dependence of the detection sensitivity are compensated for by the internal correction of the spectrofluorometer.

At the Charles University, measurements of fluorescence excitation spectra were performed on a Fluoromax 2 spectrofluorometer (Horiba) with a single emission monochromator. The fluorescence was detected in a right-angle geometry. A 715 nm long-pass filter (RG9) was used to supress the scattered excitation light (stray-light) and the second order of the excitation wavelength coming through the monochromators.

The setup at the University of South Bohemia consisted of Fluorolog 322 spectrofluorometer (Horiba) with a double emission monochromator for a better suppression of the stray-light. The fluorescence was again detected in a right-angle geometry and the same 715 nm long-pass filter was used.

2.3.3 Fluorescence emission spectra measurements

To measure the spectral profile of the fluorescence intensity, emission measurements were performed. Here, the sample is being excited at a fixed wavelength while the emission wavelength is scanned through. This allows to resolve the bands of the fluorescence spectrum.

The spectra were measured at the University of South Bohemia with the same setup as for fluorescence excitation measurements. The samples were excited at 450 nm where the absorbance of BChl *a* is minimal and the fluorescence was detected in a right-angle geometry and no filter was used.

2.4 Quenching of BChl triplet states

2.4.1 Transient absorption spectroscopy principle

In transient absorption spectroscopy, there are usually two pulses used. The First pulse, the pump, is a strong flash of light tuned to a frequency corresponding to the energy difference between the ground and excited levels of the same multiplicity (singlet-singlet or triplet-triplet). For BChl *c*, the ground state is singlet so this is a singlet-singlet transition at the Q_y band (S_0 to S_1 transition) or the Soret band (S_0 to S_3 or S_4 transition). This pulse populates the excited states and after a short period of time (typically less than a few picoseconds), most of the excited electrons are at the zeroth vibrational level of the S_1 state. At this point, some of the electrons in the S_1 state may undergo an ISC, creating a population in the T_1 state. In a longer period of time (for aggregated BChl *c* it is still below a nanosecond), the excited singlet states will all have either decayed or transferred the energy into the T_1 state. A second pulse is sent into the sample at defined delays before and after the pump pulse. It is called a probe pulse and has a much weaker intensity and a broad-spectrum (in this case a xenon lamp flash). Its purpose is to sample the electron occupancy of all the states. If the electrons are missing in the ground state (because they are in an excited state), the absorption is weaker than without the pump. Also, if the excited T_1 state is occupied, there might be a non-zero absorption from this state to higher states of the same multiplicity. One therefore observes absorption peaks at frequencies that showed no absorption before the pump. By applying the probe light at defined delays relatively to the pump pulse, one can obtain the population and decay curve of the excited states. From this curve, an exponential fitting can yield the lifetime of this state.

2.4.2 Transient absorption measurement setup

The setup for this measurement consists of an optical parametric oscillator (PG122, EKSPLA), pumped by a Q-switched Nd:YAG laser (NL303G/TH, EKSPLA). The pump intensity was set between 400-600 μJ by neutral density filters and the excitation wavelength was 740 nm. The probe light was provided by a xenon flash lamp (LS-

1130-1 Flashpack with an FX-1161 flashtube, Perkin Elmer). Two light-paths were recorded on an iCCD camera (PI-MAX 512RB, Roper Scientific) with a 2ns gate, the probe signal and the reference. Imaging spectrometer (iHR 320, Horiba Jobin Yvon) with a 100 gr/mm grating blazed at 450 nm was used before the iCCD camera. The resulting spectra were for each time delay averaged from 1000 measurement cycles and binning was used to sum all pixels corresponding to the same wavelength. A programmable timing generator (PTG, Roper Scientific) and a delay generator (DG535, Stanford Research Systems) were used to adjust the time delays between the pump pulse, probe light and the detection gate of the iCCD camera. Glass cuvettes by Hellma (10 mM path length) were used to hold the sample.

The probe light was operated at double the frequency of the pump pulse. This allowed to measure the absorption spectrum with and without the pump pulse. By subtracting those two spectra, the transient absorption spectrum was obtained.

Prior to each measurement, the spectrum of the pump pulse was recorded with a time-step of 0.5 ns to establish the time zero. The FWHM (full-width at half-maximum) of the IRF (instrument response function) was ~3 ns.

Steady-state absorption spectra were measured before and after transient absorption measurements to ensure no photo-bleaching occurs during measurement. The difference in absorbance at the Q_y band never exceeded 5 % (which can be attributed to adsorption onto the cuvette walls), therefore very little photo-destruction occurred.

2.4.3 Global analysis

The recorded transient spectra were evaluated by a global analysis. The python script performing this analysis was kindly provided by Jan Alster, Ph.D. The reconvolution fitting estimated a Gaussian profile of the IRF and the optimal IRF width obtained by the fitting was indeed around 3 ns, as measured before the transient absorption measurements. Usually, two lifetime components were used to fit the data.

The results are presented using so-called decay associated spectra (DAS), where each component is expected to have the same lifetime at all wavelengths and is plotted with a spectrum of its amplitude.

2.5 Shape and size analysis

To analyse the shape and size, a few preliminary measurements on an atomic force microscope (AFM) were done. This was done with the help of Anna Fučíková, Ph.D. at the Laboratory of Chemical Physics and Optics, Faculty of Mathematics and Physics, Charles University.

The aggregates were measured on mica. The preparation of the sample consisted of a 5 minutes incubation with the prepared solution of aggregates (15μM BChl *c*) in order to adhere the aggregates to the surface. The excess solution was then removed by a pipette tip, and deionised water was used to wash out the buffer solution. Water was left on the surface for 1 minute and removed with a pipette tip; the washing was done for a total of 3 times. The sample was dried in the end in a vacuum chamber.

The measurement was performed on an Agilent 5500 AFM/SPM Microscope combined with an optical IX73 microscope (Olympus) using ACTA cantilever (APPnano, 300 kHz, 37 Nm^{-1}, Si) in tapping mode with a scanning frequency of 1-2 Hz. Topographs were recorded by Nanowizard 3 (JPK Instruments) with a resolution of 512 × 512 pixels.

2.6 Superradiance measurements

The occurrence of superradiance is conditioned by a larger emitting dipole strength in aggregates than in individual molecules. The radiative rate constant of an electronic transition is determined by the Einstein's equation for spontaneous emission (64)

$$k_{rad} = \frac{16\pi^3}{3\varepsilon_0 hc^3}\frac{n^3}{\varepsilon_r}\nu^3|\mu|^2 \quad (2.1),$$

where *n* is the index of refraction of the closest surroundings of the studied molecule, *v* is the frequency of the transition, $|\mu|^2$ is the dipole strength, and ε_0, ε_r, h, and c are the permittivity of vacuum, dielectric constant, Planck's constant, and speed of light, respectively. The radiative rate constant can be also expressed as the quotient of the quantum yield and the radiative lifetime of this electronic transition

$$k_{rad} = \frac{\phi_{fl}}{\tau_{fl}}.$$

Since these two properties can be measured, the radiative rate constant can be determined in order to assess the dipole strength in eq. 2.1. Assuming the relative permeability in solution is very close to 1, the dielectric constant becomes equal to $\varepsilon_r = n^2$. Substituting this into eq. (2.1) and using $\lambda = \frac{c}{\nu}$ we get

$$|\mu|^2 = \frac{3\varepsilon_0 h}{16\pi^3} \frac{\lambda^3}{n} \frac{\phi_{fl}}{\tau_{fl}} \quad (2.2).$$

The only unknowns in this equation are the radiative lifetime, the quantum yield and the index of refraction. The index of refraction has to correspond to the immediate surroundings of the emitting molecule. For a free pigment in a solution, this is the index of refraction of the solvent. Monomeric BChl *c* was measured in ethanol (n_{EtOH} = 1.36). The refractive index of the Tris-HCl buffer was estimated to be the same as the refractive index of water due to low concentration of added salts and HCl (n_{TRIS} = 1.33). This value also holds for dimers of BChl *c*. However, for aggregates this has to be the index of refraction of the aggregated BChl *c,* since fluorescence may originate from inside of the aggregate. In aggregates inside chlorosomes, this value has been determined as 1.2 (79). I have adopted this value in the calculations for all the aggregates.

The quantum yield and fluorescence lifetime were measured at the Biophysics department at Wageningen University and Research. Two reference dyes have been used to determine the quantum yields, monomeric BChl *c* and HITCI, both dissolved in ethanol. Quartz cuvettes by Hellma (10 mM path length) were used to hold the sample.

2.6.1 Excited state kinetics

To measure the radiative lifetime of samples, a Hamamatsu Photonics streak camera C5680 was used. A spectral image of time- and wavelength-resolved fluorescence was obtained. A spectrograph Chromex 250is with a 50 gr/mm grating blazed at 600 nm was used. The samples were all excited at 400 nm with a Mira 900 laser (Coherent) operating at 800 nm and using a frequency doubler fs OPA-SHG (APE GmbH). The light intensity was modulated with neutral density filters to 50 µW at repetition rate of 253 kHz. The setup is further described in ((80)). Two measurement ranges were

utilised, one with a time span of 160 ps over 1024 pixels, other with a time span of 2.1 ns over 1024 pixels. Spectral resolution was approximately 5 nm.

The data were collected using High Performance Digital Temporal Analyzer 9 (Hamamatsu Photonics) and analysis was performed using GloTarAn (81). First, a sub-region of the measured image was selected to crop the spectrum only to the analysed region with the signal. On this region, a singular value decomposition was computed to determine the number of lifetime components and to get the initial estimate of the lifetime. Then, multi-exponential global fitting was performed. IRF was estimated as a Gaussian curve which provided a satisfactory fit of the leading edge. The FWHM of the IRF was approximately 15 ps for the higher temporal resolution used and 30 ps for the lower resolution.

When possible (i.e. when multiple files were measured for a single sample with exactly the same settings), multiple files were fitted at once resulting in one set of values. When settings changed (i.e. the central wavelength of the spectrometer), the files were fitted separately and the mean lifetimes were calculated.

2.6.2 Quantum yield measurements

To determine the fluorescence quantum yields of the samples, a concentration series was measured for absorbance using Agilent Cary4000 UV-Vis-NIR spectrophotometer with a full integrating sphere and for total fluorescence intensity using Horiba Fluorolog 322 spectrofluorometer, respectively. This series has been compared to a concentration series of a standard dye with a known quantum yield, in this case HITCI in ethanol with quantum yield of 0.283 (82). To cross-reference the precision of the measurements, monomeric BChl *c* with a known quantum yield of 0.21 in ethanol was measured as well (83). The fluorescence intensity was then plotted versus the absorption (absorbed photon-count) at the excitation wavelength and the linear slopes were used for the calculations of the fluorescence quantum yield (84)

$$\phi_x = \phi_{HITCI} \frac{Grad_x}{Grad_{HITCI}} \left(\frac{n_{TRIS}}{n_{EtOH}} \right)^2 \quad (2.3)$$

The subscript *x* denotes the tested sample and *n* is the index of refraction. It was always ensured not to exceed an absorbance value of 0.15 in the peak of the Q_y band (1 cm

path length) in any of the fluorescence measurements, so that reabsorption would not compromise the obtained results.

The aggregates were excited at the blue edge of the Q_y band to avoid the excitation of β-carotene so that there was no loss of excitation by energy transfer between pigments. The excitation wavelength was different for different samples: the fast-method aggregates were excited at 690 nm, slow-method aggregates at 705 nm, HITCI and chlorosomes of *Cb. tepidum* at 700 nm, and chlorosomes of *Cf. aurantiacus* at 710 nm. Since monomers have a much narrower Q_y band and because measurements cannot start closer than approx. 10 nm from the excitation wavelength, they had to be excited into the Soret band at 435 nm. This makes no impact on the measured fluorescence, because relaxation from higher excited singlet levels to the first excited singlet level occurs with a 100% efficiency and is several orders of magnitude faster compared to lifetimes of the S_1 level fluorescence decay.

The data were fitted by the least-squares method and the uncertainties of those fits were (85)

$$S = \frac{\sqrt{\frac{\sum y_i^2 - a\sum y_i - b\sum x_i y_i}{N-2}}}{\sqrt{\sum x_i^2 - \frac{\left(\sum x_i\right)^2}{N}}},$$

where x and y are the absorption and emission intensities, $a + bx$ is the equation of the fitted line, and N is the number of data points.

The overall uncertainty of a dipole strength is combined from the uncertainty of the fit in the quantum yield measurements and the uncertainty of the radiative lifetimes.

2.7 Prepared samples

2.7.1 EET efficiency β-carotene to BChl *c*

For the measurements of EET efficiency between β-carotene and BChl *c*, a series of aggregates with different concentration ratios between BChl *c* and β-carotene was prepared by both preparation methods.

The first batch consisted of slow-method aggregates prepared with a BChl *c* to β-carotene ratio of 1:0 (as a reference), 1:0.1, 1:0.5, and 1:1. Those samples were measured at Charles University.

The second batch consisted of both types of aggregates. For fast-method aggregates, concentration ratios of BChl *c* to β-carotene of 1:0.2, 1:0.4, and 1:0.6 were used along with a sample of dimers (not containing any β-carotene) as a reference. For slow-method aggregates, only concentration ratios of BChl *c* to β-carotene of 1:0 and 1:0.2 were measured. The final concentration of BChl *c* was 15 μmol/l in all samples.

2.7.2 EET efficiency BChl *c* to BChl *a*

Some of the aggregates were prepared with BChl *a* as a final acceptor of the excitation energy. BChl *a* was added to the pigment mixtures before the aggregates were formed. Due to the hydrophobicity of BChl *a*, it is expected that it is included in the structure of aggregates. The molar ratio of BChl *a* to BChl *c* was 0.25:1 or 0.1:1.

Since the fast-method aggregates showed much higher EET efficiencies than the slow-method aggregates (see section 3.2), more samples of this type of aggregates were made. A pair of BChl *c* + β-carotene and BChl *c* + β-carotene + BChl *a* was always prepared to compare the fluorescence. The sample pairs containing BChl *a* were in ratios of BChl *c* to β-carotene to BChl *a* as follows: 1:0.2:0.1, 1:0.2:0.25, 1:0.4:0.25, and 1:0.6:0.25. A sample that would not contain β-carotene was not tested since this method of preparation yields only dimers of BChl *c* when no aggregation-inducing agent is added; only aggregates prepared by this method were measured for EET efficiency.

For slow-aggregates, only two pairs of samples were prepared, the samples containing BChl *a* were in ratios of 1:0:0.25 and 1:0.2:0.25.

A slow-method sample pair in a ratio of 1:0:0.25 without the block co-polymer was also prepared to determine whether the co-polymer envelope has any effect on the EET efficiency between BChl *c* and BChl *a*.

The final concentration of BChl *c* was 15 μmol/l in all samples.

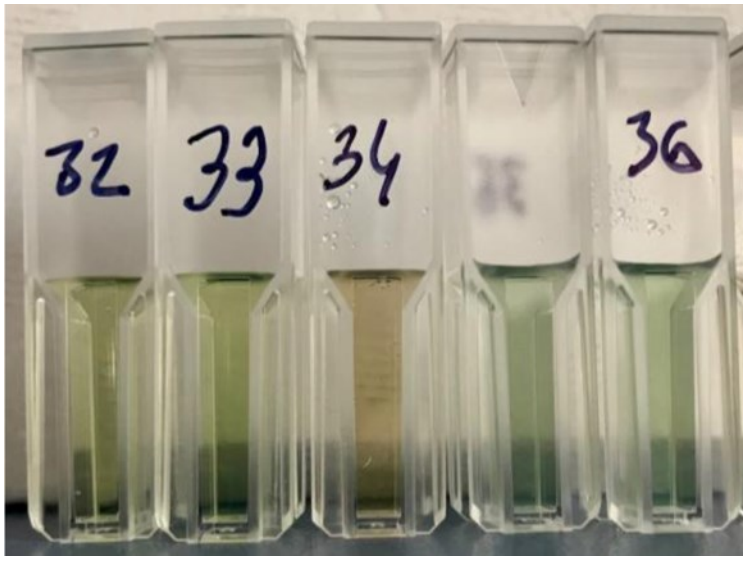

Figure 12: Photo of the prepared slow-method aggregates in a solution containing various amounts of β-carotene, BChl *a* and other pigments. Samples 32 and 33 contain only BChl *c*, 34 contains BChl *c* and β-carotene mixture, 35 and 36 contain BChl *c* and BChl *a*.

2.7.3 Quenching of BChl triplet states

One sample of slow-method aggregates with BChl *c* to β-carotene ratio of 1:0.3 was prepared along with two fast-method aggregates with BChl *c* to β-carotene ratios of 1:0.25 and 1:0.5. The final concentration of BChl *c* was 30 μM for the slow-method aggregates and 15 μM for the fast-method aggregates.

2.7.4 Shape and size analysis

Only one sample prepared by the slow method was visualised using AFM. The ratio of BChl *c* to β-carotene was 1:0.2. The final concentration of BChl *c* was 10 μmol/l.

2.7.5 Superradiance measurements

Samples for measurements of superradiance contained a series of different concentration ratios of BChl *c* to β-carotene. Six samples were prepared with a final concentration of BChl *c* 15 μmol/l by each of the preparation methods. The ratios of BChl *c* to β-carotene were 1:0, 1:0.1, 1:0.2, 1:0.3, 1:0.5, and 1:1. This resulted in 11 samples of aggregates and one sample of dimers (fast method, 1:0). In addition, multiple solutions of monomeric BChl *c* in EtOH and HITCI solutions in EtOH were

prepared as well. All of these solutions were measured for lifetimes and quantum yields.

Apart from artificial aggregates, chlorosomes isolated from two different species of bacteria were measured for comparison; those were chlorosomes of *Cf. aurantiacus* and *Cb. tepidum*. Different sets of each chlorosomes were prepared, under aerobic and anaerobic conditions. The anaerobic samples were prepared by adding sodium dithionite (15 mM final concentration) to the 20mM Tris-HCl buffer and incubated for at least 2 hours in sealed cuvettes. Before measurements, the dithionite level was checked by absorbance measurement at the 300 nm region where the reduced form of dithionite absorbs strongly. The absorption in this region was always saturated, therefore no free oxygen was present in the samples. Excitation quenching occurs in chlorosomes from *Cb. tepidum* at aerobic conditions since they are strictly anaerobic bacteria.

The other set of chlorosomes was prepared using a regular Tris-HCl buffer just like all BChl *c* aggregates and dimers, therefore dissolved oxygen was present in samples.

3 Results and discussion

3.1 Efficiency of EET from β-carotene to BChl *c*

Excitation spectra can be compared with $1-T$ spectra to determine the efficiency of energy transfer between two pigments. When a single emitting molecule is measured for absorption ($1-T$) and fluorescence excitation spectrum, the amplitudes of those two spectra will differ (one shows the number of photons absorbed, the other the number of photons absorbed and then emitted), but the shape of both curves should be exactly the same. Normalising the spectra leads to the curves being identical.

If we have a mixture of two pigments that do not interact (i.e. no transfer of excitation energy occurs), the $1-T$ spectrum has the shape of the absorption of both pigments combined, but the excitation spectrum will bear the shape of the absorption only of the pigment fluorescence of which was measured. However, should there be an energy transfer from one pigment to the other, this would add signal to the excitation spectrum measured at the fluorescence of the second one. Then, the difference between the $1-T$ spectrum and the excitation spectrum would correspond exactly to the number of photons absorbed by this other pigment and not transferred to the pigment measured for fluorescence. Using this logic, the efficiency of the EET can be determined, as long as the fluorescence at the measured wavelength belongs only to one pigment, the final acceptor of the excitation energy. Also, the normalisation of the spectra cannot occur at a random wavelength, but the spectra need to be normalised at a wavelength where only the fluorescing pigment absorbs. In aggregates with β-carotene, this is in the region of the Q_y band. This identical shape of $1-T$ absorption spectra and excitation spectra is shown later in Figure 16.

In aggregates, a minor complication is a shift of the spectrum and change of the absorption coefficient due to the different environment – the energy levels are different for a molecule surrounded by the aggregate and by a solvent. Therefore, aggregates with the added β-carotene have to be compared to the same type of aggregates without any added pigments as a baseline – subtracting the two $1-T$ spectra yields the absorption of all the pigments added into the aggregate, and subtracting the corresponding excitation spectrum from the $1-T$ spectrum of the aggregates with the added pigments yields the absorption of the added pigment not transferring any energy

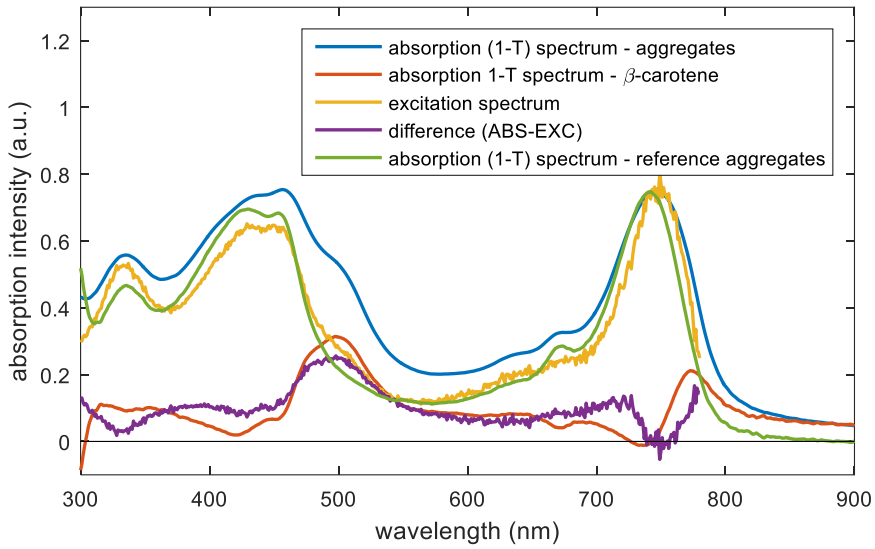

Figure 13: EET from β-carotene in slow-method aggregates (BChl *c* to β-carotene 1:0.2). Subtraction of the excitation spectrum (orange) from the absorption (blue) yields the amount of β-carotene not transferring energy to BChl *c* (purple). The total amount of β-carotene is determined by subtracting the absorption of β-carotene-free aggregates (green, normalised to the amplitude of the blue curve) from the blue curve (orange). Measured at the University of South Bohemia.

to the aggregates. The measured and subtracted spectra for slow-method aggregates (BChl *c* to β-carotene ratio 1:0.2) are shown in Figure 13.

Especially in the fast-method aggregates, the shift of the Q_y band depends on the amount of the added β-carotene, and therefore there will be a discrepancy in the spectrum subtraction at this wavelength. However, the shorter wavelengths are not affected by different amounts of β-carotene. Comparing the amplitudes of the absorption peak of the pigments not transferring energy to BChl *c* with the peak of all the added pigments, one calculates the proportion of the added pigment not transferring any absorbed energy. This was compared at 500 nm which was determined experimentally as a suitable wavelength, the maximum of absorption of β-carotene in aggregates.

Serious problems were caused by the scattering, as mentioned in section 2.3.1. The same scattering problem was encountered during fluorescence measurements. The correction for the excitation spectra was made by measuring silica particles (Ludox, Sigma Aldrich) as a non-fluorescent scattering solution. An optimal case would be a

measurement of the scattering of a solution with the same particle sizes and degree of polydispersity, but Ludox particles are a reasonably close estimate. The excitation spectra of Ludox were measured under the same conditions as the samples and then subtracted from the excitation spectra of samples to yield the best overlap in the Q_y region.

Another problem was caused by the lamp correction in the Fluoromax 2 spectrometer. An old correction file was present and initially was thought to be the source of errors. A new correction file was measured, but no significant improvement in the recorded data was observed. There were still peaks that obviously originated from the excitation lamp but were not corrected for (seen in Figure 14 and Figure 15, orange curve). One of those peaks was often seen exactly in the Q_y band (at 763-765 nm) which made a precise analysis difficult. It is suspected that the motor turning the monochromator grating was loose, turning with a hysteresis.

For some samples, it was possible to measure them on a Fluorolog 332 with a double monochromator at the University of South Bohemia; however, it was not possible for all the samples.

At first, measurements were performed at Charles University. The set of tested samples contained slow-method aggregates and the measurements revealed straight away that the measurements will not lead to any meaningful information. For all tested samples, the amount of β-carotene not transferring excitation to BChl *c* was measured to be larger than the total amount of β-carotene in each sample (see Figure 14). The most likely cause for this nonsensical result is the influence of scattering on the spectra. Moreover, a distinct carotenoid shoulder is seen in the measured excitation spectrum (orange in Figure 14). This clearly indicates that some energy transfer from β-carotene to BChl *c* is happening, therefore non-zero EET efficiency is expected. (The remaining figures for aggregates measured at Charles University are shown in Appendix A, Figures A.1 and A.2.)

Even though a scattering spectrum of Ludox solution was subtracted from the measured excitation spectra (simulating the scattering of artificial BChl *c* aggregates), it was not enough. The spectrofluorometer at Charles University has only a single

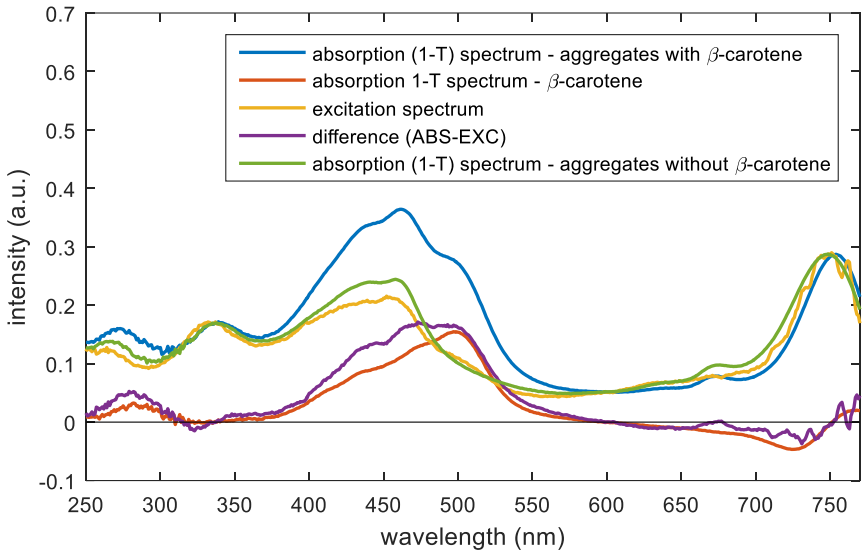

Figure 14: The absorption $(1-T)$ spectrum (blue) and the excitation spectrum (orange) of the slow-method aggregates (BChl *c* to β-carotene ratio 1:0.5) as measured at Charles University. The red curve represents the amount of all β-carotene in the sample (blue curve minus green curve), the purple curve should represent the fraction of β-carotene not transferring excitation energy to BChl *c* aggregates (blue curve minus orange curve). All spectra are normalised to the absorption intensity in the Q_y band. This shows that the setup at Charles University introduces significant errors into the measurements.

monochromator and since the fluorescence intensity of the aggregates is weak (shown in section 3.5), the errors in the recorded fluorescence excitation spectrum are significant. The correction of scattering during absorption measurements by an integrating sphere was not ideal either. A test measurement was then performed on a sample containing no other pigments than BChl *c* (see Figure 15).

The test clearly proves that although the orange line should be identical to the blue line, errors in measurement clearly affect the measured data. Therefore it was decided to measure the emission spectra on a spectrofluorometer with a double monochromator at the collaborating laboratory at the Faculty of Science, University of South Bohemia.

Even though the same test (aggregates with no other pigment than BChl *c*) did not yield two exactly identical spectra by methods of absorption measurement and fluorescence excitation measurement, the spectra are much more alike and tend to differ only in the short-wavelength region where scattering is high (see Figure 16).

Therefore, the measurements at the University of South Bohemia were deemed acceptably accurate for slow-method aggregates. On the other hand, the same test for

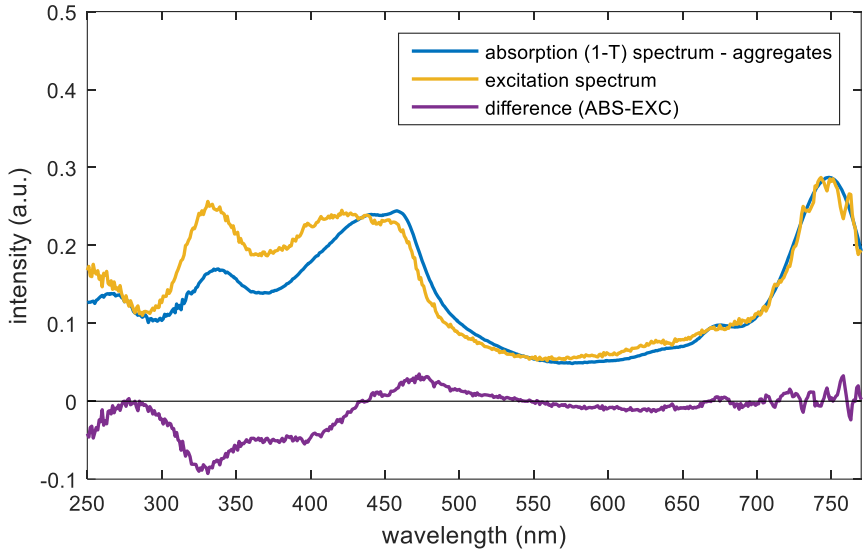

Figure 15: The absorption (1-T) spectrum (blue) with the excitation spectrum (orange) of the slow-method aggregates (BChl *c* to β-carotene ratio 1:0) as measured at Charles University. The purple curve should be a constant zero at all wavelengths. All spectra are normalised to the absorption intensity. This shows that the setup at Charles University introduces significant errors into the measurements.

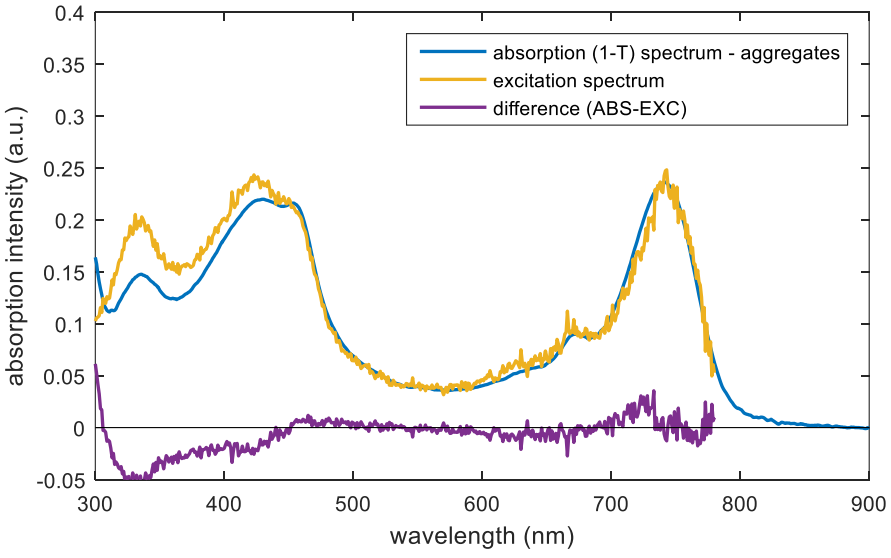

Figure 16: The absorption and excitation spectrum of slow-method aggregates (only BChl *c* and co-polymer) illustrating that no energy is lost by EET between BChl *c* molecules. Measurements performed at the University of South Bohemia.

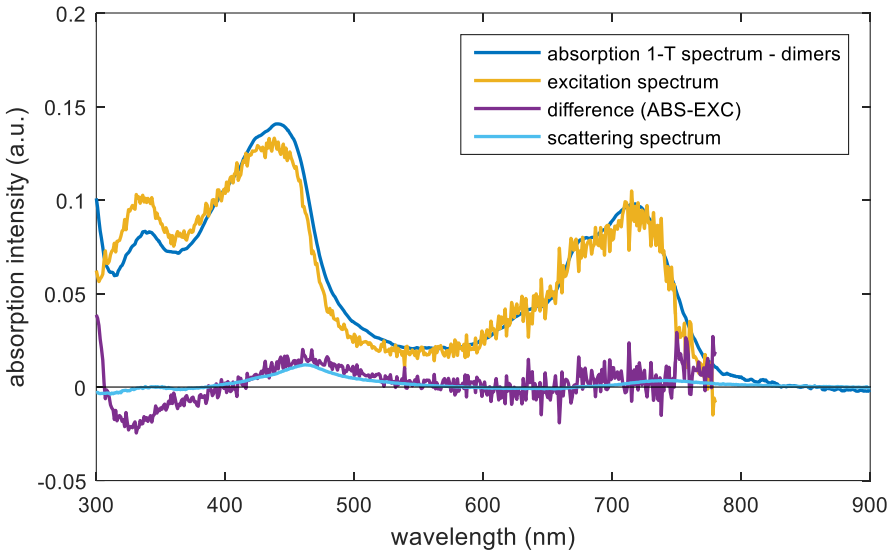

Figure 17: The absorption (1-T) spectrum (blue) with the excitation spectrum (orange) of fast-method aggregates (BChl *c* to β-carotene ratio 1:0) as measured at the University of South Bohemia. The purple curve should be a constant zero at all wavelengths. Scattering spectrum of the sample is shown for comparison (cyan). All spectra are normalised to absorption intensity. This shows that the scattering by this type of samples introduces significant errors into the measurements.

dimers of BChl *c* (the reference for fast-method aggregates containing only BChl *c*) showed that a non-negligible amount of scattering is present even above 500 nm (see Figure 17).

For slow-method aggregates, the absorption $(1-T)$ spectra corresponded well to the excitation spectra, even though some obvious scattering was visible in the blue region. The measured spectra have already been shown in Figure 13. In this concrete example (slow method of preparation, BChl *c* to β-carotene ratio of 1:0.2), the efficiency of EET from β-carotene to BChl *c* was determined to be 20 %.

In measurements of the fast-method aggregates, the excitation spectra seem to be distorted (see Figure 18, Figure 19, and Figure A.3 in Appendix A). The total amount of β-carotene is determined by absorption measurements with a small integrating sphere, therefore this value is considered reasonably accurate (the shape of the $1-T$ spectrum is similar to the one published in (59)), although a full integrating sphere would most likely produce better results. However, it seems that the excitation

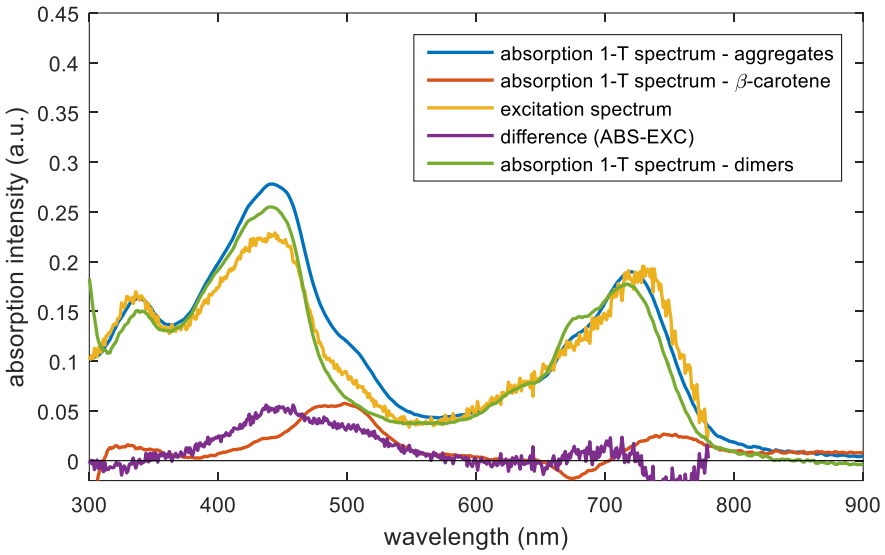

Figure 18: EET from β-carotene in fast-method aggregates (BChl *c* to β-carotene 1:0.2). Subtraction of the excitation spectrum (orange) from the absorption spectrum (blue) yields the amount of β-carotene not transferring energy to BChl *c* (purple). The total amount of β-carotene is determined by subtracting the absorption of β-carotene-free aggregates (normalised to the amplitude of the blue curve) from the blue curve (red).

spectrum is not entirely reliable, since the shape of the spectrum of β-carotene that does not transfer energy to BChl *c* is different. It is somewhat similar to the shape of β-carotene as measured at Charles University in the slow-method aggregates (large intensity at the blue end), which was proven unreliable. Just by comparing these (non-corresponding) spectra of β-carotene, the efficiency of energy transfer was determined at 500 nm to be 40 % for aggregates prepared from BChl *c* to β-carotene ratio 1:0.2, 27 % for 1:0.4, and 26 % for 1:.0.6.

The scattering definitely influences the measured spectra. The purple curve (Figure 18 and Figure 19), corresponding to only the part of β-carotene not transferring energy to BChl *c*, cannot by definition rise above the curve of total β-carotene content in the aggregates. However, in both types of aggregates, it does rise above the theoretical maximum. Also, the shapes of the spectra for total β-carotene content and for the fraction of β-carotene not transferring energy to BChl *c* are different, which they should not. A scattering spectrum of BChl *c* dimers is shown in Figure 17 (cyan curve). It clearly shows that the error in the measured spectra is due to the uncorrected

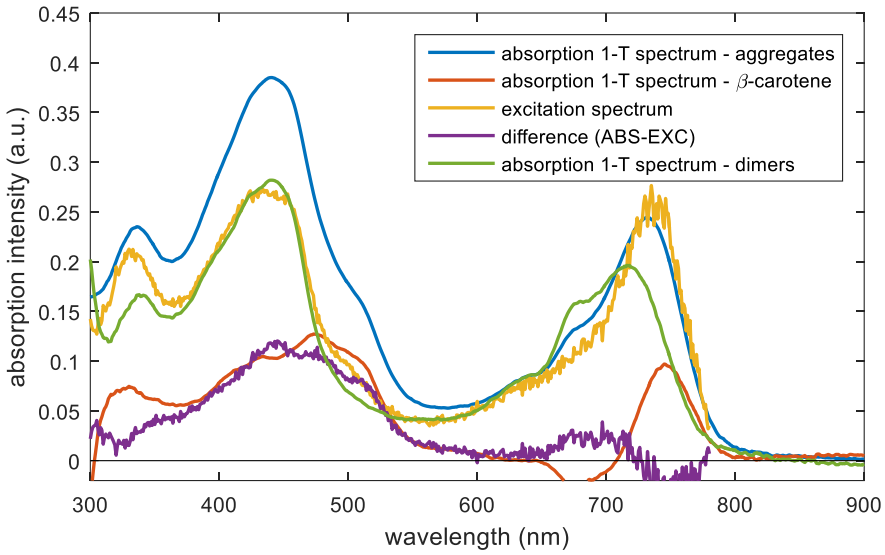

Figure 19: EET from β-carotene in fast-method aggregates (BChl *c* to β-carotene 1:0.2). Subtraction of the excitation spectrum (orange) from the absorption spectrum (blue) yields the amount of β-carotene not transferring energy to BChl *c* (purple). The total amount of β-carotene is determined by subtracting the absorption of β-carotene-free aggregates (normalised to the amplitude of the blue curve) from the blue curve (red).

scattering. Moreover, it seems that the reason why the β-carotene spectra for slow-method aggregates are more accurate is due to increased Rayleigh scattering during the fluorescence excitation measurements, which seem to compensate the specific scattering present in the $1-T$ spectra at the wavelength of β-carotene absorption (Figure 13).

If the scattering was corrected for, the measured EET efficiency would presumably get higher for fast-method aggregates.

Another factor that complicates the evaluation of EET efficiency in the fast-method aggregates is that the reference aggregates (without β-carotene) are not in fact aggregates, but only dimers. Some minor shifts of Soret band are observed when comparing dimers to aggregates with β-carotene. This would introduce some errors in the determination of EET efficiency, estimated to be on the order of 10 %. The EET efficiency would be measured to be seemingly lower if the Soret band of the aggregates shifts towards red. However, the scattering has a larger effect on the measurements.

A related issue of subtracting the dimer spectrum of the wrong amplitude can happen. Unlike the slow-method aggregates, the Q_y band of the fast-method aggregates consists of two peaks that change shape when more β-carotene is added (blue and green curve in Figure 18 and Figure 19). The normalisation of the spectra of aggregates and dimers could not have been done in the Q_y band but rather at a vibration peak of the Q_y band at 635 nm. Since the absorbance is low at this wavelength, there is room for a lot of error. This step directly influences the resulting spectrum of the total amount of β-carotene, therefore influencing the acquired efficiencies. This is another major cause of errors in determining the EET efficiency in the fast-method aggregates.

Both slow-method and fast-method aggregates clearly show EET from β-carotene to BChl *c* as a shoulder at ~500 nm in excitation spectra. The accurate determination of its efficiency is impossible due to the scattering (all aggregates) and the lack of an appropriate reference for the spectrum of the fast-method aggregates without carotenoids.

A full integrating sphere for both the absorption and excitation measurements is necessary for more reliable measurements.

3.2 Efficiency of EET from BChl *c* to BChl *a*

In samples with BChl *a* as the final acceptor of energy, one needs to take a different approach to assess the efficiency of the energy transfer from BChl *c* to BChl *a*. Both of these pigments fluoresce in the red region of the spectrum, therefore, one cannot settle with the assumption that all the energy from the higher-energy molecule is either transferred or dissipated in a non-radiative way. In this case, emission spectra need to be evaluated. Fluorescence intensities of BChl *a* and BChl *c* when both pigments are present were compared to the fluorescence intensity of BChl *c* alone in the aggregates. The decrease in the fluorescence intensity of BChl *c* is assumed to be only due to the interaction with BChl *a*, because BChl *a* is the only added compound.

It is presumed that the shape of the BChl *c* Q_y band does not change with the addition of BChl *a* (this assumption is proven by fitting the BChl *c* and BChl *a* emission bands in Appendix B figures B.1 through B.7). This way, by comparing the intensities of fluorescence at the same wavelength of the BChl *c* Q_y band (at a wavelength where there is no emission from BChl *a*; 750 nm was used) in a sample with and without BChl *a*, the ratio of these values corresponds to the ratio of energy transferred from

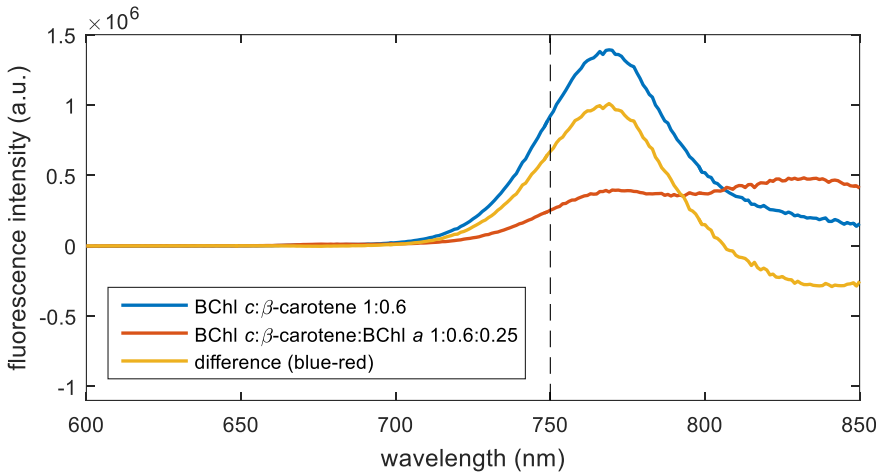

Figure 20: An illustration of how the EET efficiency from BChl *c* to BChl *a* was determined (fast-method aggregates with ratio of BChl *c* to β-carotene 1:0.6). The ratio of the orange (spectrum of aggregates containing BChl *c* and BChl *a* subtracted from the spectrum of aggregates containing no BChl *a*) and blue (spectrum of aggregates containing no BChl *a*) curve gives the EET efficiency (here 73 %). Black vertical line shows wavelength where the amplitude was compared. Spectra are adjusted for slightly different concentrations of BChl *c*.

BChl *c* (illustrated in Figure 20). Both samples need to have the same amount of BChl *c*, which needs to be confirmed spectroscopically or it is necessary to compensate for the difference.

In general, no significant scattering in the emission spectra was observed and therefore the fluorescence spectra are accurate.

The results for all measured aggregates are summarised in Table 1. For fast-method aggregates, the efficiency of energy transfer of 95 % was reached when BChl *c* to BChl a were in a ratio of 1:0.25 (as seen in Figure 21). When the ratio of BChl a was reduced to 1:0.1 (which is closer to the actual ratio in chlorosomes), the efficiency dropped a little, but not substantially, to 88 % (Figure B.10). Adding β-carotene reduced the efficiency more; increasing the BChl *c* to β-carotene ratio from 1:0.2 to 1:0.4 reduced the EET efficiency to 88 % and a further increase to 1:0.6 reduced the efficiency to 73 % (Figure 20). Figures for other measured samples are shown in appendix, Figures B.8 through B.11.

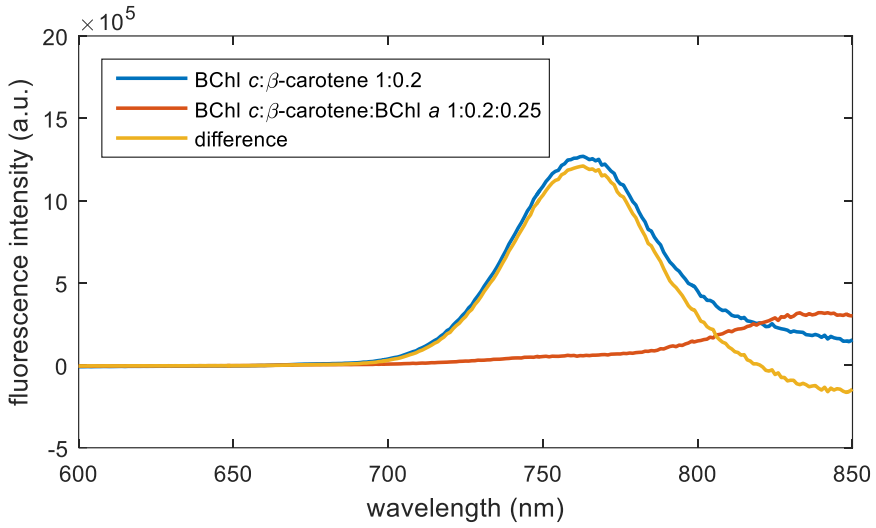

Figure 21: The emission spectra of fast-method aggregates with (red) and without (blue) added BChl *a* and their difference (orange) indicating EET efficiency of 95 %.

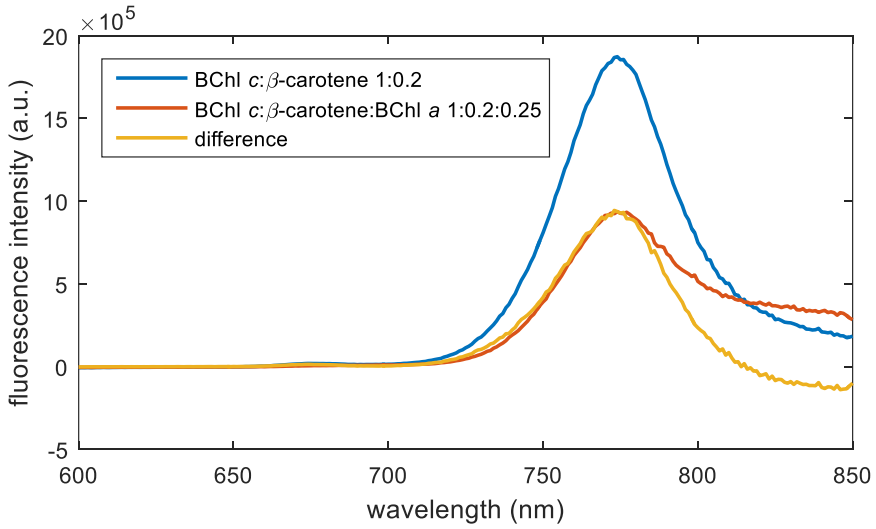

Figure 22: The emission spectra of slow-method aggregates with (red) and without (blue) added BChl *a* and their difference (orange) indicating EET efficiency of 47 %.

Slow-method aggregates yielded less positive results, the EET efficiency did not surpass ²/₃. For a sample with no β-carotene, the efficiency was still 65 %, but adding just a small amount of β-carotene (to the BChl *c* to β-carotene ratio of 1:0.2) reduced the efficiency to 47 % (Figure 22).

It was hypothesised whether the co-polymer in the envelope around the aggregates cannot hinder the EET. However, in two samples prepared by the slow method, differing only in the presence of the co-polymer, the EET efficiency was identically

65 %. Therefore, some other effect lowers the EET efficiency from BChl *c* to BChl *a* in the slow-method aggregates.

One possible explanation could lie in the inherent order and disorder of each type of aggregates due to the preparation procedure itself. During the fast method the formation of aggregates is very random, and upon injection into the buffer aggregates are formed in a disordered manner. Moreover, the aggregates "mature" for approximately a day after preparation, increasing the red shift of the Q_y band indicating further aggregation processes are possible and are in fact happening. On the other hand, the slow-method aggregates take a longer time to organise but once created, no further changes are visible in the absorption spectra. Therefore it is theorised that the slow-method aggregates are more orderly (this is supported by the results in 3.5). This would increase the probability that BChl *a* is not interwoven into the aggregate structure in slow-method aggregates, but rather it may form secluded domains within the structure. Energy transfer would be still possible, but it would be nowhere near as efficient as in fast-method aggregates where there are possibly smaller domains or single molecules of BChl *a* scattered across the structure. This is supported by the decrease in EET efficiency upon including β-carotene (discussed below), which is more pronounce than in fast-method aggregates. Having small localised domains of BChl *a* would extend the time necessary for an exciton to travel from BChl *c* to BChl *a* compared to aggregates where BChl *a* is spread more evenly throughout the whole structure.

Another explanation could be a reverse EET from BChl *a* to BChl *c*. In slow-method aggregates, the energy levels of BChl *c* aggregates are closer to the levels of BChl *a* than in fast-method aggregates. The closer the energy levels are, the more probable is the reverse energy transfer from BChl *a* to BChl *c*. This is expressed by the Boltzmann distribution, where the ratio of the populations of two energy levels depends on the energy difference between those two levels (k – Boltzmann constat, T – temperature):

$$\frac{p_{\mathrm{BChl}\,c}}{p_{\mathrm{BChl}\,a}} = e^{\frac{E_{\mathrm{BChl}\,a} - E_{\mathrm{BChl}\,c}}{\mathrm{k}T}}.$$

The decreased efficiency with the addition of β-carotene in general supports both of these theories. Adding β-carotene can introduce hindrance to the otherwise omnidirectional energy transfer, blocking some directions. The more physical

Table 1: Summary of efficiencies of energy transfer from BChl *c* to BChl *a* and the efficiencies of conversion of the accepted energy into fluorescence.

sample #	preparation method	BChl *c* :β-carotene:Bchl *a*	reference sample #	EET efficiency BChl *c* to BChl *a*
1	slow, with co-polymer	1:0.0:0	-	-
2		1:0.0:0.25	1	65
3		1:0.2:0	-	-
4		1:0.2:0.25	3	47
5	slow, without co-polymer	1:0.0:0	-	-
6		1:0.0:0.25	5	65
7	fast, without co-polymer	1:0.2:0	-	-
8		1:0.2:0.1	7	88
9		1:0.2:0.25	7	95
10		1:0.4:0	-	-
11		1:0.4:0.25	10	88
12		1:0.6:0	-	-
13		1:0.6:0.25	12	73

obstacles (i.e. β-carotene) are added, the lower the EET efficiency, for the pathway to BChl *a* gets longer and the probability of the absorbed energy being radiated by BChl *c* increases. This is supported by the increased fluorescence from BChl *c* in aggregates with higher concentration of β-carotene (red curve in Figure 20 and Figure 21) even though BChl *a* is present. Also, fast-method aggregates with higher β-carotene content have the Q_y band of BChl *c* aggregates more red-shifted (i.e. closer to the energy level of BChl *a*), which could allow for easier reverse EET from BChl *a* to BChl *c* by reducing the energy difference between the two energy levels.

Whether the effects of β-carotene on the EET efficiency from BChl *c* to BChl *a* are purely due to presenting a physical obstacle or whether it is caused by EET from BChl *a* to BChl *c*, that is purely speculative and would need investigation. However, it is a fact that adding β-carotene decreases the otherwise high EET efficiency from BChl *c* to BChl *a*.

3.3 Quenching of BChl *c* triplet states

The data for slow-method aggregates were already published in (43). Here the results are described again and compared to the fast-method aggregates.

Slow-method aggregates showed two lifetime components, 9.5 ns and 1.2 µs (Figure 23). In fast-method aggregates, these lifetimes are slightly different. For BChl *c* to β-

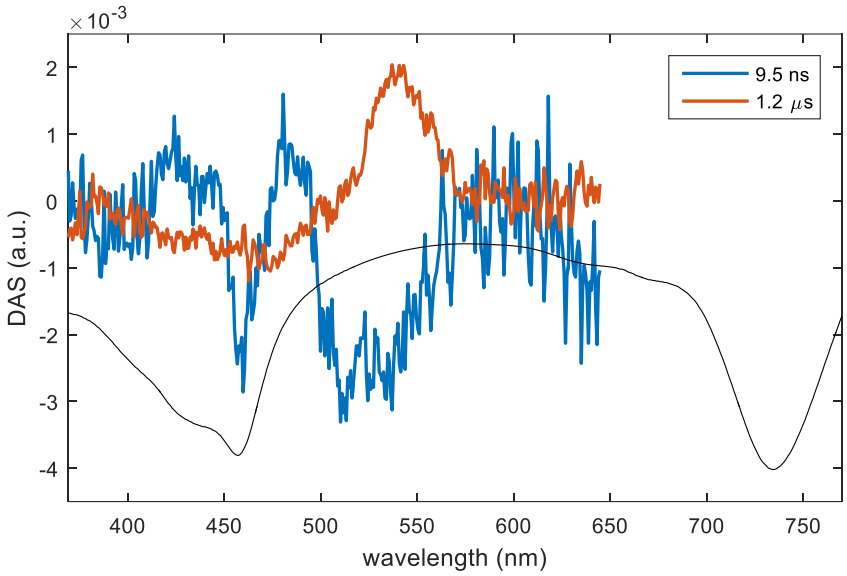

Figure 23: Decay associated spectra (DAS) of slow-method aggregates (BChl *c* to β-carotene ratio 1:0.3) at aerobic conditions. Inverted steady-state absorption spectrum (black line) is displayed for reference.

carotene concentration ratio of 1:0.25 the fast component is 4.4 ns while the slow component amounts to 2.1 µs (Figure 24). For a concentration ratio of 1:0.5, the lifetimes are similar, 4.5 ns and 2.2 µs (Figure 25).

In both types of aggregates, the longer component (red in all three figures) represents the decay of the carotenoid triplet state. The negative peak at around 400-500 nm is the ground-state bleaching (GSB) – a decrease in absorbance due to electrons missing in the S_0 state (therefore not available to be excited to the S_2 or higher states, decreasing the absorbance in that spectral region). Those electrons are in the T_1 state which shows a new absorption band at approximately 540 nm, corresponding to T_1 to T_x transitions and being called excited state absorption (ESA). The shorter component corresponds to the process of formation of these carotenoid triplet states by triplet EET from BChl *c*. As a result, this curve is similar to a mirror image of the β-carotene decay curve. One peak at the wavelength of the Soret band of BChl *c* disrupts this symmetry. Due to its wavelength, it is attributed to the decay of BChl *c*.

It has been found that the formation of β-carotene triplet states is happening with a time constant on the order of nanoseconds. The measured ~4.5ns and 9.5ns

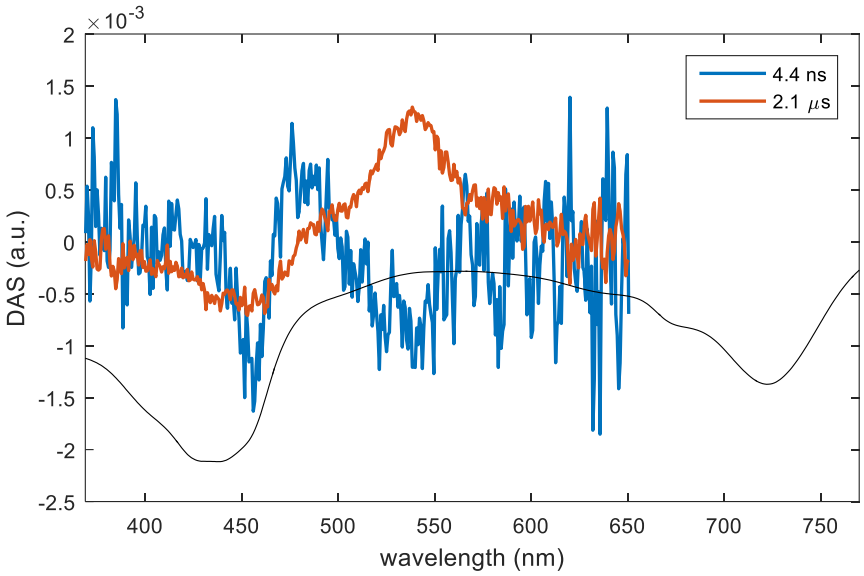

Figure 24: DAS of fast-method aggregates (BChl *c* to β-carotene ratio 1:0.25) at aerobic conditions. Inverted steady-state absorption spectrum (black line) is displayed for reference.

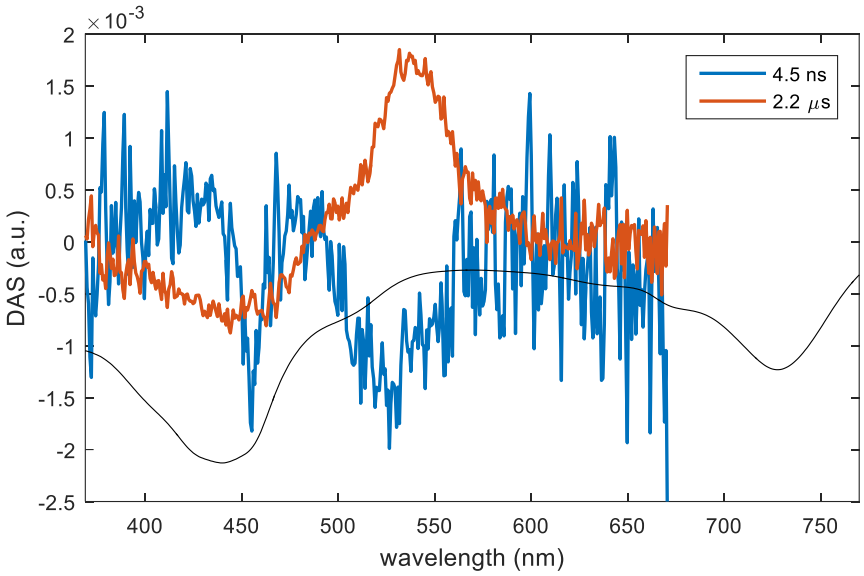

Figure 25: DAS of fast-method aggregates (BChl *c* to β-carotene ratio 1:0.5) at aerobic conditions. Inverted steady-state absorption spectrum (black line) is displayed for reference.

components represent the lifetime of BChl *c* triplet states shortened by the EET to β-carotene. Since the excitation wavelength was at 740 nm, which is below the estimated energy of β-carotene S_1 state at approximately 670 nm (86), the β-carotene triplet state cannot originate from a singlet fission (SF) (87).

The carotenoid triplet states do not originate from ISC as in most molecules, but from triplet energy transfer from (B)Chls. Except for this path, another, much faster mechanism exists (87). The carotenoid S_1 state can be described as a coupled pair of triplet states (88). Decay of this coupling may initiate the fast transition of the S_1 state into T_1 state.

The results show that β-carotene indeed accepts energy from the triplet states of BChl *c*. A time constant of 9.5 ns for the quenching of BChl *c* triplet states of slow-method aggregates is almost two orders of magnitude slower than in some pigment-protein complexes (89), but it is comparable to the triplet quenching rate in chlorosomes, being only two times slower (43). In fast-method aggregates, the time constant of ~4.5 ns is even closer to the rate in chlorosomes. In both chlorosomes and artificial aggregates, another important factor of protection against BChl *c* triplet formation is the shortened excited state lifetime. Both of these mechanism contribute to the fact that the quenching efficiency of BChl *c* seems to approach 100 % (90).

3.4 Shape and size analysis

A sample of slow-method aggregates was measured by AFM, indicating elongated structures of no more than several nanometres long (Figure 26). Artefacts of the probe tip sticking to the surface or formed salt crystals are shown as small circular dots in the image; those are not the aggregates (determined by optical microscopy). Despite the low spatial resolution, the shapes and sizes can be distinguished. Whether or not this is representative of the other aggregates cannot be said at this point, more measurements would be necessary.

The observed aggregates tended to form clusters on the surface. This would be a welcomed property if the clustering happened only on the surface, resulting in richer and denser depositions onto a substrate. However, if the clustering happened before, in a solution, this would be a hindrance to the potential applications.

Precipitation from solution can be influenced by the pH of the buffer. So far, pH 8.0 was used since low pH tends to dissociate the magnesium ion from the chlorin ring (91). A slight adjustment to the pH may be possible – a report shows that BChl *c* aggregates do not instantaneously degrade at low pH (91) – adjusting their surface

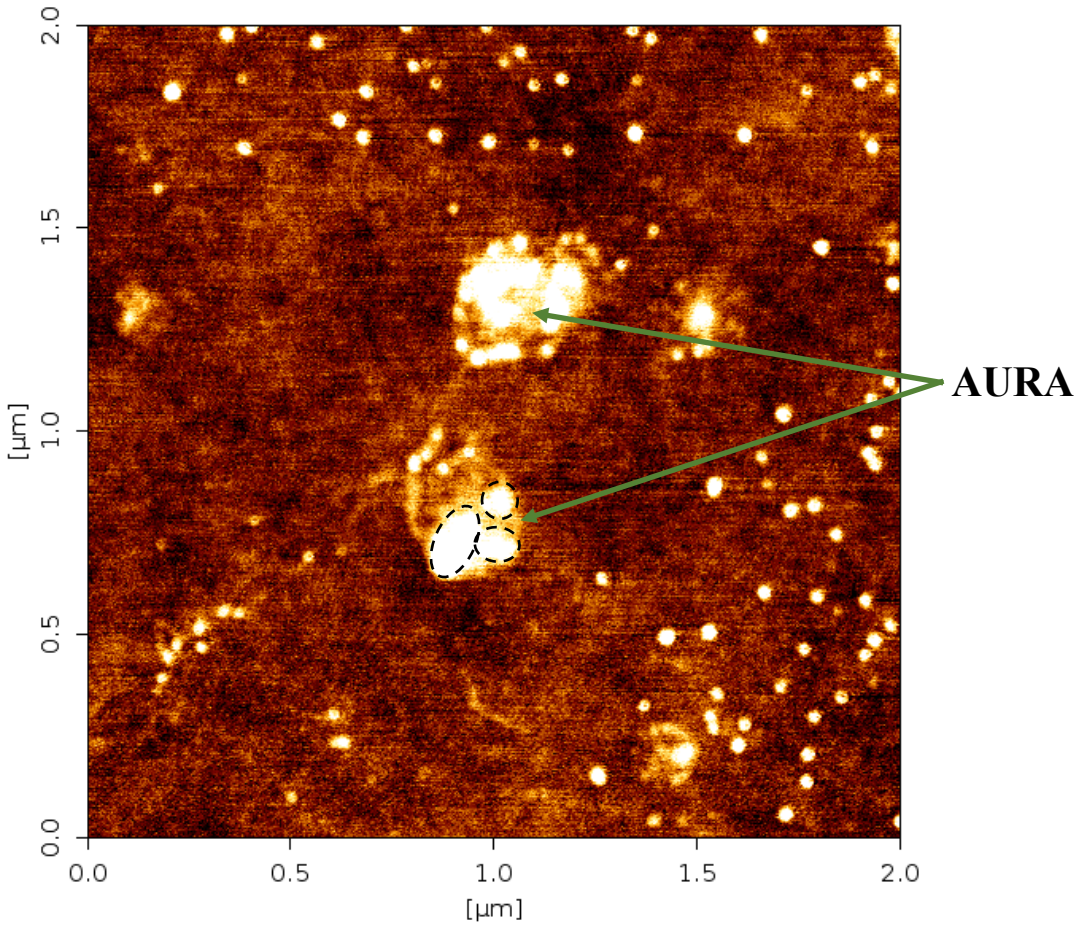

Figure 26: AFM topograph of slow-method aggregates dried on mica surface. The two large structures in the centre seem to be composed of multiple aggregates, each of them elongated as indicated by outlines for the bottom one. It is not certain whether the medium gluing the aggregates together is the leftover buffer salt or whether the pigments are leaking upon drying.

charge (zeta-potential) to a point where the aggregates would electrostatically repel each other. This might also make it easier to attach the aggregates to surfaces if they are charged with the opposite charge.

During the measurements, the probe was constantly sticking to the surface. It is suspected that a hygroscopic layer of leftover buffer salts was covering the whole dried surface. This complicated the measurements and quickly reduced the resolution of the used probe. A new method of sample preparation is therefore necessary for further measurements.

The used method was a result of several trial-and-error procedures, some resulting in no depositions at all and some resulting in a film of indistinguishable dried buffer and aggregates. Nevertheless, a further tweaking of this procedure is necessary.

An optimal solution may be to perform the measurements in a buffer with a submerged tip so that it is known for sure that no film of buffer salts covers the sample. Then, a higher resolution may be achieved. Furthermore, by doing this, it will be possible to find out whether clustering happened due to drying or already prior to that. A better way to ensure a richer deposition of aggregates onto the surface is also necessary – it was difficult to find any aggregates at all on the sample prepared in this way.

Also, an aura around the detected clusters of aggregates is present. It is not known whether this is an error of measurement due to probe tip being covered in buffer salts after a few scans, whether it is just dried buffer, or whether a leakage from the interior of aggregates is observed.

Therefore, further investigation of these samples would be necessary to find out possible leakage and clustering. Also, so far it is unknown whether added pigments (β-carotene or BChl *a*) affect the shape and size of the aggregates.

3.5 Superradiance measurements

3.5.1 Excited state kinetics

The aggregates and dimers show a two-exponential fluorescence decay according to singular value decomposition (SVD). One component is purely positive, corresponding to the observed fluorescence. This component is of a longer lifetime of the two and typically between 20 and 30 ps. The other, shorter lifetime component, is different for the two types of aggregates. An example of recorded spectra is given in Figure 27.

For slow-method aggregates, the second component is purely negative, smaller in amplitude (although not more than 30%), and slightly red-shifted (approx. by 5 nm) as seen in Figure 28. It may be attributed to a relaxation from higher states, probably from the Soret band. It is present in all measured slow-method aggregates in a very similar relative amplitude, therefore it is not related to energy transfer from β-carotene to BChl *c*.

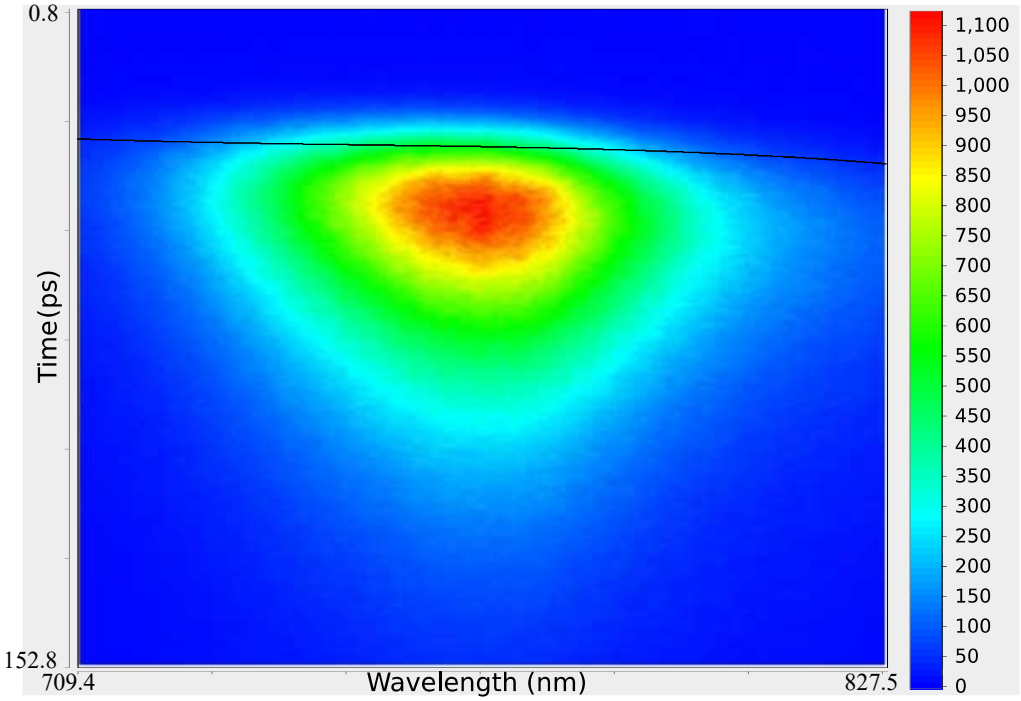

Figure 27: Image from streak camera of the number of photons detected from the slow-method aggregates with BChl *c* to β-carotene ratio 1:0.2. Black curve corresponds to the time-zero curve, it is not a line due to dispersion around central wavelength.

For fast-method aggregates the faster component is positive at the blue end of the spectrum and negative at the red end, pointing at a down-hill excitation energy transfer within the Q_y band – decaying at the blue end relaxing into the red end. This component is approximately half the amplitude of the primary longer component, as seen in Figure 29. Again, the relative amplitude of this component does not change much with addition of β-carotene to the structure, therefore its relation to β-carotene is unlikely. If such a component were to be counted towards a mean lifetime in eq. 2.2, it would only result in a higher dipole strength indicating more superradiance (discussed at the end of this section). The measured lifetimes are shown in Table 2 and are discussed together with quantum yields and dipole strengths in sections 3.5.3 and 3.5.4.

In chlorosomes, two to three significant lifetime components were identified due to the presence of BChl *a* and its fluorescence. In chlorosomes of *Cf. aurantiacus*, three components were identified by SVD. One component represents the emission from BChl *c* aggregates, one emission from BChl *a* in the baseplate, and one component is

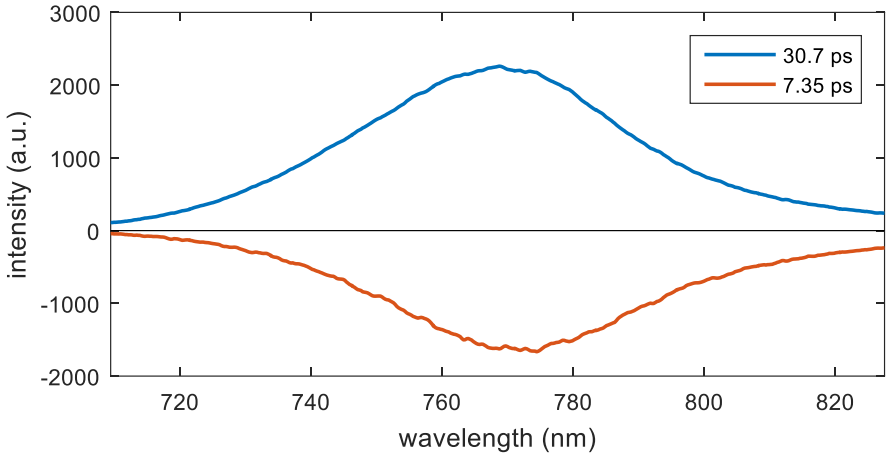

Figure 28: Decay associated spectra for two decay components of slow-method aggregates, BChl *c* to β-carotene ratio 1:0.2.

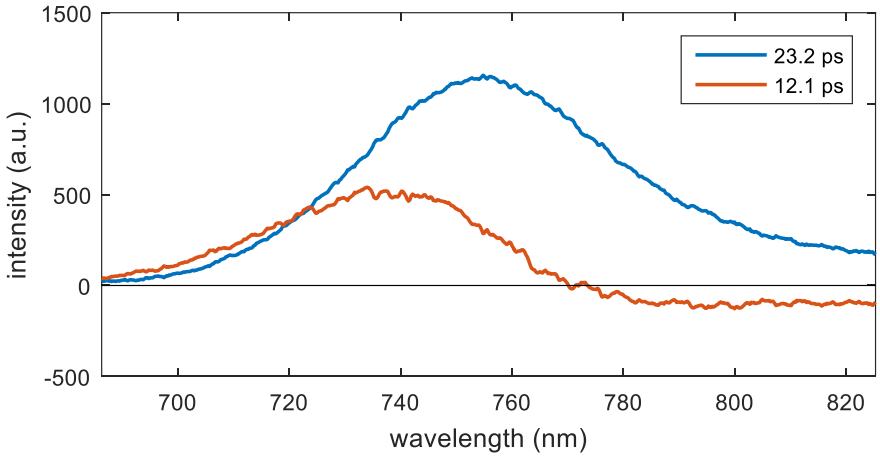

Figure 29: Decay associated spectra for two decay components of fast-method aggregates, BChl *c* to β-carotene ratio 1:0.2.

mostly non-radiative and represents energy transfer within the BChl *c* Q_y manifold, and from BChl *c* to BChl *a*. Under aerobic conditions (Figure 30), the BChl *c* component had a lifetime of 18.4 ps, the BChl *a* 234 ps, and the third component was similar in shape to the one identified in the fast-method aggregates (~8 ps). Under anaerobic conditions (Figure 31), BChl *c* decayed with a lifetime of 25.1 ps, BChl *a* with a lifetime of 462 ps, and the third component was purely negative like in slow-method aggregates (~8 ps).

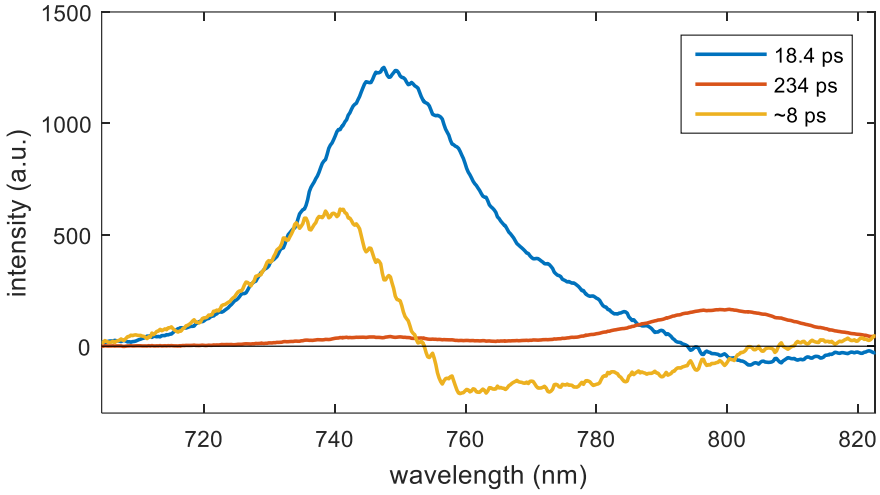

Figure 30: Decay associated spectra for the decay components of *Cf. aurantiacus* chlorosomes, aerobic.

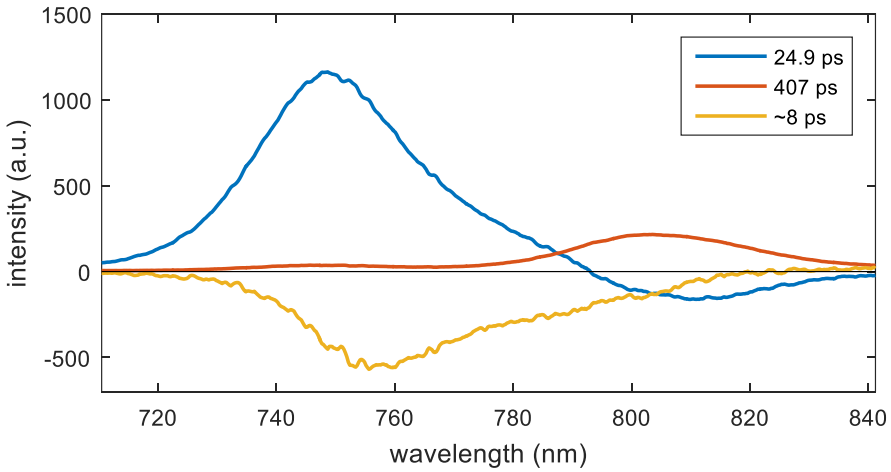

Figure 31: Decay associated spectra for the decay components of *Cf. aurantiacus* chlorosomes, anaerobic.

In chlorosomes of *Cb. tepidum*, the fluorescence intensity was much lower due to a much lower quantum yield, especially under aerobic conditions, where the excitation is quenched. This complicated the fitting of the decay spectrum. Under aerobic conditions, three components were identified in the SVD (although the third one being very weak). However, only in one of three measurements these three components were successfully fitted – in two out of three cases the fitting process by a global analysis collapsed two lifetime components into one. Those files were therefore fitted with only two components, arriving at values similar to those achieved in the first measurement. Lifetimes provided by the first measurements were 22.6 ps (BChl *c*), 25.7 ps (BChl *a*),

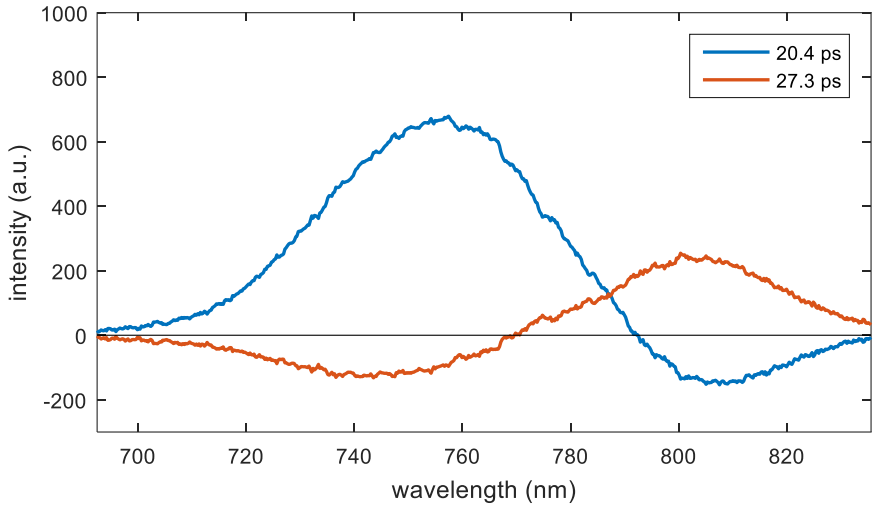

Figure 32: Decay associated spectra for the decay components of *Cb. tepidum* chlorosomes, aerobic.

and ~1.5 ps (low amplitude component similar to the minor component in fast-method aggregates). The other two measurements (Figure 32) yielded lifetimes of 20.4 ps (BChl *c*) and 27.3 ps (BChl *a*). Under anaerobic conditions, the third component was visible in the SVD only in one of the three measurements, so a reasonable contribution by the third component to the overall decay data is arguable at best. Therefore, these data were also fitted with only two components in the end (Figure 33), the best fit yielding the lifetimes of 22.9 ps (BChl *c*) and 41.1 ps (BChl *a*). It is, however, possible that especially the BChl *a* lifetimes are underestimated due to a very weak signal under both aerobic and anaerobic conditions. This is mainly due to the low BChl *a* content, but also the overall quantum yield is low, which makes fitting by multiple components difficult.

In Figure 32, the negative signal of both components is likely an artefact of the fitting. The signal was low, which is visible from the jagged lines. Moreover, the lifetimes of the fitted components do not differ very much, therefore it is highly probable that the negative components are used by the algorithm to compensate for deviations. No energy transfer from BChl *c* to BChl *a* is expected at aerobic conditions. Later in it is argued that reverse EET from BChl *a* to BChl *c* could be happening, but it should be more prominent under anaerobic conditions than under aerobic. In Figure 33, the energy transfers might be possible.

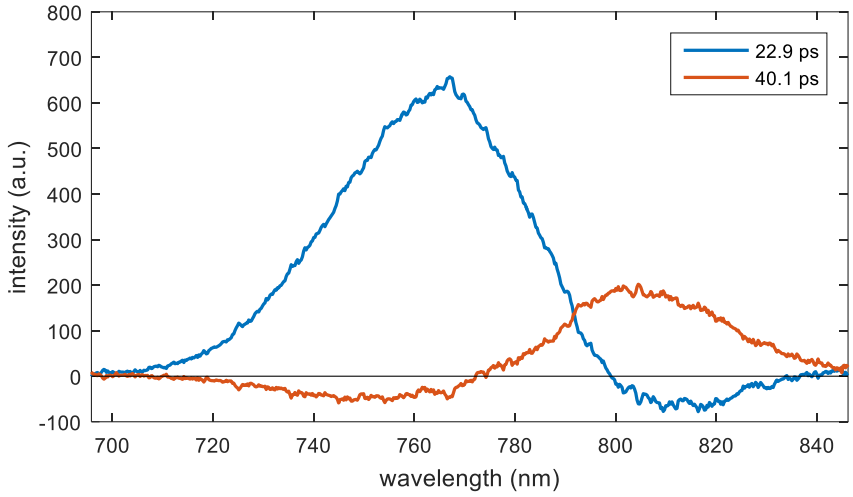

Figure 33: Decay associated spectra for the decay components of *Cb. tepidum* chlorosomes, anaerobic.

In monomers, a spectral relaxation phenomenon similar to that of energy transfer from blue to the red end of the emission spectrum just like in the fast-method aggregates occurs, although with much smaller relative amplitude and much longer lifetime (Figure 34). This further supports the claims that the shorter lifetime components measured in aggregates, which are mostly non-radiative, are related to the internal reorganisation of the excited energy inside BChl *c*. In slow method aggregates, the fact that the curve is purely negative might be related to the decay speed of this component. The components were measured to be around 8 ps, which is the estimated resolution of the setup in the highest resolution settings. Therefore, any faster processes are not determined reliably.

There are other factors that could affect the shorter lifetime component. Solvent relaxation could be happening. The relaxation can take effect on timescales varying between femtoseconds to hundreds of picoseconds ((92), (93)). The shape of the faster component in fast-method aggregates and monomers indicates energy relaxation from lower to higher energies, which is in accord with the solvent relaxation effect. This effect is corroborated by the spectral profile of the streak camera image and the tilted time-zero curve (see Figure 27), clearly showing that the red part of the spectrum starts to relax later. Some of the effects on its tilt result from dispersion, however, an overall trend is visible. The shift towards longer wavelengths at slightly later times could be caused by solvent relaxation.

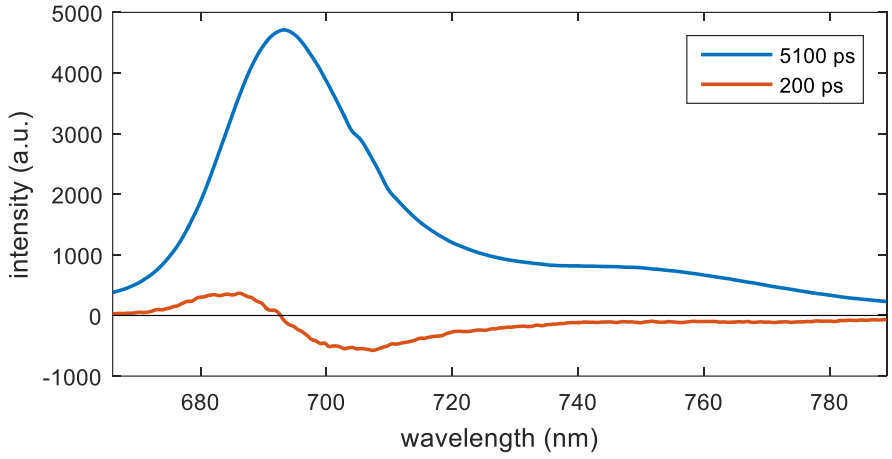

Figure 34: Decay associated spectra for two decay components of monomeric BChl *c*.

This would need to be investigated further to determine which hypothesis is correct. However, it is irrelevant for this measurement. It would be merely an internal relaxation (solvent relaxation or some other internal reorganisation) and in effect would not affect the radiative lifetimes. It would only affect the spectral profile and the time-zero curve, which is being compensated for by the modelled dispersion.

Then, artefacts of the measurement setup could play a role for the apparent decay components, but since the effects are not the same for all measurements, this explanation is also unlikely.

Due to all the reasons listed above, only the longer lifetime components of BChl *c* are counted towards the radiative lifetime. Should the shorter components be included in the calculation, the mean lifetime of the aggregates would be shortened even more compared to monomers; and therefore, the resulting dipole strength would be greater than calculated. Hence, the results of the dipole strength in the aggregates might be underestimated.

3.5.2 Quantum yield

The quantum yields were calculated using equation 2.3 and the measurements showed that both methods of preparation produce significantly different aggregates. All slow-method aggregates have quantum yields at least 3-fold higher than the corresponding aggregates prepared by the fast method.

The resulting quantum yields and lifetimes of all measured aggregates are given in Table 2, as well as the dipole strength calculated using Equation 2.2.

3.5.3 Dipole strength

The indices of refraction were used as follows: for aggregates and chlorosomes 1.2, for dimers (fast method, BChl *c* to β-car ratio of 1:0) 1.33, for monomers 1.36. Reasons for this are explained in section 2.6. The emission maxima are at 777 nm for the slow-method aggregates, 757 nm for the fast-method aggregates 674 nm for monomers, 750 nm for chlorosomes of *Cf. aurantiacus* and 770 nm for chlorosomes of *Cb. tepidum*.

The calculated dipole strengths (Table 2) show that the different methods of preparation create aggregates with different properties not only in terms of a red shift in absorption. The dipole strengths of fast-method aggregates are not substantially

Table 2: Measured quantum yields and lifetimes of artificial BChl *c* aggregates, BChl *c* monomers, and native chlorosomes of *Cb. tepidum* and *Cf. aurantiacus*. τ_1 corresponds to the main radiative lifetime (positive peak in DAS), τ_2 corresponds to the faster lifetime component that has non-radiative properties for the slow-method aggregates and mixed properties for the fast-method aggregates and monomers. The lifetimes of BChl *a* in the baseplate of chlorosomes are not included. The calculated dipole strength is given with a standard deviation.

		Bchlc : Bcar	quantum yield	τ_1 (ps)	τ_2 (ps)	$\lvert\mu\rvert^2$ (D^2)	$\Delta\lvert\mu\rvert^2$ (D^2)
slow method, polymer		1 : 0.0	0.00179	25.2	6.68	88.6	8.9
		1 : 0.1	0.00190	28.3	7.11	83.6	9.1
		1 : 0.2	0.00234	30.7	7.35	94.7	11.2
		1 : 0.3	0.00203	32.4	7.15	78	8.2
		1 : 0.5	0.00226	34.6	7.53	81.4	10.1
		1 : 1.0	0.00228	34.9	8.58	81.3	7.8
fast method, no polymer		1 : 0.0	0.000506	19.9	11.2	26.4	2.9
		1 : 0.1	0.000512	21.2	10.5	27.8	3.3
		1 : 0.2	0.000648	23.2	12.1	32.3	3.1
		1 : 0.3	0.000638	22.2	9.59	33.2	3.8
		1 : 0.5	0.000667	21.9	9.02	35.3	3.9
		1 : 1.0	0.000712	22.2	8.87	37.1	4.1
BChl *c* monomers		1 : 0.0	0.213	5050	~200	31.4	2.9
Cf. aurantiacus	aerobic	- : -	0.00242	18.4	~8	148	29
	anaerobic	- : -	0.00649	25.1	~8	290	87
Cb. tepidum	aerobic	- : -	0.000946	21.1	~1.5	54.4	6.1
	anaerobic	- : -	0.00337	22.9	-	179	26

different from that of monomers of BChl *c*, therefore, it is improbable that superradiance occurs there. If any superradiance is to occur, it is in these aggregates with a high in β-carotene content, which exhibit up to a 25% increase in the dipole strength when compared to monomers.

On the other hand, aggregates created prepared by the slow method that are supposed to mimic chlorosomes including the envelope show dipole strengths higher by approximately 150 to 200 %. This indicates that superradiance is present in those aggregates and the emission occurs from states that are still delocalised over several molecules.

To further investigate superradiance of BChl *c* aggregates, chlorosomes isolated from *Cf. aurantiacus* and *Cb. tepidum* were studied in the same way. Since there is BChl *a* present in the baseplate, two peaks of fluorescence were recorded – one corresponding to the emission of the BChl *c* aggregates inside the chlorosome envelope, the other corresponding to the emission of BChl *a* in the baseplate (Figure 35 and Figure 36). Because we are interested only in the superradiance of aggregated BChl *c*, only the first emission peak was considered, both lifetime-wise and quantum yield-wise. The

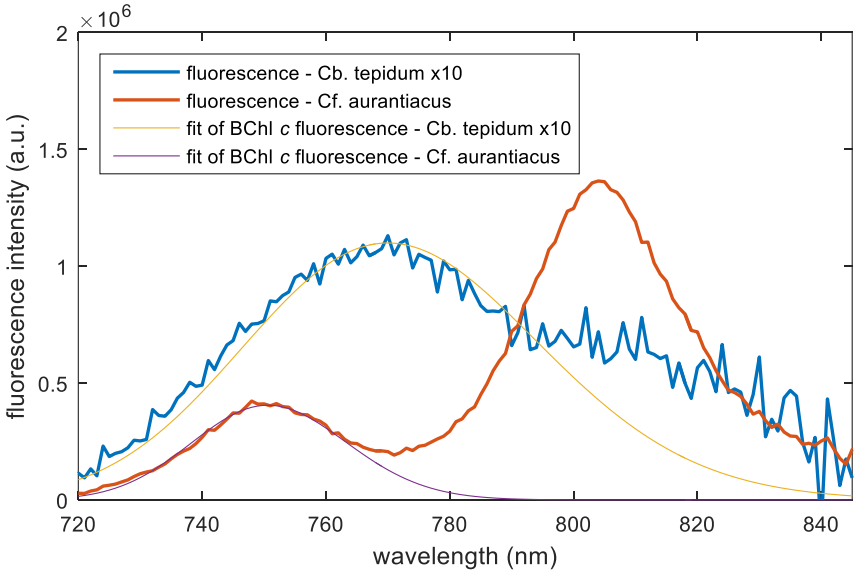

Figure 35: Fluorescence emission of chlorosomes (aerobic conditions) – *Cf. aurantiacus* chlorosomes in red with the fit of the contribution of its BChl *c* (purple), *Cb. tepidum* chlorosomes in blue with the fit of the contribution of its BChl *c* (orange). Both curves of *Cb. tepidum* are multiplied by a factor of 10 for better visibility.

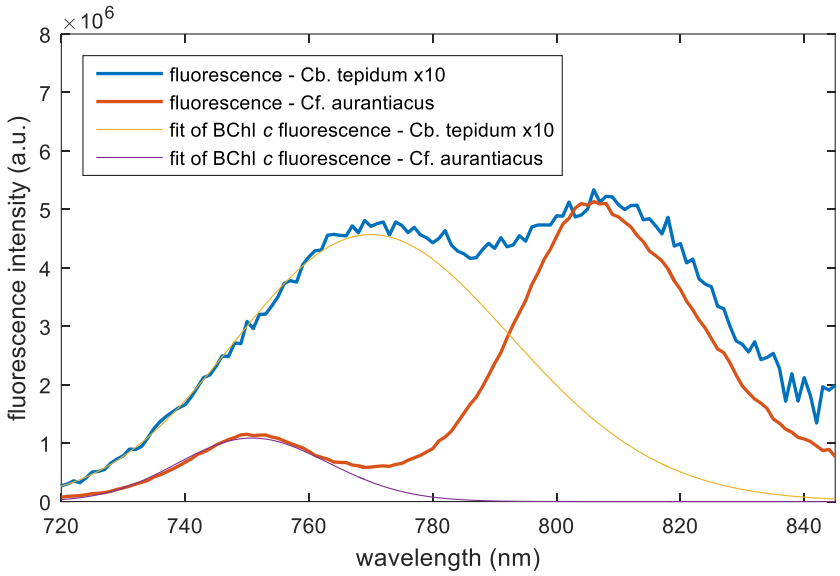

Figure 36: Fluorescence emission of chlorosomes (anaerobic conditions) – *Cf. aurantiacus* chlorosomes in red with the fit of the contribution of its BChl *c* (purple), *Cb. tepidum* chlorosomes in blue with the fit of the contribution of its BChl *c* (orange). Both curves of *Cb. tepidum* are multiplied by a factor of 10 for better visibility.

emission spectrum was thus fitted with Gaussian functions to separate the two fluorescence peaks. The area under the Gaussian curve estimating the peak of BChl *c* aggregates was used as the fluorescence intensity.

This is justified, because energy transfer from BChl *c* to BChl *a* is another non-radiative pathway for the excitation to decay with. This decreases the quantum yield and radiative lifetime proportionally, therefore the measured dipole strength is not influenced.

The fluorescence lifetime is determined by the inverse sum of all the rate constants of different decay pathways

$$\tau_{fl} = \frac{1}{k_{rad} + \sum k_{non-rad}},$$

where subscripts *rad* and *non-rad* distinguish the radiative and non-radiative decay pathways. The quantum yield is given by the same formula multiplied by the radiative rate constant

$$\phi_{fl} = \frac{k_{rad}}{k_{rad} + \sum k_{non-rad}} .$$

Adding another decay pathway, the quenching, lowers both values by the same factor, therefore their ratio, which determines the radiative rate constant, remains the same

$$k_{rad} = \frac{\phi_{fl}}{\tau_{fl}} .$$

Using this logic, the same argument could be made for the excitation quenching under aerobic condition, where the dipole strength would be identical for the aerobic and anaerobic conditions.

However, the results are different than what was expected by the theory outlined above. The dipole strength in *Cf. aurantiacus* chlorosomes under aerobic conditions is increased 4.7 fold compared to monomeric BChl *c*. Under anaerobic conditions, the increase is 9.2-fold.

In *Cb. tepidum*, the increase in dipole strength is 1.7 fold under aerobic conditions but under anaerobic conditions, which are natural to these bacteria, the dipole strength increases 5.7 fold.

The explanation for the different measured dipole strengths lies with the reverse transfer from BChl *a* to the BChl *c* aggregates. This increases the detected lifetime of BChl *c*. However, since those photons that would otherwise be emitted by BChl *a* are now emitted by BChl *c*, the quantum yield of BChl *c* increases as well. In fact, it increases more than the lifetime, because even though the excitation is transferred back to BChl *c* at later times, it still decays with the lifetime of BChl *c*, just delayed as if the excitation pulse arrived later. Doubling the amount of photons emitted from BChl *c* then doubles its quantum yield, but the lifetime does not increase so significantly. This effect is demonstrated in Figure 37 where a re-excitation in later times is simulated. The blue curve models the decay of BChl *c* when no reverse energy transfer occurs. If, however, re-excitation is allowed at later times, the red curve is what the decay curve looks like; it is composed of a series of smaller exponential decay curves with the same lifetime as the blue curve, but shifted in time. Fitting the red curve with a mono-exponential decay function (convolution of a Gaussian IRF and an exponential function) gives a longer lifetime (in the case given by Figure 37, the lifetime is 45 %

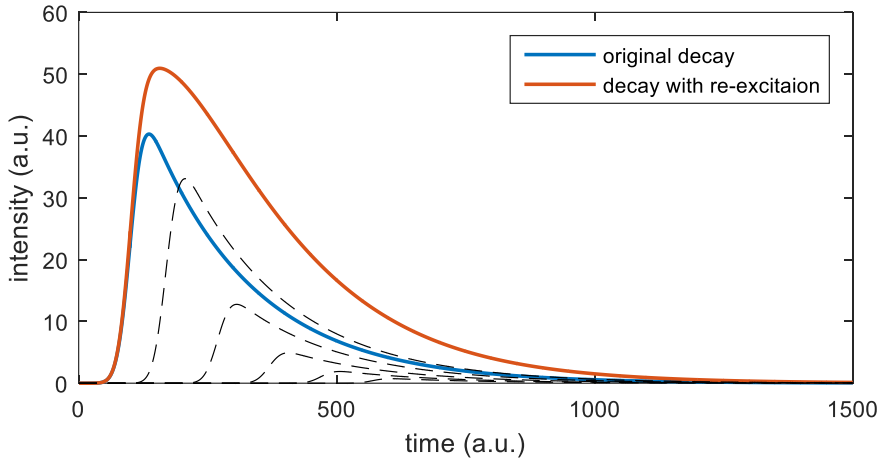

Figure 37: An illustration of the effects of re-excitation of BChl *c* on the recorded decay curves. The original decay (blue) has a time constant of 20 a.u., the simulated decay curve (red) has a time constant of 29 a.u. This is an increase of lifetime by 45 %, however, the intensity (area under curve) is larger by 81 % for the simulated (red) curve. The thin black dashed lines show some of the delayed decay curves included in the red curve (multiplied by 20). The effect here serves only illustrative purposes.

longer). Also the intensity, i.e. the area under the curve, is larger, but it is larger by 81 %. Therefore, even though the actual dipole strength remains the same, the ratio of the measured quantum yield to the fluorescence lifetime changes significantly.

In chlorosomes, the quenching is caused primarily by quinones (94) that are activated by the different redox potential under aerobic conditions (95), not by oxygen itself. Quinones are present in the interior of chlorosomes and quench the BChl *c* aggregates (94), especially in anaerobic bacteria like *Cb. tepidum* (but not so much in facultative anaerobe, *Cf. aurantiacus*). Therefore, the ratio of intensity of BChl *a* fluorescence to that of BChl *c* is lower under aerobic conditions than under anaerobic conditions – the probability of energy transfer to BChl *a* is significantly decreased. This can be seen from comparing Figure 35 to Figure 36 showing the fluorescence under aerobic and anaerobic conditions. For chlorosomes of *Cf. aurantiacus*, the peak intensity of BChl *a* increases approximately 3.8-fold while BChl *c* increases 2.8-fold. For chlorosomes of *Cb. tepidum*, the peak intensity of BChl *a* increases approximately 20-fold while BChl *c* increases 4.3-fold. This is in contrast to measurements reported in (94) where for *Cb. tepidum* more than 10-fold increase in BChl *c* fluorescence was reported and

in (96) where a more than 40-fold increase was reported. On the other hand, the results reported in both (94) and (96) show a much smaller intensity of BChl *a* fluorescence – it is likely that the *Cb. tepidum* used in their work contained a much smaller ratio of BChl *a*.

Because the quenching under aerobic conditions reduces the intensity of BChl *c*, much less EET to BChl *a* is happening. This also reduces the probability of the reverse energy transfer from BChl *a* that would affect the measured lifetimes of BChl *c*. However, since the sample was excited at 400 nm during the lifetime measurements, it is possible that some small amount of BChl *a* was excited – although the Soret band of BChl *a* peaks at approx. 350 nm in most environments, there is still some absorption at 400 nm. This direct excitation of BChl *a* could then lead to reverse EET.

To put the reverse EET into perspective, assuming the fluorescence of both BChl *a* and BChl *c* is happening from the lowest states, those corresponding to emission wavelengths of 810 nm and 770 nm respectively in chlorosomes of *Cb. tepidum*, the Boltzmann distribution of the populations of these states is

$$\frac{p_{\mathrm{BChl}\,c}}{p_{\mathrm{BChl}\,a}} = e^{\frac{E_{\mathrm{BChl}\,a} - E_{\mathrm{BChl}\,c}}{\mathrm{k}T}} = e^{\frac{\mathrm{hc}}{\mathrm{k}T}\left(\frac{1}{\lambda_{\mathrm{BChl}\,a}} - \frac{1}{\lambda_{\mathrm{BChl}\,c}}\right)}.$$

Evaluating this (h – Planck's constant, c – speed of light, k – Boltzmann constant, T – thermodynamic temperature, and λ – the wavelength corresponding to the states of BChl *a* and *c*) for room temperature (293 K) and wavelengths given above, the ratio of populations of both states is 0.043. This means that (if the lifetimes of both populations are the same) there is an increase of the measured quantum yield of 4.3 %, leading to an overestimation of the dipole strength by no more than 4.3%. In chlorosomes of *Cb. tepidum*, the quenching of BChl *c* is so strong under aerobic conditions that almost no excitation is transferred to BChl *a*, as can be seen from Figure 35. Whether the observed emission of BChl *a* originated from a direct excitation at 400 nm or it was due to the EET from BChl *c* cannot be distinguished. Direct excitation cannot be higher at anaerobic conditions and therefore its contribution is not significant in *Cb. tepidum* at any conditions.

The lifetime ratio also plays a role in this reverse EET. The larger the ratio of BChl *a* to BChl *c* lifetimes, the larger the probability of transferring the energy back. In *Cb. tepidum* under anaerobic conditions, the lifetime of BChl *a* is measured to be

approximately double that of BChl *c*. However, under aerobic conditions, they are almost identical. This means that this effect does not increase the probability of reverse EET in chlorosomes of *Cb. tepidum* under aerobic conditions.

Thus, unless there is another major factor influencing the results, the measured dipole strength under aerobic conditions for chlorosomes of *Cb. tepidum* reflects its real value.

For chlorosomes of *Cf. aurantiacus*, the situation is different. The emission peaks of BChl *c* and BChl *a* are farther apart, with maxima at 750 and 805 nm. This yields a BChl *c* to BChl *a* population ratio of 0.011. However, these chlorosomes do not have such an efficient quenching mechanism – they do not require anaerobic conditions for efficient EET from BChl *c* to BChl *a* as oxygen does not pose a threat to their reaction centre (57). Also, these chlorosomes contain more BChl *a* relatively to BChl *c* than the chlorosomes of *Cb. tepidum* (1:100 in *Cb. tepidum* (97), 1:25 in *Cf. aurantiacus* (98)). This makes the direct excitation of BChl *a* more prominent. However, the primary effect here is the much longer lifetime of BChl *a*, which significantly increases the probability of reverse EET.

So far it was proven in *Cb. tepidum* that the dipole strength is increased approximately two times even when the reverse EET does not influence the results. A delocalisation of emission over a minimum of 2 molecules and moderate superradiance is still indicated. This is also true for artificial aggregates, which do not contain any BChl *a* and no reverse energy transfer may occur. The β-carotene present in the aggregates (and chlorosomes) transfers the excitation to BChl *c* from its S_2 state (59) with a rate constant faster by at least 2 orders of magnitude than the fluorescence lifetime of BChl *c* (62), therefore bearing no real impact on the data.

The aggregates prepared by the slow method are exhibiting an even larger dipole strength than aggregates in chlorosomes of *Cb. tepidum* and 2-3-fold larger dipole strength than the fast-method aggregates and monomers. The reason for this may be hypothesised that aggregates created by a slow solvent exchange turn out to contain more tightly packed and ordered pigments because of the method of preparation where the pigments have enough time to organise in non-aqueous environment, as was outlined above. On the other hand, aggregates created by the fast method may be more

disordered because the formation is faster, happening immediately upon injection into buffer.

The increased dipole strength in some of the samples also implies that the excitation travels more fluidly through the aggregates. The aggregation of pigments causes the quantum yield to drop, which reduces the probability of a de-excitation by radiative decay, while the increased dipole strength allows for faster energy transfer times within the aggregate compared to monomeric pigments. Even larger dipole strengths were observed in BChl *c* aggregates in chlorosomes from *Cb. tepidum* under anaerobic conditions and *Cf. aurantiacus*, but these may be, at least partly, overestimated due to a reverse energy transfer from BChl *a*.

3.5.4 Effects of β-carotene on aggregates

So far it has been proven that, depending on the preparation procedure, aggregates may exhibit superradiance. In most of the measured aggregates there has been β-carotene present. If we plot the fluorescence quantum yield as a function of β-carotene concentration, the quantum yields may rise slightly with the amount of β-carotene added (Figure 38). This is in agreement with the aggregation inducing properties of β-carotene, because more β-carotene provides a better long-range order in the aggregates (99), increasing the strength of interactions when the fast method of preparation is used (59). The different confidence intervals in Figure 38 are caused by the method of fitting – the relative errors were always similar, so for four to five times larger values this means four to five times larger confidence intervals. A possible trend might be visible in the lifetime dependence of the radiative component (τ_1 in Table 2) – while in slow-method aggregates the lifetimes seem to get longer when more β-carotene is added, in fast method aggregates they seem to remain the same (Figure 39). Also, a slight trend is visible when it comes to a dipole strength dependence on the amount of β-carotene inside the aggregates (Figure 40). While the dipole strength gets larger with the addition of more β-carotene in the fast-method aggregates, in slow-method aggregates it seems to be the other way around. Both of those trends may have the same explanation – disorder. Fast method aggregates are more disordered in general. Adding more β-carotene to the mixture improves the long-range order of the pigments (99), increasing the dipole strength and the interactions between molecules. On the other hand, in slow method aggregates, where molecules are very orderly already, incorporating more β-carotene may introduce disorder, because the otherwise

neatly stacked aggregates get their structure disrupted by high amounts of β-carotene that breaks those condensed stacks apart. This may make the disorder more significant and in turn decrease the dipole strength.

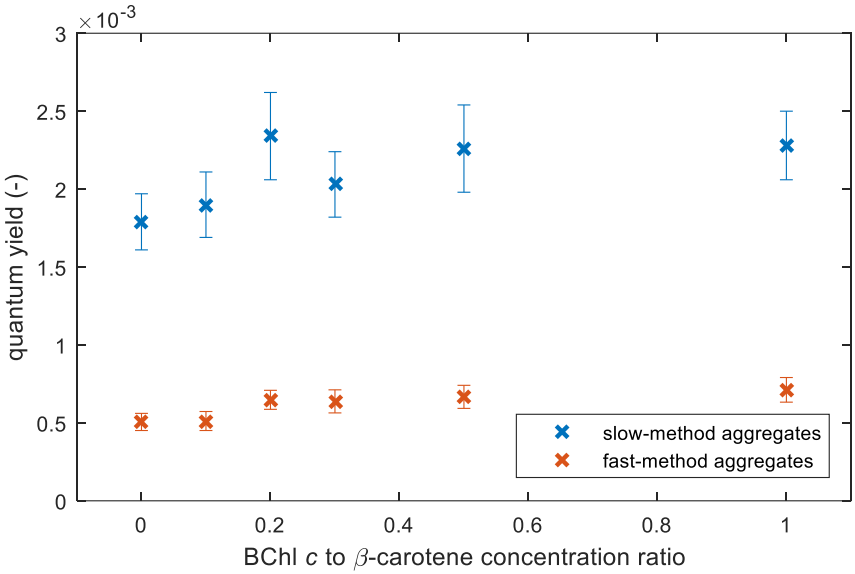

Figure 38: Dependence of measured quantum yield on relative concentration of BChl *c* to β-carotene for both types of prepared aggregates.

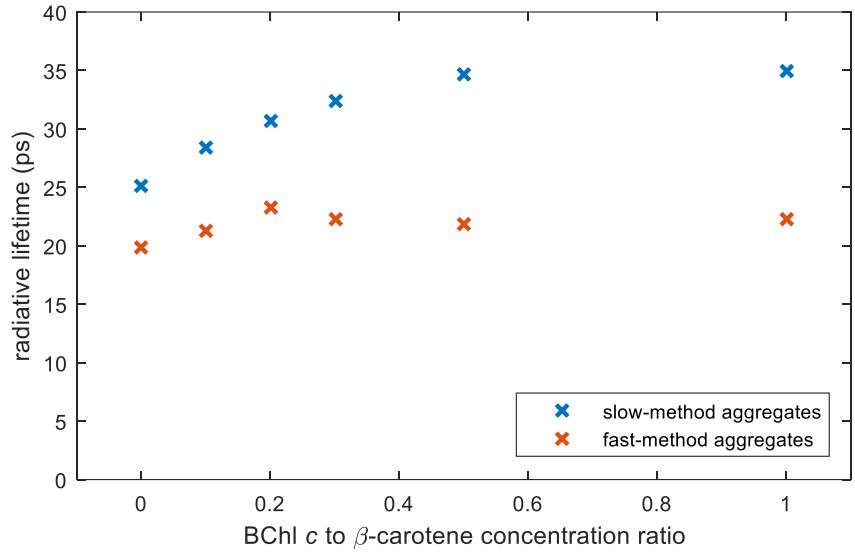

Figure 39: Dependence of radiative lifetime on relative concentration of BChl *c* to β-carotene for both types of prepared aggregates. Error bars for measurement uncertainty were too small to visualise.

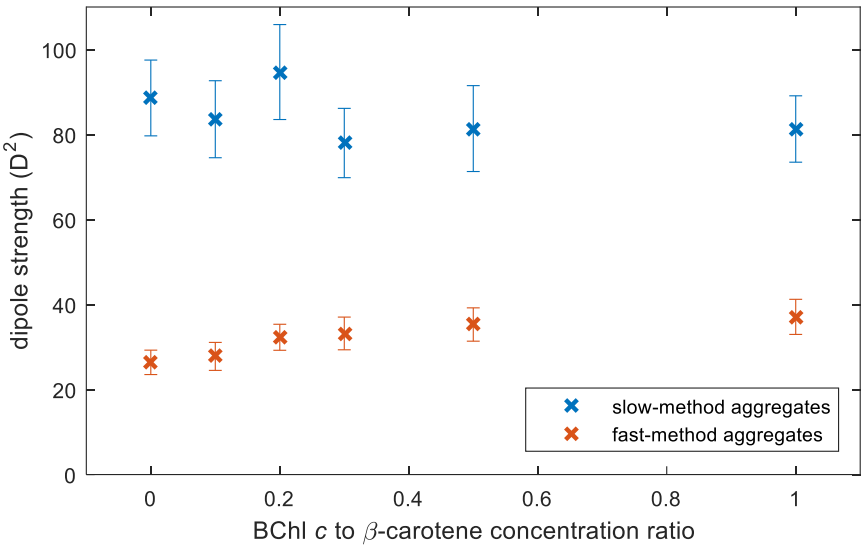

Figure 40: Dependence of dipole strength lifetime on relative concentration of BChl *c* to β-carotene for both types of prepared aggregates.

This means that in fast method aggregates the emission is delocalised very little or not at all, while in aggregates prepared by the slow method the emission appears to be delocalised over at least 3 molecules. In chlorosomes, there is delocalised emission present. In chlorosomes of *Cb. tepidum*, this delocalisation includes at least 2 molecules. Whether the delocalisation is even more pronounced in chlorosomes of *Cf. aurantiacus*, or it is an effect of the artefacts, is not clear.

4 Conclusions

4.1 EET efficiency

Efficiency of EET from β-carotene to BChl *c* aggregates and then to BChl *a* has been studied in two types of artificial aggregates of BChl *c*. The slow-method aggregates prepared by a method of slow dripping of an aqueous buffer into dissolved pigments exhibit EET efficiency from β-carotene to BChl *c* of approximately 20 %. This value is reasonably reliable, despite various factors affecting the measurements, most importantly scattering, because these effects were not too pronounced at the wavelengths of carotenoid absorption. The scattering was even more pronounced during the measurements of the fast-method aggregates prepared by a rapid injection of pigments into an aqueous buffer. Artificial aggregates with molar concentration ratios of BChl *c* to β-carotene of 1:0.2, 1:0.4, and 1:0.6 yielded EET efficiencies of 40 %, 27 % and 26 %; however, these values are deemed to be rather inaccurate and likely underestimated due to strong scattering and the lack of an appropriate reference without β-carotene. The decreasing efficiency with more added β-carotene shows that it would be inefficient to put large amounts of β-carotene as an absorber into artificial aggregates, were they to be used in solar cells. This is unexpected since the EET efficiency from β-carotene to BChl *c* in chlorosomes is much higher, 50-80 % ((60), (61), (62)). Thus, additional pigments filling in the absorption gap in the green region would have to be found.

Also, it was determined from these measurements that the method of comparing excitation spectra with $1-T$ absorption spectra is not suitable for highly scattering samples unless a full integrating sphere is used. However, the demands of this method for equipment are lower than for determining the rate constants, which requires highly time-resolved measurements and is less accurate for non-scattering samples.

The EET efficiency from BChl *c* to BChl *a* was determined by emission spectra measurements. Intriguingly high EET efficiencies were found, where fast-method aggregates reached 95 % efficiency. The efficiency decreased with the addition of β-carotene and with the decrease of BChl *a* concentration, although not significantly in the latter case. In slow-method aggregates, the same trend was observed, although at lower efficiencies in general, the maximum efficiency being 65 % for a sample without

β-carotene. The co-polymer used for the preparation of these aggregates did not affect the EET efficiency to BChl *a*. The high efficiencies observed with the fast-method aggregates are promising with respect to their potential applications.

4.2 Quenching of BChl *c* triplet states

In all artificial BChl *c* aggregates (prepared both by the slow and the fast method), β-carotene triplet states were measured to have a lifetime on the order of 1-2 μs. It has been shown that the β-carotene triplet states arise from the quenching of triplet states of BChl *c*. Therefore, triplet states of BChl *c* are being formed in artificial aggregates. However, more importantly, all the triplet states of BChl *c* are quenched by β-carotene.

It has also been measured that these triplet states of BChl *c* are quenched with a time constant of approximately 4.5 ns in the case of the fast-method aggregates and 9.5 ns in the case of slow-method aggregates. Together with a highly shortened excited state lifetime of the aggregated BChl *c*, these two mechanisms protect the artificial aggregates from oxidative damage. This is a very important finding with regard to the potential use of these aggregates is photovoltaics.

4.3 Size and shape of artificial aggregates

From the one sample of slow-method aggregates measured, typical sizes of approximately 100 nm over the longest dimension can be expected for these aggregates. The dried aggregates tend to cluster together. It would be interesting to verify whether this clustering happens only after drying or it is a process ongoing already in solution. It is arguable whether drying of the aggregates results in leakage of their interior or the observed aura around the clusters was due to leftover salts from the Tris-HCl buffer.

In the preliminary measurements, the deposition of aggregates on mica was not ideal. A new method of deposition will need to be developed so that richer depositions of aggregates on the surface are achieved. Possibly, measurements with a submerged tip might be required to avoid damage to the aggregates by drying. Also, measuring in buffer would eliminate the contamination by leftover buffer salts.

4.4 Superradiance measurements

The dipole strengths were measured for both types of aggregates and were compared to chlorosomes of *Cf. aurantiacus* and *Cb. tepidum*. The dipole strength of monomeric BChl *c* was determined to be 31.4 D^2. The dipole strengths of fast-method aggregates ranged from 26.4 D^2 in a sample with no β-carotene (i.e. BChl *c* dimers) to 37.1 D^2 in a sample with a molar ratio of BChl *c* to β-carotene of 1:1. If any superradiance and elevated values of dipole strength are observed, then only in the aggregates high in β-carotene content.

In slow method aggregates, the results are very different. Larger dipole strengths are recorded for aggregates with less β-carotene, 88.6 D^2 in a sample with no β-carotene, and decreasing with addition of β-carotene to 81.3 D^2 in a sample with BChl *c* to β-carotene ratio of 1:1. All samples exhibit superradiance and the emission is delocalised over at least 3 molecules.

In chlorosomes, the values of dipole strength are mostly measured to be even higher. Different values are obtained under aerobic and anaerobic conditions. The reason for this is suspected to be a reverse EET from BChl *a* to BChl *c* aggregates. Under aerobic conditions, the excitation is quenched in *Cb. tepidum* and the resulting fluorescence from BChl *c* is not affected by a re-excitation from BChl *a*. In *Cb. tepidum*, this makes the measured dipole strength of 54.4 D^2 reliable. However, this mechanism is not present in *Cf. aurantiacus* and it is therefore possible that the value of 148 D^2 measured under aerobic conditions is overestimated.

Both chlorosomes and artificial aggregates exhibit strong exciton interactions. In the case of the slow-method aggregates and chlorosomes it leads to the occurrence of superradiance. In chlorosomes of *Cb. tepidum*, an emission occurs from a state which is delocalized over at least 2 molecules. In chlorosomes of *Cf. aurantiacus*, the reliable value for the dipole strength could not be determined, but were the measured values accurate, it would correspond to emission from a state delocalised over a minimum of 5 molecules.

The emitting dipole strength larger than for a monomer increases the EET rate within and out of the BChl *c* aggregate, while the quantum yield reduced by aggregation leads to smaller losses of excitation due to emission.

5 References

(1) TACHIBANA, Yasuhiro, Lionel VAYSSIERES, and James R. DURRANT. Artificial photosynthesis for solar water-splitting. Nature Photonics. 2012, 6(8), 511-518. DOI: 10.1038/nphoton.2012.175. ISSN 1749-4885. Available at: http://www.nature.com/articles/nphoton.2012.175

(2) CONCEPCION, J. J., R. L. HOUSE, J. M. PAPANIKOLAS, and T. J. MEYER. Chemical approaches to artificial photosynthesis. Proceedings of the National Academy of Sciences. 2012, 109(39), 15560-15564. DOI: 10.1073/pnas.1212254109. ISSN 0027-8424. Available at: http://www.pnas.org/cgi/doi/10.1073/pnas.1212254109

(3) BERARDI, Serena, Samuel DROUET, Laia FRANCÀS, Carolina GIMBERT-SURIÑACH, Miguel GUTTENTAG, Craig RICHMOND, Thibaut STOLL, and Antoni LLOBET. Molecular artificial photosynthesis. Chem. Soc. Rev. 2014, 43(22), 7501-7519. DOI: 10.1039/C3CS60405E. ISSN 0306-0012. Available at: http://xlink.rsc.org/?DOI=C3CS60405E

(4) GUST, Devens, Thomas A. MOORE, and Ana L. MOORE. Solar Fuels via Artificial Photosynthesis. Accounts of Chemical Research. 2009, 42(12), 1890-1898. DOI: 10.1021/ar900209b. ISSN 0001-4842. Available at: https://pubs.acs.org/doi/10.1021/ar900209b

(5) KALYANASUNDARAM, K and M GRAETZEL. Artificial photosynthesis: biomimetic approaches to solar energy conversion and storage. Current Opinion in Biotechnology. 2010, 21(3), 298-310. DOI: 10.1016/j.copbio.2010.03.021. ISSN 09581669. Available at: https://linkinghub.elsevier.com/retrieve/pii/S0958166910000649

(6) KAY, Andreas and Michael GRAETZEL. Artificial photosynthesis. 1. Photosensitisation of titania solar cells with chlorophyll derivatives and related natural porphyrins. The Journal of Physical Chemistry. 1993, 97(23), 6272-6277. DOI: 10.1021/j100125a029. ISSN 0022-3654. Available at: https://pubs.acs.org/doi/abs/10.1021/j100125a029

(7) EBERHART, Michael S., Leah M. Rader BOWERS, Bing SHAN, Ludovic TROIAN-GAUTIER, M. Kyle BRENNAMAN, John M. PAPANIKOLAS, and Thomas J. MEYER. Completing a Charge Transport Chain for Artificial Photosynthesis. Journal of the American Chemical Society. 2018, 140(31), 9823-9826. DOI: 10.1021/jacs.8b06740. ISSN 0002-7863. Available at: https://pubs.acs.org/doi/10.1021/jacs.8b06740

(8) BLANKENSHIP, Robert E. Molecular mechanisms of photosynthesis. 2nd ed. Chichester: Wiley Blackwell, 2014. ISBN 978-1-4051-8976-7.

(9) THE NATURE OF LIGHT RADIATED BY OUR SUN. Center for Coastal Physical Oceanography [online]. Norfolk, Virginia, 2003 [cit. 2020-04-21]. Available at: http://www.ccpo.odu.edu/SEES/ozone/class/Chap_4/4_3.htm

(10) KE, Bacon, *Photosynthesis: Photobiochemistry and Photobiophysics*. 10th.Walnut Creek, USA: Sptringer, Dordrecht, 2001. DOI: 10.1007/0-306-48136-7. ISBN 978-0-7923-6334-7.

(11) SCHULZE-MAKUCH, Dirk and Louis Neal IRWIN. *Life in the Universe: Expectations and* Constraints. 2nd. Springer-Verlag Berlin Heidelberg, 2008. ISBN 978-3-540-76817-3.

(12) BUTTERFIELD, Nicholas J. and Barry LOMAX. Proterozoic photosynthesis - a critical review. Palaeontology. 2015, 58(6), 953-972. DOI: 10.1111/pala.12211. ISSN 00310239. Available at: http://doi.wiley.com/10.1111/pala.12211

(13) TICE, Michael M. and Donald R. LOWE. Photosynthetic microbial mats in the 3,416-Myr-old ocean. Nature. 2004, 431(7008), 549-552. DOI: 10.1038/nature02888. ISSN 0028-0836. Available at: http://www.nature.com/articles/nature02888

(14) NISBET, E.G. and C.M.R. FOWLER. The Early History of Life. Treatise on Geochemistry. Elsevier, 2014, 2014, , 1-42. DOI: 10.1016/B978-0-08-095975-7.00801-9. ISBN 9780080983004. Available at: https://linkinghub.elsevier.com/retrieve/pii/B9780080959757008019

(15) CARDONA, Tanai. Early Archean origin of heterodimeric Photosystem I. Heliyon. 2018, 4(3). DOI: 10.1016/j.heliyon.2018.e00548. ISSN 24058440. Available at: https://linkinghub.elsevier.com/retrieve/pii/S2405844017336290

(16) Illustrated Glossary of Organic Chemistry. UCLA Department of Chemistry & Biochemistry [online]. Los Angeles, 2016 [cit. 2020-04-22]. Available at: http://www.chem.ucla.edu/~harding/IGOC/C/chlorophyll.html. Website managed by Dr. Steve Hardinger.

(17) GOVINDJEE, Govindjee, ed. Bioenergetics of Photosynthesis. London: Academic Press, 1975, 118, 120. ISBN 0122943503.

(18) OMLC [online]. Scott Prahl & Steve Jacques, 2018 [cit. 2020-04-22]. Available at: https://omlc.org/

(19) KATO, Masaru, Jenny Z. ZHANG, Nicholas PAUL, and Erwin REISNER. Protein film photoelectrochemistry of the water oxidation enzyme photosystem II. Chem. Soc. Rev. 2014, 43(18), 6485-6497. DOI: 10.1039/C4CS00031E. ISSN 0306-0012. Available at: http://xlink.rsc.org/?DOI=C4CS00031E

(20) FRANK, Harry A. and Richard J. COGDELL. Carotenoids in Photosynthesis. Photochemistry and Photobiology. 1996, 63(3), 257-264. DOI: 10.1111/j.1751-1097.1996.tb03022.x. ISSN 0031-8655. Available at: http://doi.wiley.com/10.1111/j.1751-1097.1996.tb03022.x

(21) STRANGE, Claudia, ed. Carotenoids in Nature. Switzerland: Springer, 2016.

(22) LOKA BHARATHI, P.A. Sulfur Cycle. Encyclopedia of Ecology. Elsevier, 2008, 2008, s. 3424-3431. DOI: 10.1016/B978-008045405-4.00761-8. ISBN 9780080454054. Dostupné také z: https://linkinghub.elsevier.com/retrieve/pii/B9780080454054007618

(23) SALTON, M R J and P OWEN. Bacterial Membrance Structure. Annual Review of Microbiology. 1976, 30(1), 451-482. DOI: 10.1146/annurev.mi.30.100176.002315. ISSN 0066-4227. Available at: http://www.annualreviews.org/doi/10.1146/annurev.mi.30.100176.002315

(24) VOGL, Kajetan, Marcus TANK, Gregory S. ORF, Robert E. BLANKENSHIP, and Donald A. BRYANT. Bacteriochlorophyll f: properties of chlorosomes containing the "forbidden

chlorophyll". Frontiers in Microbiology. 2012, 3. DOI: 10.3389/fmicb.2012.00298. ISSN 1664-302X. Available at: http://journal.frontiersin.org/article/10.3389/fmicb.2012.00298/full

(25) BLANKENSHIP, Robert E., John M. OLSON, and Mette MILLER. Antenna Complexes from Green Photosynthetic Bacteria. Anoxygenic Photosynthetic Bacteria. Dordrecht: Kluwer Academic Publishers, 2004, , 399-435. Advances in Photosynthesis and Respiration. DOI: 10.1007/0-306-47954-0_20. ISBN 0-7923-3681-X. Available at: http://link.springer.com/10.1007/0-306-47954-0_20

(26) PŠENČÍK, Jakub, Aaron M. COLLINS, Lassi LILJEROOS, et al. Structure of Chlorosomes from the Green Filamentous Bacterium Chloroflexus aurantiacus. Journal of Bacteriology. 2009, 191(21), 6701-6708. DOI: 10.1128/JB.00690-09. ISSN 0021-9193. Available at: https://JB.asm.org/content/191/21/6701

(27) PŠENČÍK, J., T.P. IKONEN, P. LAURINMÄKI, M.C. MERCKEL, S.J. BUTCHER, R.E. SERIMAA, and R. TUMA. Lamellar Organization of Pigments in Chlorosomes, the Light Harvesting Complexes of Green Photosynthetic Bacteria. Biophysical Journal. 2004, 87(2), 1165-1172. DOI: 10.1529/biophysj.104.040956. ISSN 00063495. Available at: https://linkinghub.elsevier.com/retrieve/pii/S0006349504735961

(28) OOSTERGETEL, Gert T., Michael REUS, Aline GOMEZ MAQUEO CHEW, Donald A. BRYANT, Egbert J. BOEKEMA, and Alfred R. HOLZWARTH. Long-range organization of bacteriochlorophyll in chlorosomes of Chlorobium tepidum investigated by cryo-electron microscopy. FEBS Letters. 2007, 581(28), 5435-5439. DOI: 10.1016/j.febslet.2007.10.045. ISSN 00145793. Available at: http://doi.wiley.com/10.1016/j.febslet.2007.10.045

(29) OOSTERGETEL, Gert T., Herbert VAN AMERONGEN, and Egbert J. BOEKEMA. The chlorosome: a prototype for efficient light harvesting in photosynthesis. Photosynthesis Research. 2010, 104(2-3), 245-255. DOI: 10.1007/s11120-010-9533-0. ISSN 0166-8595. Available at: http://link.springer.com/10.1007/s11120-010-9533-0

(30) PROKHORENKO, V.I., D.B. STEENSGAARD, and A.R. HOLZWARTH. Exciton Theory for Supramolecular Chlorosomal Aggregates: 1. Aggregate Size Dependence of the Linear Spectra. Biophysical Journal. 2003, 85(5), 3173-3186. DOI: 10.1016/S0006-3495(03)74735-3. ISSN 00063495. Available at: https://linkinghub.elsevier.com/retrieve/pii/S0006349503747353

(31) LI, Hui and Donald A. BRYANT. Envelope Proteins of the CsmB/CsmF and CsmC/CsmD Motif Families Influence the Size, Shape, and Composition of Chlorosomes in Chlorobaculum tepidum. Journal of Bacteriology. 2009, 191(22), 7109-7120. DOI: 10.1128/JB.00707-09. ISSN 0021-9193. Available at: https://JB.asm.org/content/191/22/7109

(32) MARTISKAINEN, Jari, Juha LINNANTO, Robertas KANANAVIČIUS, Viivi LEHTOVUORI, and Jouko KORPPI-TOMMOLA. Excitation energy transfer in isolated chlorosomes from Chloroflexus aurantiacus. Chemical Physics Letters. 2009, 477(1-3), 216-220. DOI: 10.1016/j.cplett.2009.06.080. ISSN 00092614. Available at: https://linkinghub.elsevier.com/retrieve/pii/S0009261409007751

(33) SAVIKHIN, Sergei, Yinwen ZHU, Robert E. BLANKENSHIP, and Walter S. STRUVE. Ultrafast Energy Transfer in Chlorosomes from the Green Photosynthetic Bacterium Chloroflexus aurantiacus. The Journal of Physical Chemistry. 1996, 100(9), 3320-3322. DOI: 10.1021/jp953734k. ISSN 0022-3654. Available at: https://pubs.acs.org/doi/10.1021/jp953734k

(34) PŠENČÍK, Jakub, Ying-Zhong MA, Juan B. ARELLANO, Jan HÁLA, and Tomas GILLBRO. Excitation Energy Transfer Dynamics and Excited-State Structure in Chlorosomes of Chlorobium phaeobacteroides. Biophysical Journal. 2003, 84(2), 1161-1179. DOI: 10.1016/S0006-3495(03)74931-5. ISSN 00063495. Available at: https://linkinghub.elsevier.com/retrieve/pii/S0006349503749315

(35) LODISH, Harvey, Arnold BERK, S Lawrence ZIPURSKY, Paul MATSUDAIRA, David BALTIMORE, and James DARNELL. Molecular Cell Biology. 4th. New York: W. H. Freeman, 2000. ISBN 0-7167-3136-3.

(36) SAKURAI, Hidehiro, Takuro OGAWA, Michiko SHIGA, and Kazuhito INOUE. Inorganic sulfur oxidising system in green sulfur bacteria. Photosynthesis Research. 2010, 104(2-3), 163-176. DOI: 10.1007/s11120-010-9531-2. ISSN 0166-8595. Available at: http://link.springer.com/10.1007/s11120-010-9531-2

(37) GAO, Xinliu, Erica Wunderlich MAJUMDER, Yisheng KANG, Hai YUE a Robert E. BLANKENSHIP. Functional analysis and expression of the mono-heme containing cytochrome c subunit of alternative complex III in Chloroflexus aurantiacus. Archives of Biochemistry and Biophysics. 2013, 535(2), 197-204. DOI: 10.1016/j.abb.2013.04.002. ISSN 00039861. Dostupné také z: https://linkinghub.elsevier.com/retrieve/pii/S0003986113001069

(38) KING, Jeremy D., Chelsea L. MCINTOSH, Christopher M. HALSEY, Bryan M. LADA, Dariusz M. NIEDZWIEDZKI, Jason W. COOLEY a Robert E. BLANKENSHIP. Metalloproteins Diversified: The Auracyanins Are a Family of Cupredoxins That Stretch the Spectral and Redox Limits of Blue Copper Proteins. Biochemistry. 2013, 52(46), 8267-8275. DOI: 10.1021/bi401163g. ISSN 0006-2960. Dostupné také z: https://pubs.acs.org/doi/10.1021/bi401163g

(39) Carotenoids Database [online]. Junko Yabuzaki, 2019 [cit. 2020-04-22]. Available at: http://carotenoiddb.jp/

(40) HARADA, Jiro, Kenji V. P. NAGASHIMA, Shinichi TAKAICHI, Norihiko MISAWA, Katsumi MATSUURA, and Keizo SHIMADA. Phytoene Desaturase, CrtI, of the Purple Photosynthetic Bacterium, Rubrivivax gelatinosus, Produces both Neurosporene and Lycopene. Plant and Cell Physiology. 2001, 42(10), 1112-1118. DOI: 10.1093/pcp/pce140. ISSN 1471-9053. Available at: http://academic.oup.com/pcp/article/42/10/1112/1876695/Phytoene-Desaturase-CrtI-of-the-Purple

(41) PINTA, Violaine, Soufian OUCHANE, Martine PICAUD, Shinichi TAKAICHI, Chantal ASTIER, and Françoise REISS-HUSSON. Characterization of unusual hydroxy- and ketocarotenoids in Rubrivivax gelatinosus: involvement of enzyme CrtF or CrtA. Archives of

Microbiology. 2003, 179(5), 354-362. DOI: 10.1007/s00203-003-0538-3. ISSN 0302-8933. Available at: http://link.springer.com/10.1007/s00203-003-0538-3

(42) KIM, Hanyoup, Hui LI, Julia A. MARESCA, Donald A. BRYANT a Sergei SAVIKHIN. Triplet Exciton Formation as a Novel Photoprotection Mechanism in Chlorosomes of Chlorobium tepidum. Biophysical Journal. 2007, 93(1), 192-201. DOI: 10.1529/biophysj.106.103556. ISSN 00063495. Dostupné také z: https://linkinghub.elsevier.com/retrieve/pii/S0006349507712717

(43) VINKLÁREK, Ivo S., David BÍNA, Tomáš MALINA, Aaron M. COLLINS, Radek LITVÍN, Jan ALSTER, and Jakub PŠENČÍK. Triplet state quenching of bacteriochlorophyll c aggregates in a protein-free environment of a chlorosome interior. Chemical Physics. 2020, 529. DOI: 10.1016/j.chemphys.2019.110542. ISSN 03010104. Available at: https://linkinghub.elsevier.com/retrieve/pii/S0301010419305920

(44) HOLT, N. E. Carotenoid Cation Formation and the Regulation of Photosynthetic Light Harvesting. Science. 2005, 307(5708), 433-436. DOI: 10.1126/science.1105833. ISSN 0036-8075. Available at: https://www.sciencemag.org/lookup/doi/10.1126/science.1105833

(45) LATOWSKI, Dariusz, Paulina KUCZYŃSKA, and Kazimierz STRZAŁKA. Xanthophyll cycle – a mechanism protecting plants against oxidative stress. Redox Report. 2013, 16(2), 78-90. DOI: 10.1179/174329211X13020951739938. ISSN 1351-0002. Available at: http://www.tandfonline.com/doi/full/10.1179/174329211X13020951739938

(46) MUSAZADE, Elshan, Roman VOLOSHIN, Nathan BRADY, et al. Biohybrid solar cells: Fundamentals, progress, and challenges. Journal of Photochemistry and Photobiology C: Photochemistry Reviews. 2018, 35, 134-156. DOI: 10.1016/j.jphotochemrev.2018.04.001. ISSN 13895567. Available at: https://linkinghub.elsevier.com/retrieve/pii/S1389556718300030

(47) GRÄTZEL, Michael. Recent Advances in Sensitised Mesoscopic Solar Cells. Accounts of Chemical Research. 2009, 42(11), 1788-1798. DOI: 10.1021/ar900141y. ISSN 0001-4842. Available at: https://pubs.acs.org/doi/10.1021/ar900141y

(48) CAO, Huanqi, Weidong HE, Yiwu MAO, Xiao LIN, Ken ISHIKAWA, James H. DICKERSON, and Wayne P. HESS. Recent progress in degradation and stabilisation of organic solar cells. Journal of Power Sources. 2014, 264, 168-183. DOI: 10.1016/j.jpowsour.2014.04.080. ISSN 03787753. Available at: https://linkinghub.elsevier.com/retrieve/pii/S0378775314005801

(49) GRÄTZEL, Michael. Photoelectrochemical cells. Nature. 2001, 414(6861), 338-344. DOI: 10.1038/35104607. ISSN 0028-0836. Available at: http://www.nature.com/articles/35104607

(50) CHERIAN, Suman and Carl C. WAMSER. Adsorption and Photoactivity of Tetra(4-carboxyphenyl)porphyrin (TCPP) on Nanoparticulate TiO 2. The Journal of Physical Chemistry B. 2000, 104(15), 3624-3629. DOI: 10.1021/jp994459v. ISSN 1520-6106. Available at: https://pubs.acs.org/doi/10.1021/jp994459v

(51) GRÄTZEL, Michael. Mesoporous oxide junctions and nanostructured solar cells. 1999, 4(4), 314-321. DOI: 10.1016/S1359-0294(99)90013-4. ISSN 13590294. Available at: https://linkinghub.elsevier.com/retrieve/pii/S1359029499900134

(52) ZENG, Wangdong, Yiming CAO, Yu BAI, et al. Efficient Dye-Sensitised Solar Cells with an Organic Photosensitiser Featuring Orderly Conjugated Ethylenedioxythiophene and Dithienosilole Blocks. Chemistry of Materials. 2010, 22(5), 1915-1925. DOI: 10.1021/cm9036988. ISSN 0897-4756. Available at: https://pubs.acs.org/doi/10.1021/cm9036988

(53) BESSHO, Takeru, Shaik M. ZAKEERUDDIN, Chen-Yu YEH, Eric Wei-Guang DIAU, and Michael GRÄTZEL. Highly Efficient Mesoscopic Dye-Sensitised Solar Cells Based on Donor-Acceptor-Substituted Porphyrins. Angewandte Chemie International Edition. 2010, 49(37), 6646-6649. DOI: 10.1002/anie.201002118. ISSN 14337851. Available at: http://doi.wiley.com/10.1002/anie.201002118

(54) LUKASHEV, E. P., V. A. NADTOCHENKO, E. P. PERMENOVA, O. M. SARKISOV, and A. B. RUBIN. Electron phototransfer between photosynthetic reaction centers of the bacteria Rhodobacter sphaeroides and semiconductor mesoporous TiO2 films. Doklady Biochemistry and Biophysics. 2007, 415(1), 211-216. DOI: 10.1134/S1607672907040138. ISSN 1607-6729. Available at: http://link.springer.com/10.1134/S1607672907040138

(55) WANG, Mingdong, Fangyan XIE, Jun DU, et al. Degradation mechanism of organic solar cells with aluminum cathode. Solar Energy Materials and Solar Cells. 2011, 95(12), 3303-3310. DOI: 10.1016/j.solmat.2011.07.020. ISSN 09270248. Available at: https://linkinghub.elsevier.com/retrieve/pii/S0927024811004235

(56) ABDULRAZZAQ, Omar A., Viney SAINI, Shawn BOURDO, Enkeleda DERVISHI, and Alexandru S. BIRIS. Organic Solar Cells: A Review of Materials, Limitations, and Possibilities for Improvement. Particulate Science and Technology. 2013, 31(5), 427-442. DOI: 10.1080/02726351.2013.769470. ISSN 0272-6351. Available at: http://www.tandfonline.com/doi/abs/10.1080/02726351.2013.769470

(57) BLANKENSHIP, Robert E. and Katsumi MATSUURA. Antenna Complexes from Green Photosynthetic Bacteria. Light-Harvesting Antennas in Photosynthesis. Dordrecht: Springer Netherlands, 2003, 2003, , 195-217. Advances in Photosynthesis and Respiration. DOI: 10.1007/978-94-017-2087-8_6. ISBN 978-90-481-5468-5. Available at: http://link.springer.com/10.1007/978-94-017-2087-8_6

(58) BALABAN, Teodor Silviu, Hitoshi TAMIAKI, and Alfred R. HOLZWARTH. Chlorins Programmed for Self-Assembly. Supermolecular Dye Chemistry. Berlin/Heidelberg: Springer-Verlag, 2005, , 1-38. Topics in Current Chemistry. DOI: 10.1007/b137480. ISBN 3-540-27758-7. Available at: http://www.springerlink.com/index/10.1007/b137480

(59) ALSTER, J., T. POLÍVKA, J.B. ARELLANO, P. CHÁBERA, F. VÁCHA, and J. PŠENČÍK. B-Carotene to bacteriochlorophyll c energy transfer in self-assembled aggregates mimicking chlorosomes. Chemical Physics. 2010, 373(1-2), 90-97. DOI:

10.1016/j.chemphys.2010.02.006. ISSN 03010104. Available at: https://linkinghub.elsevier.com/retrieve/pii/S0301010410000546

(60) VAN DORSSEN, R.J., P.D. GEROLA, J.M. OLSON, and J. AMESZ. Optical and structural properties of chlorosomes of the photosynthetic green sulfur bacterium Chlorobium limicola. Biochimica et Biophysica Acta (BBA) - Bioenergetics. 1986, 848(1), 77-82. DOI: 10.1016/0005-2728(86)90162-3. ISSN 00052728. Available at: https://linkinghub.elsevier.com/retrieve/pii/0005272886901623

(61) MELØ, T.B., N.-U. FRIGAARD, K. MATSUURA, and K. RAZI NAQVI. Electronic energy transfer involving carotenoid pigments in chlorosomes of two green bacteria: Chlorobium tepidum and Chloroflexus aurantiacus. Spectrochimica Acta Part A: Molecular and Biomolecular Spectroscopy. 2000, 56(10), 2001-2010. DOI: 10.1016/S1386-1425(00)00289-4. ISSN 13861425. Available at: https://linkinghub.elsevier.com/retrieve/pii/S1386142500002894

(62) PŠENČÍK, Jakub, Ying-Zhong MA, Juan B. ARELLANO, Jesús GARCIA-GIL, Alfred R. HOLZWARTH, and Tomas GILLBRO. Excitation energy transfer in Chlorosomes of chlorobium phaeobacteroides strain CL1401: The role of carotenoids. Photosynthesis Research. 2002, 71(1/2), 5-18. DOI: 10.1023/A:1014943312031. ISSN 01668595. Available at: http://link.springer.com/10.1023/A:1014943312031

(63) CELARDO, Giuseppe L., Fausto BORGONOVI, Marco MERKLI, Vladimir I. TSIFRINOVICH, and Gennady P. BERMAN. Superradiance Transition in Photosynthetic Light-Harvesting Complexes. The Journal of Physical Chemistry C. 2012, 116(42), 22105-22111. DOI: 10.1021/jp302627w. ISSN 1932-7447. Available at: http://pubs.acs.org/doi/10.1021/jp302627w

(64) MONSHOUWER, René, Malin ABRAHAMSSON, Frank VAN MOURIK, and Rienk VAN GRONDELLE. Superradiance and Exciton Delocalization in Bacterial Photosynthetic Light-Harvesting Systems. The Journal of Physical Chemistry B. 1997, 101(37), 7241-7248. DOI: 10.1021/jp963377t. ISSN 1520-6106. Available at: https://pubs.acs.org/doi/10.1021/jp963377t

(65) GROSS, M. a S. HAROCHE. Superradiance: An essay on the theory of collective spontaneous emission. Physics Reports. 1982, 93(5), 301-396. DOI: 10.1016/0370-1573(82)90102-8. ISSN 03701573. Dostupné také z: https://linkinghub.elsevier.com/retrieve/pii/0370157382901028

(66) KLINGER, Pavel, Juan B. ARELLANO, František VÁCHA, Jan HÁLA, and Jakub PŠENČÍK. Effect of Carotenoids and Monogalactosyl Diglyceride on Bacteriochlorophyll c Aggregates in Aqueous Buffer: Implications for the Self-assembly of Chlorosomes¶. Photochemistry and Photobiology. 2004, 80(3), 572-578. DOI: 10.1111/j.1751-1097.2004.tb00131.x. ISSN 00318655. Available at: http://doi.wiley.com/10.1111/j.1751-1097.2004.tb00131.x

(67) GIRI, Dhurba. High Performance Liquid Chromatography (HPLC) : Principle, Types, Instrumentation and Applications. Laboratory Info [online]. Nepal, 2020 [cit. 2020-04-24]. Available at: https://laboratoryinfo.com/hplc/

(68) PERSSON, Søren, Carsten P. SÖNKSEN, Niels-Ulrik FRIGAARD, Raymond P. COX, Peter ROEPSTORFF, and Mette MILLER. Pigments and proteins in green bacterial chlorosomes studied by matrix-assisted laser desorption ionisation mass spectrometry. European Journal of Biochemistry. 2000, 267(2), 450-456. DOI: 10.1046/j.1432-1327.2000.01019.x. ISSN 00142956. Available at: http://doi.wiley.com/10.1046/j.1432-1327.2000.01019.x

(69) STANIER, R.Y. and J.H.C. SMITH. The chlorophylls of green bacteria. Biochimica et Biophysica Acta. 1960, 41(3), 478-484. DOI: 10.1016/0006-3002(60)90045-7. ISSN 00063002. Available at: https://linkinghub.elsevier.com/retrieve/pii/0006300260900457

(70) TSUJI, K., S. Takaichi, K. Matsuura, K. Shimada, Specificity of carotenoids in chlorosomes of the green filamentous bacterium, Chloroflexus aurantiacus, in: P. Mathis (Ed.), Photosynthesis: from Light to Biosphere, Vol. 3, Kluwer Academic Publisher, Dordrecht, 1995, pp. 99–103.

(71) YOUNG, A and G BRITTON, ed. Carotenoids in photosynthesis. 1. Springer Netherlands, 1993. ISBN 978-94-011-2124-8.

(72) MIYATAKE, Tomohiro and Hitoshi TAMIAKI. Self-aggregates of natural chlorophylls and their synthetic analogues in aqueous media for making light-harvesting systems. Coordination Chemistry Reviews. 2010, 254(21-22), 2593-2602. DOI: 10.1016/j.ccr.2009.12.027. ISSN 00108545. Available at: http://linkinghub.elsevier.com/retrieve/pii/S0010854509003555

(73) ALSTER, Jan, Anita ZUPCANOVA, Frantisek VACHA and Jakub PŠENČÍK. Effect of quinones on formation and properties of bacteriochlorophyll c aggregates. Photosynthesis Research. 2008, 95(2-3), 183-189. DOI: 10.1007/s11120-007-9259-9. ISSN 0166-8595. Available at: http://link.springer.com/10.1007/s11120-007-9259-9

(74) MATĚNOVÁ, Martina, Viviana LORELEI HORHOIU, Florian-Xuan DANG, Petr POSPÍŠIL, Jan ALSTER, Jaroslav V. BURDA, Teodor SILVIU BALABAN, and Jakub PŠENČÍK. Energy transfer in aggregates of bacteriochlorophyll c self-assembled with azulene derivatives. Phys. Chem. Chem. Phys. 2014, 16(31), 16755-16764. DOI: 10.1039/C4CP01311E. ISSN 1463-9076. Available at: http://xlink.rsc.org/?DOI=C4CP01311E

(75) POSPÍŠIL, Petr. Samoorganizace a přenos excitační energie v bakteriochlorofylových agregátech (in Czech). Prague, 2010. Diploma thesis. Charles University, Faculty of Mathematics and Physics, Department of chemical physics and optics. Thesis supervisor Pšenčík, Jakub.

(76) ALSTER, J., T. POLÍVKA, J. B. ARELLANO, P. HŘÍBEK, F. VÁCHA, J. HÁLA, and J. PŠENČÍK. Self-assembly and energy transfer in artificial light-harvesting complexes of bacteriochlorophyll c with astaxanthin. Photosynthesis Research. 2012, 111(1-2), 193-204. DOI: 10.1007/s11120-011-9670-0. ISSN 0166-8595. Available at: http://link.springer.com/10.1007/s11120-011-9670-0

(77) COLLINS, A. M., J. A. TIMLIN, S. M. ANTHONY, and G. A. MONTAÑO. Amphiphilic block copolymers as flexible membrane materials generating structural and functional mimics of green bacterial antenna complexes. Nanoscale. 2016, 8(32), 15056-15063. DOI:

10.1039/C6NR02497A. ISSN 2040-3364. Available at: http://xlink.rsc.org/?DOI=C6NR02497A

(78) NAQVI, K. Razi, M. N. MERZLYAK a T. B. MELØ. Absorption and scattering of light by suspensions of cells and subcellular particles: an analysis in terms of Kramers–Kronig relations. Photochem. Photobiol. Sci. 2004, 3(1), 132-137. DOI: 10.1039/B304781D. ISSN 1474-905X. Dostupné také z: http://xlink.rsc.org/?DOI=B304781D

(79) TANG, Kuo-Hsiang, Liying ZHU, Volker S. URBAN, Aaron M. COLLINS, Pratim BISWAS, and Robert E. BLANKENSHIP. Temperature and Ionic Strength Effects on the Chlorosome Light-Harvesting Antenna Complex. Langmuir. 2011, 27(8), 4816-4828. DOI: 10.1021/la104532b. ISSN 0743-7463. Available at: https://pubs.acs.org/doi/10.1021/la104532b

(80) VAN OORT, Bart, Sukumaran MURALI, Emilie WIENTJES, Rob B.M. KOEHORST, Ruud B. SPRUIJT, Arie VAN HOEK, Roberta CROCE, and Herbert VAN AMERONGEN. Ultrafast resonance energy transfer from a site-specifically attached fluorescent chromophore reveals the folding of the N-terminal domain of CP29. chemical Physics. 2009, 357(1-3), 113-119. DOI: 10.1016/j.chemphys.2008.10.052. ISSN 03010104. Available at: https://linkinghub.elsevier.com/retrieve/pii/S0301010408005120

(81) SNELLENBERG, Joris-Joost. Glotaran: a tool for interactive global and target analysis of time-resolved spectroscopy and microscopy data. Amsterdam, 2010. Master's thesis. VU University Amsterdam. Supervisor Ivo van Stokkum.

(82) RURACK, Knut and Monika SPIELES. Fluorescence Quantum Yields of a Series of Red and Near-Infrared Dyes Emitting at 600−1000 nm. Analytical Chemistry. 2011, 83(4), 1232-1242. DOI: 10.1021/ac101329h. ISSN 0003-2700. Available at: https://pubs.acs.org/doi/10.1021/ac101329h

(83) BRUNE, Daniel C., Robert E. BLANKENSHIP, and Gilbert R. SEELY. FLUORESCENCE QUANTUM YIELDS AND LIFETIMES FOR BACTERIOCHLOROPHYLL c. Photochemistry and Photobiology. 1988, 47(5), 759-763. DOI: 10.1111/j.1751-1097.1988.tb02776.x. ISSN 0031-8655. Available at: http://doi.wiley.com/10.1111/j.1751-1097.1988.tb02776.x

(84) A Guide to Recording Fluorescence Quantum Yields. Stanmore, United Kingdom. Available at: http://www.horiba.com/fileadmin/uploads/Scientific/Documents/Fluorescence/quantumyieldstrad.pdf

(85) THOMPSON, David E. Curve Fitting. David E. Thompson [online]. USA: University of Idaho, 2010 [cit. 2020-04-30]. Available at: https://www.engr.uidaho.edu/thompson/courses/ME330/lecture/least_squares.html

(86) POLÍVKA, Tomáš a Harry A. FRANK. Molecular Factors Controlling Photosynthetic Light Harvesting by Carotenoids. Accounts of Chemical Research. 2010, 43(8), 1125-1134. DOI: 10.1021/ar100030m. ISSN 0001-4842. Dostupné také z: https://pubs.acs.org/doi/10.1021/ar100030m

(87) GRADINARU, C. C., J. T. M. KENNIS, E. PAPAGIANNAKIS, I. H. M. VAN STOKKUM, R. J. COGDELL, G. R. FLEMING, R. A. NIEDERMAN a R. VAN GRONDELLE. An unusual pathway of excitation energy deactivation in carotenoids: Singlet-to-triplet conversion on an ultrafast timescale in a photosynthetic antenna. Proceedings of the National Academy of Sciences. 2001, 98(5), 2364-2369. DOI: 10.1073/pnas.051501298. ISSN 0027-8424. Dostupné také z: http://www.pnas.org/cgi/doi/10.1073/pnas.051501298

(88) POLAK, D., , A.J. MUSSER, et al. Band-edge Excitation of Carotenoids Removes S* Revealing Triplet-pair Contributions to the S1 Absorption Spectrum. ArXiv: Chemical Physics. 2019. Dostupné také z: https://arxiv.org/ftp/arxiv/papers/1901/1901.04900.pdf

(89) TEJEDA-FERRARI, Marely E., Chelsea L. BROWN, Gabriela C. C. C. COUTINHO, et al. Electronic Structure and Triplet-Triplet Energy Transfer in Artificial Photosynthetic Antennas. Photochemistry and Photobiology. 2019, 95(1), 211-219. DOI: 10.1111/php.12979. ISSN 00318655. Dostupné také z: http://doi.wiley.com/10.1111/php.12979

(90) KVÍČALOVÁ, Zuzana, Jan ALSTER, Eckhard HOFMANN, Petro KHOROSHYY, Radek LITVÍN, David BÍNA, Tomáš POLÍVKA, and Jakub PŠENČÍK. Triplet–triplet energy transfer from chlorophylls to carotenoids in two antenna complexes from dinoflagellate Amphidinium carterae. Biochimica et Biophysica Acta (BBA) - Bioenergetics. 2016, 1857(4), 341-349. DOI: 10.1016/j.bbabio.2016.01.008. Available at: https://www.sciencedirect.com/science/article/pii/S0005272816000104

(91) ISHII, Takasada, Kaku UEHARA, Yukihiro OZAKI, and Mamoru MIMURO. The Effects of pH and Ionic Strength on the Aggregation of Bacteriochlorophyll c in Aqueous Organic Media: The Possibility of Two Kinds of Aggregates. Photochemistry and Photobiology. 1999, 70(5), 760-765. DOI: 10.1111/j.1751-1097.1999.tb08280.x. ISSN 0031-8655. Available at: http://doi.wiley.com/10.1111/j.1751-1097.1999.tb08280.x

(92) JIMENEZ, Ralph, Graham R. FLEMING, P. V. KUMAR, and M. MARONCELLI. Femtosecond solvation dynamics of water. Nature. 1994, 369(6480), 471-473. DOI: 10.1038/369471a0. ISSN 0028-0836. Available at: http://www.nature.com/articles/369471a0

(93) LAKOWICZ, Joseph R. Principles of Fluorescence Spectroscopy. 3rd Ed. New York: Springer US, 2006. ISBN 978-0387-31278-1.

(94) FRIGAARD, N.-U., Shinichi TAKAICHI, Masamitsu HIROTA, Keizo SHIMADA, and Katsumi MATSUURA. Quinones in chlorosomes of green sulfur bacteria and their role in the redox-dependent fluorescence studied in chlorosome-like bacteriochlorophyll c aggregates. Archives of Microbiology. 1997, 167(6), 343-349. DOI: 10.1007/s002030050453. ISSN 0302-8933. Available at: http://link.springer.com/10.1007/s002030050453

(95) BLANKENSHIP, Robert E., Peiling CHENG, Timothy P. CAUSGROVE, Daniel C. BRUNE, Stephanie Hsiao-Hsien WANG, Jin-Ug CHOH, and Jian WANG. REDOX REGULATION OF ENERGY TRANSFER EFFICIENCY IN ANTENNAS OF GREEN PHOTOSYNTHETIC BACTERIA. Photochemistry and Photobiology. 1993, 57(1), 103-107. DOI: 10.1111/j.1751-1097.1993.tb02263.x. ISSN 0031-8655. Available at: http://doi.wiley.com/10.1111/j.1751-1097.1993.tb02263.x

(96) FRIGAARD, Niels-Ulrik, Katsumi MATSUURA, Masamitsu HIROTA, Mette MILLER, and Raymond P. COX. Studies of the location and function of isoprenoid quinones in chlorosomes from green sulfur bacteria. Photosynthesis Research. 1998, 58(1), 81-90. DOI: 10.1023/A:1006043706652. ISSN 01668595. Available at: http://link.springer.com/10.1023/A:1006043706652

(97) BRYANT, Donald A., Elena V. VASSILIEVA, Niels-Ulrik FRIGAARD, and Hui LI. Selective Protein Extraction from Chlorobium tepidum Chlorosomes Using Detergents. Evidence That CsmA Forms Multimers and Binds Bacteriochlorophyll a †. Biochemistry. 2002, 41(48), 14403-14411. DOI: 10.1021/bi026599s. ISSN 0006-2960. Available at: https://pubs.acs.org/doi/10.1021/bi026599s

(98) FEICK, RG, M FITZPATRICK, and RC FULLER. Isolation and characterization of cytoplasmic membranes and chlorosomes from the green bacterium Chloroflexus aurantiacus. J Bacteriol. 1982, 150(2), 905-15. Available at: https://JB.asm.org/content/174/15/5021

(99) PŠENČÍK, Jakub, Juan B. ARELLANO, Teemu P. IKONEN, Carles M. BORREGO, Pasi A. LAURINMÄKI, Sarah J. BUTCHER, Ritva E. SERIMAA a Roman TUMA. Internal Structure of Chlorosomes from Brown-Colored Chlorobium Species and the Role of Carotenoids in Their Assembly. Biophysical Journal. 2006, 91(4), 1433-1440. DOI: 10.1529/biophysj.106.084228. ISSN 00063495. Dostupné také z: https://linkinghub.elsevier.com/retrieve/pii/S0006349506718549

List of Figures

List of Tables

List of abbreviations

AFM	Atomic force microscopy
ASCII	American Standard Code for Information Interchange
ATP	Adenosine triphosphate
(B)Chl	(Bacterio)Chlorophyll
Cb.	Chlorobaculum
Cf.	Chloroflexus
CIGS	Copper indium gallium (di)selenide
DAS	Decay associated spectra
DSSC	Dye-sensitised solar cell
EET	Excitation energy transfer
ESA	Excited state absorption
EtOH	Ethanol
FMO	Fenna-Matthews-Olson
FNR	Ferredoxin-NADP+ reductase
FWHM	Full-width at half-maximum
GSB	Ground-state bleaching
HITCI	1,1',3,3,3',3'-hexamethylindotricarbocyanine iodide
HPLC	High-performance liquid chromatography
iCCD	Intensified charge coupled device
IRF	Instrument response function
ISC	Intersystem crossing
LHCII	Light-harvesting complex II
MeOH	Methanol

MES	2-(N-morpholino)ethanesulfonic acid
MGDG	monogalactosyl diglyceride
NADP	Nicotinamide adenine dinucleotide
Nd:YAG	Neodymium-doped Yttrium Alluminium Garnet
NIR	Near Infrared
OPA	Optical parametric amplifier
OPV	Organic photovoltaics
OSC	Organic solar cell
PEO-b-PBD	Poly(butadiene(1,2 addition))-block-ethylene oxide
PSI or PSII	Photosystem I or II
RC	Reaction centre
SHG	Second harmonic generator
SVD	Singular value decomposition
THF	Tetrahydrofuran
Tris	tris(hydroxymethyl)aminomethane
UV	Ultra-violet
Vis	Visible

Appendix A

The following figures are the remaining figures not shown in section 3.1. They illustrate the spectra from which the EET efficiency between β-carotene and BChl *c* aggregates was determined. The first two figures (A.1 and A.2) are inaccurate since they were measured on a spectrofluorometer with only a single emission monochromator. The last figure (A.3) is deemed less inaccurate, although scattering affected those data significantly, too.

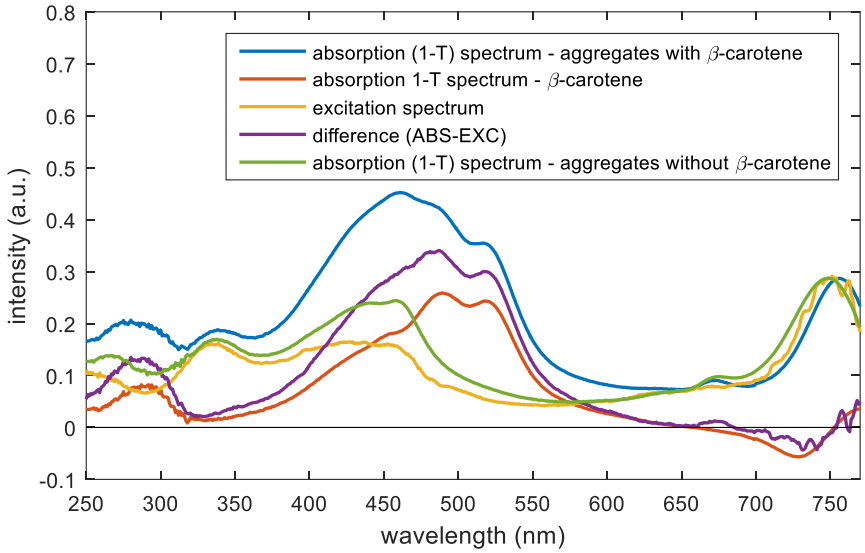

Figure A.1: EET from β-carotene in slow-method aggregates (BChl *c* to β-carotene 1:1). Subtraction of the excitation spectrum (orange) from the absorption (blue) yields the amount of β-carotene not transferring energy to BChl *c* (purple). The total amount of β-carotene is determined by subtracting the absorption β-carotene-free aggregates (normalised to the amplitude of the blue curve) from the blue curve (red). Measured at Charles University (proven inaccurate).

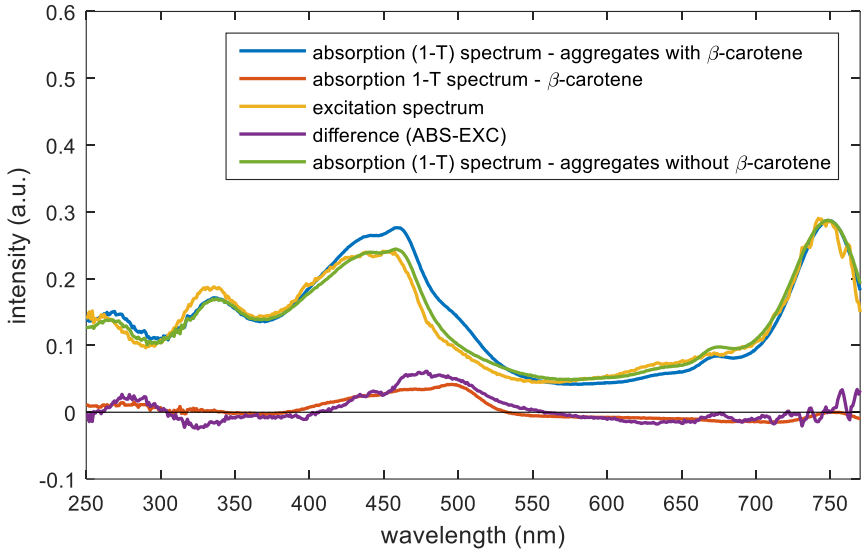

Figure A.2: EET from β-carotene in slow-method aggregates (BChl *c* to β-carotene 1:0.1). Subtraction of the excitation spectrum (orange) from the absorption (blue) yields the amount of β-carotene not transferring energy to BChl *c* (purple). The total amount of β-carotene is determined by subtracting the absorption β-carotene-free aggregates (normalised to the amplitude of the blue curve) from the blue curve (red). Measured at Charles University (proven inaccurate).

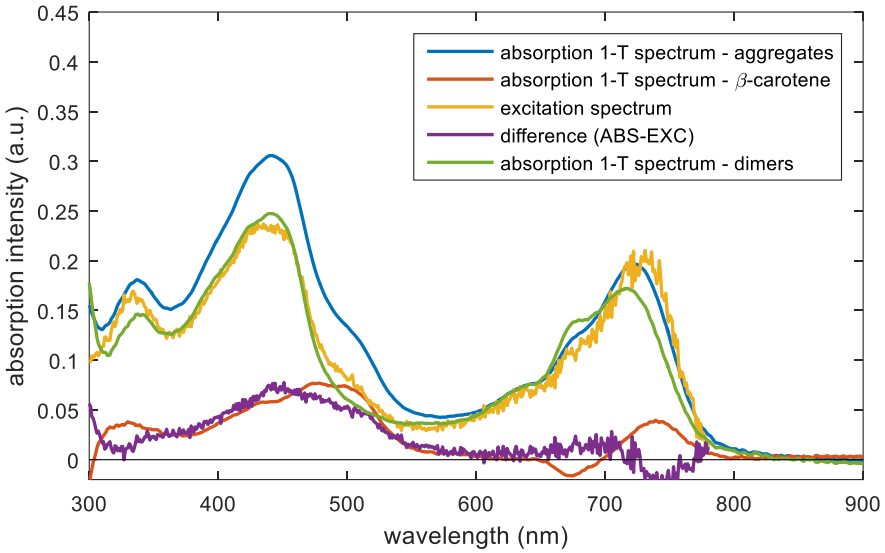

Figure A.3: EET from β-carotene in fast-method aggregates (BChl *c* to β-carotene 1:0.4). Subtraction of the excitation spectrum (orange) from the absorption (blue) yields the amount of β-carotene not transferring energy to BChl *c* (purple). The total amount of β-carotene is determined by subtracting the absorption β-carotene-free aggregates (normalised to the amplitude of the blue curve) from the blue curve (red). Measured at the University of South Bohemia.

Appendix B

The following figures demonstrate that the addition of β-carotene or BChl *a* does not affect the shape of the emission spectrum.

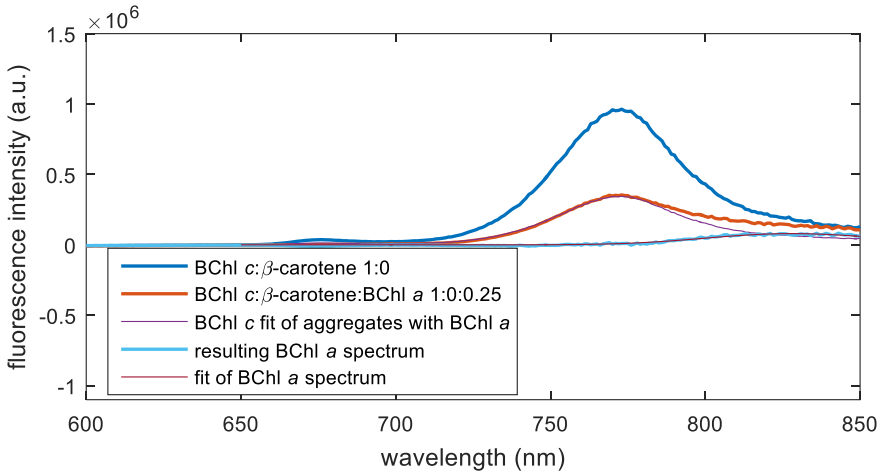

Figure B.1: Spectrum of the emission of slow-method aggregates with (blue) and without (red) BChl *a*. The latter were fitted (purple) with the BChl *c* emission spectrum and a Gaussian function for the BChl *a* emission (magenta). The Gaussian fit closely follows the BChl *a* emission spectrum obtained by a subtraction of the purple line from the red line.

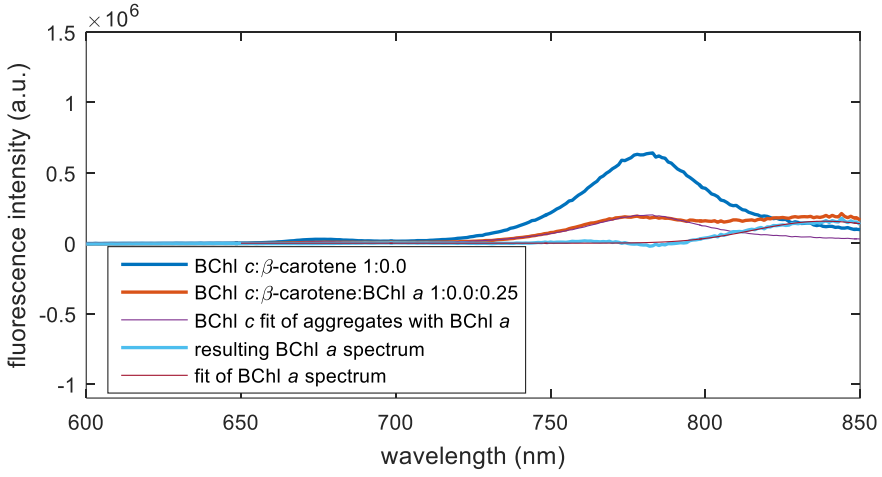

Figure B.2: Spectrum of the emission of polymer-free slow-method aggregates with (blue) and without (red) BChl *a*. The latter were fitted (purple) with the BChl *c* emission spectrum and a Gaussian function for the BChl *a* emission (magenta). The Gaussian fit closely follows the BChl *a* emission spectrum obtained by a subtraction of the purple line from the red line.

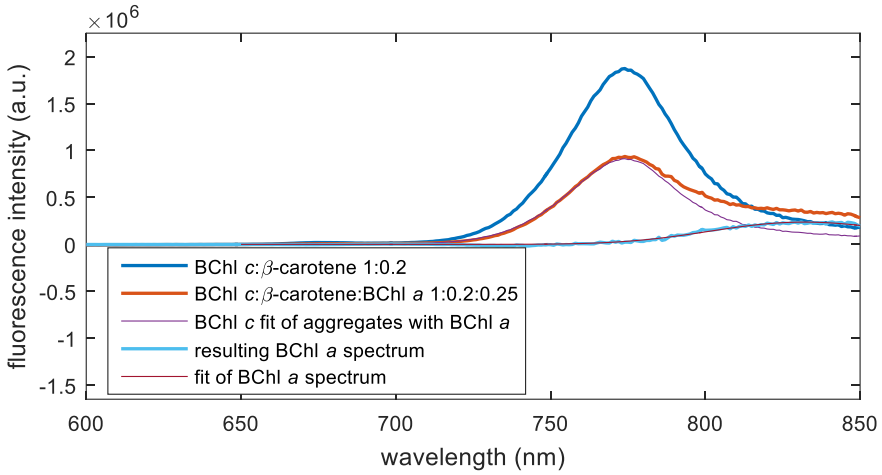

Figure B.3: Spectrum of the emission of slow-method aggregates with (blue) and without (red) BChl *a*. The latter were fitted (purple) with the BChl *c* emission spectrum and a Gaussian function for the BChl *a* emission (magenta). The Gaussian fit closely follows the BChl *a* emission spectrum obtained by a subtraction of the purple line from the red line.

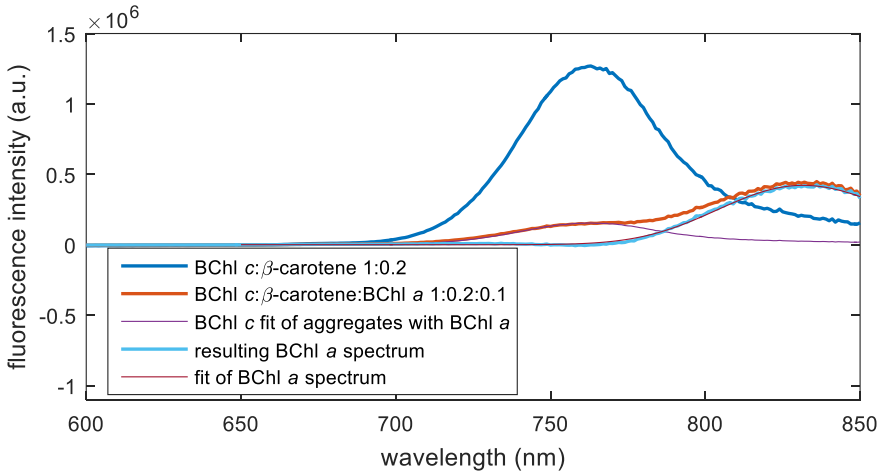

Figure B.4: Spectrum of the emission of fast-method aggregates with (blue) and without (red) BChl *a*. The latter were fitted (purple) with the BChl *c* emission spectrum and a Gaussian function for the BChl *a* emission (magenta). The Gaussian fit closely follows the BChl *a* emission spectrum obtained by a subtraction of the purple line from the red line.

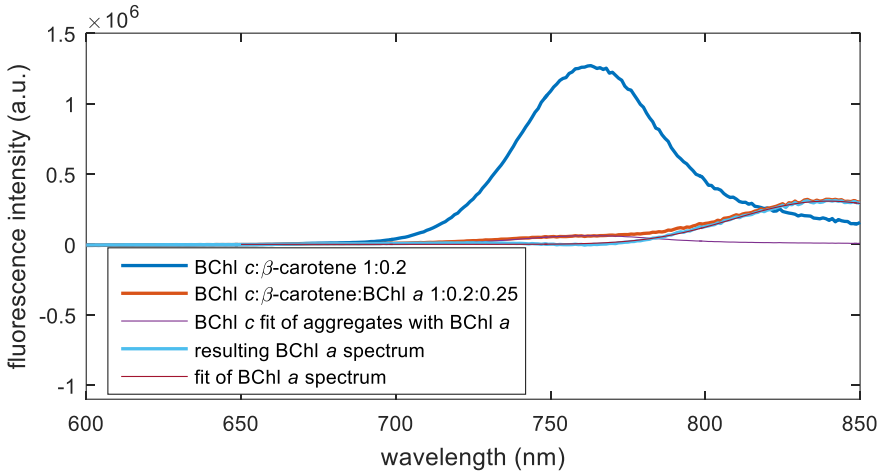

Figure B.5: Spectrum of the emission of fast-method aggregates with (blue) and without (red) BChl *a*. The latter were fitted (purple) with the BChl *c* emission spectrum and a Gaussian function for the BChl *a* emission (magenta). The Gaussian fit closely follows the BChl *a* emission spectrum obtained by a subtraction of the purple line from the red line.

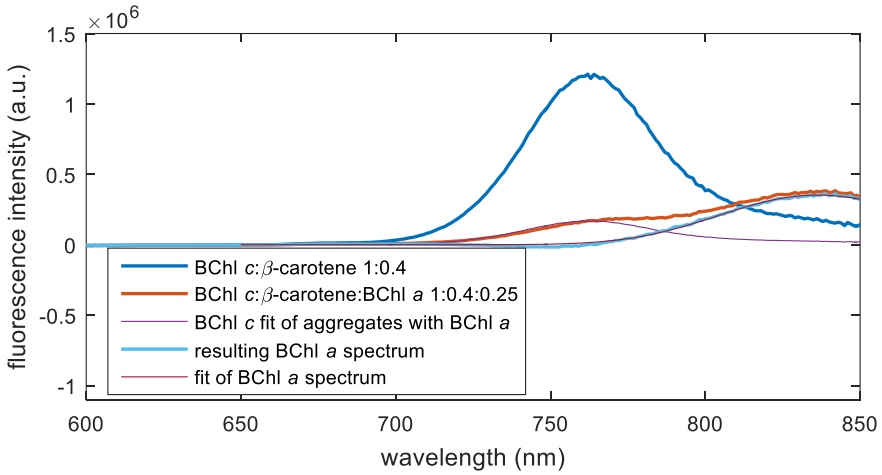

Figure B.6: Spectrum of the emission of fast-method aggregates with (blue) and without (red) BChl *a*. The latter were fitted (purple) with the BChl *c* emission spectrum and a Gaussian function for the BChl *a* emission (magenta). The Gaussian fit closely follows the BChl *a* emission spectrum obtained by a subtraction of the purple line from the red line.

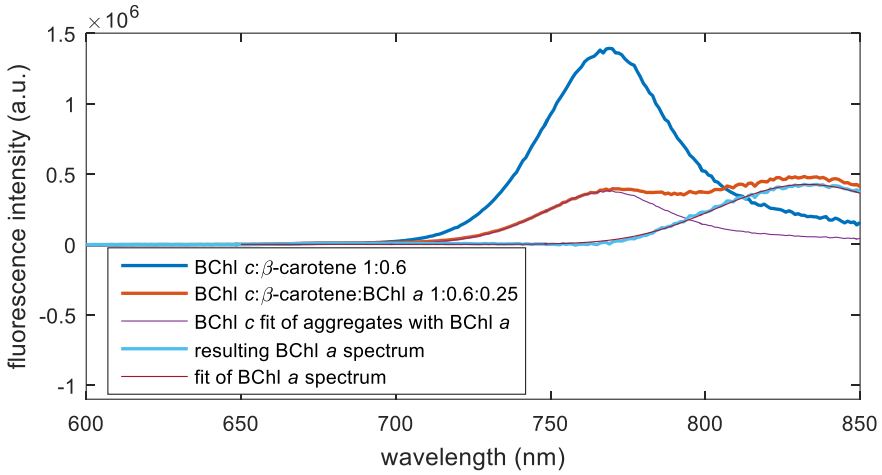

Figure B.7: Spectrum of the emission of fast-method aggregates with (blue) and without (red) BChl *a*. The latter were fitted (purple) with the BChl *c* emission spectrum and a Gaussian function for the BChl *a* emission (magenta). The Gaussian fit closely follows the BChl *a* emission spectrum obtained by a subtraction of the purple line from the red line.

The following figures show the emission spectra from which the EET efficiency between BChl *c* and BChl *a* was determined. These are the remaining figures not shown in section 3.2.

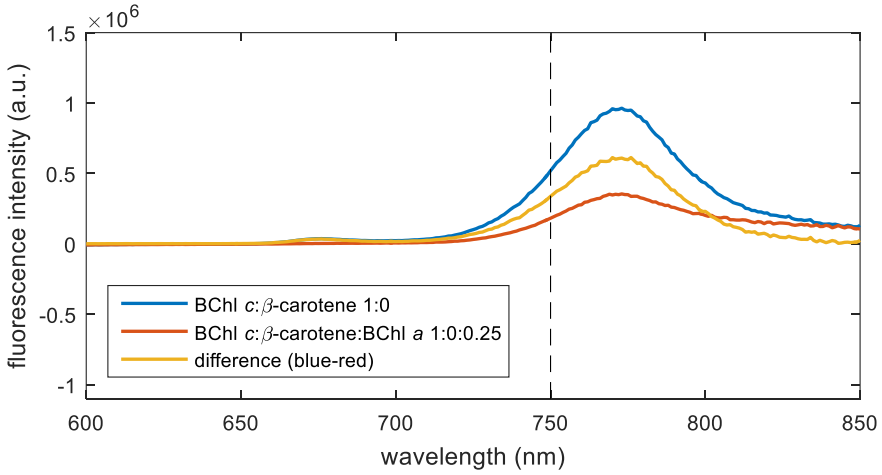

Figure B.8: The emission spectra of slow-method aggregates with (red) and without (blue) added BChl *a* and their difference (orange) indicating EET efficiency of 65 %.

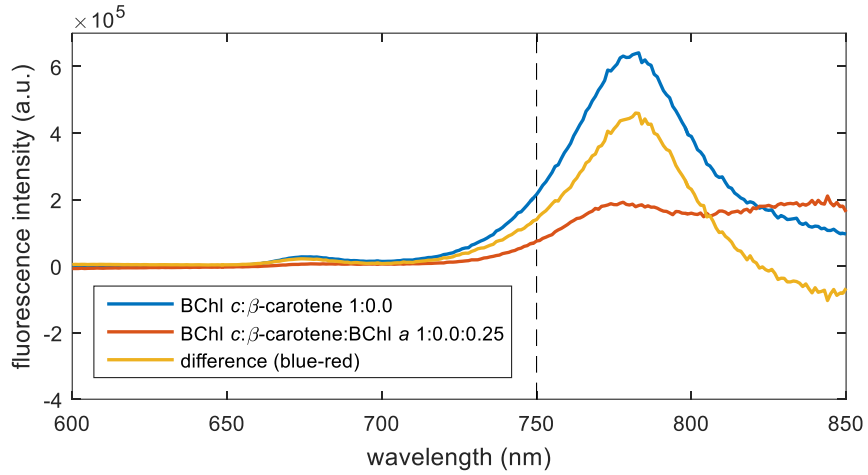

Figure B.9: The emission spectra of polymer-free slow-method aggregates with (red) and without (blue) added BChl *a* and their difference (orange) indicating EET efficiency of 65 %.

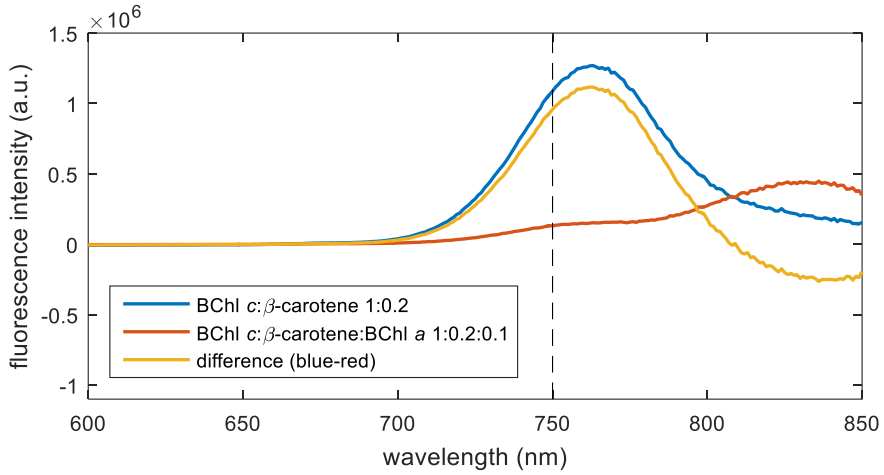

Figure B.10: The emission spectra of fast-method aggregates with (red) and without (blue) added BChl *a* and their difference (orange) indicating EET efficiency of 88 %.

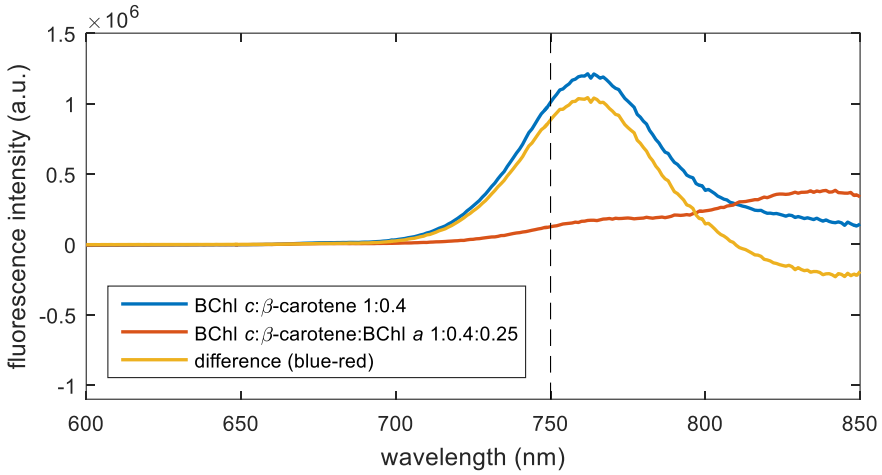

Figure B.11: The emission spectra of fast-method aggregates with (red) and without (blue) added BChl *a* and their difference (orange) indicating EET efficiency of 88 %.

Appendix C

The contents of the attachments are described in this section.

Quantum yields

The folder *Quantum yields* contains a XLS file where the results are visualised for each measured sample. The results of absorption and emission intensities are listed for each measurement along with the calculated uncertainties. The slopes of the emission vs absorption plot (Eq.2.3) are used for the evaluation of the quantum yields.

The folder also contains all the measured spectra in ASCII (emission spectra) or CSV (absorption spectra) format along with the Matlab scripts used to analyse the spectra and enumerate the results. The wavelengths for the integration of the emission intensity were selected manually for each sample and the selected wavelengths are listed with each sample in the attached XLS file (next to each sample, the first two sheets). The final calculations are shown in two tables (the last two sheets of the file). The results are then summarised in the thesis in Table 2.

Streak camera data

The folder *Streak camera data* contains the IMG files that were measured and processed for background, jitter and shading corrections. Those files contain an ASCII header with the information about the measurement setup and binary UTF-8 encoded map of recorded intensities. These files were processed using the GloTarAn software (as mentioned in 2.6.1).

Streak camera fits

The folder *Streak camera fits* contains the output from the GloTarAn software. Those data are in the XML format native to the software. They can be loaded to GloTarAn to view all the calculated values.